Exploring NK-92 Cell Cultures with Spectral Flow Cytometry and Metabolic Profiling

DIPLOMARBEIT

zur Erlangung des akademischen Grades

Diplom-Ingenieur

im Rahmen des Studiums

Technische Chemie

eingereicht von

Philipp Brunmayr, MSc
01506503

am Institut für Verfahrenstechnik, Umwelttechnik und technische Biowissenschaften
der Fakultät für Technische Chemie
der Technischen Universität Wien

Betreuung: Univ.Prof. Dipl.-Ing. Dr.nat.techn. Oliver Spadiut

Mitwirkung: Bence Kozma, PhD
Valentin Von Werz, MSc

Wien, 20. November 2023

Philipp Brunmayr

Exploring NK-92 Cell Cultures with Spectral Flow Cytometry and Metabolic Profiling

DIPLOMA THESIS

submitted in partial fulfillment of the requirements for the degree of

Diplom-Ingenieur

in

Technical Chemistry

by

Philipp Brunmayr, MSc
01506503

to the Institute of Chemical, Environmental and Bioscience Engineering

at the Faculty of Technical Chemistry

at the Vienna University of Technology

Advisor: Univ.Prof. Dipl.-Ing. Dr.nat.techn. Oliver Spadiut

Assistance: Bence Kozma, PhD
Valentin Von Werz, MSc

Vienna, November 20, 2023

Philipp Brunmayr

Erklärung zur Verfassung der Arbeit

Philipp Brunmayr, MSc

Hiermit erkläre ich, dass ich diese Arbeit selbständig verfasst habe, dass ich die verwendeten Quellen und Hilfsmittel vollständig angegeben habe und dass ich die Stellen der Arbeit – einschließlich Tabellen, Karten und Abbildungen –, die anderen Werken oder dem Internet im Wortlaut oder dem Sinn nach entnommen sind, auf jeden Fall unter Angabe der Quelle als Entlehnung kenntlich gemacht habe.

Wien, 20. November 2023

Philipp Brunmayr

Acknowledgements

I want to express my deep gratitude to Univ. Prof. Oliver Spadiut for the opportunity to conduct my diploma thesis in his amazing research group for Integrated Bioprocess Development at the Vienna University of Technology.

I am also deeply grateful to my co-supervisor, Bence Kozma, for his invaluable guidance and countless hours of insightful discussions, adding a touch of wisdom to my academic journey. I would also like to extend my sincere thanks to Valentin, whose project I had the privilege of contributing to. The conducive and relaxed working environment fostered by both mentors made the research experience productive and enjoyable.

Hats off to my master's colleague Karim, whose friendship injected a sense of humor into our collaborative efforts. Working with him wasn't just a productivity boost; it was a joyride. Also, let's not forget the bioprocess engineering team. You guys are the lab legends, and the fantastic collegues who made every experiment feel awesome.

On a personal note, I would like to express my heartfelt appreciation to my girlfriend, Sarah. She's been there for me through thick and thin, and her sense of humor has been a real lifesaver. I couldn't have done this without her support, love, and encouragement.

Heartfelt thanks to my family, whose love and encouragement have been the pillars of my academic journey. They have always supported me emotionally and financially and I am forever grateful for their love and care.

Finally, to everyone who played a part, your assistance and encouragement have been invaluable and I am deeply grateful for your support. To everyone who gave a hand, a joke, or a word of encouragement, thank you.

Abstract

Adoptive cell therapy represents a promising approach in cancer treatment that involves the administration of *ex vivo* activated, expanded and genetically modified allogeneic or autologous immune cells. Natural killer cells have emerged as versatile and safe candidates for this therapy due to their innate ability to target and eliminate abnormal cells and modulate immune responses. Our study focuses on the NK-92 cell line, which reflects the characteristics of highly activated blood-derived NK cells that exhibit high cytotoxicity. This method offers a cost-effective alternative to allogeneic primary NK cells by reducing donor-to-donor variability and eliminating the need for expensive cell isolation and purification techniques, enabling their use as an off-the-shelf therapeutic agent.

Despite the potential of NK cell-based therapies, expansion processes remain poorly understood and lack standardization. Rapid adaptations in immune cell metabolism further complicate the predictability of lymphocyte expansion. We aim to employ Quality by Design principles to ensure consistent qualitative and quantitative characteristics of therapeutic NK cells. By elucidating the interaction between quality attributes and process parameters, we aim to ensure the consistent quality of the living product. To overcome the challenges that arise from the slow growth kinetics of NK-92 cells, our study employed a pseudo-static cultivation method for daily phenotypic characterization, assessment of cytokine production, and comparative cytotoxicity evaluation. Furthermore, we aimed to gain a deeper understanding of the basic metabolic requirements of the NK-92 expansion process by monitoring nutrient uptake and metabolite release.

Our investigation uncovered a metabolic fingerprint of NK-92 cells, characterized by heavy utilization of L-serine, L-arginine, L-asparagine, and L-glutamine. Moreover, we observed the development of a dysfunctional phenotype characterized by reduced metabolic activity, cytotoxicity, impaired degranulation, and downregulation of activating receptors. We hypothesized that this is associated with shear stress induced during cell handling or linked to nutrient depletion and the accumulation of inhibitory metabolites. Furthermore, our research has demonstrated that flow cytometry is the optimal method to evaluate cellular cytotoxicity because of its superior sensitivity, applicability, and the information density of the obtained data. In conclusion, the insights gained from this project provide a valuable basis for future experiments that will allow us to understand and improve the manufacturing process of therapeutic NK cells.

Kurzfassung

Die adoptive Zelltherapie stellt einen vielversprechenden Ansatz in der Krebstherapie dar, der die Verabreichung von *ex vivo* aktivierten, expandierten und eventuell genetisch modifizierten allogenen oder autologen Immunzellen beinhaltet. Natürliche Killerzellen haben sich aufgrund ihrer angeborenen Fähigkeit, abnormale Zellen zu erkennen und zu eliminieren sowie Immunantworten zu modulieren, als vielseitige und sichere Kandidaten für die Zelltherapie herausgestellt. Unsere Studie konzentriert sich auf die NK-92-Zelllinie, die die Eigenschaften hochaktivierter, aus Blut gewonnener NK-Zellen mit hoher Zytotoxizität widerspiegelt. Dieser Ansatz bietet eine kostengünstige Alternative zu allogenen primären NK-Zellen, reduziert die Spender-zu-Spender-Variabilität und den Bedarf an teuren Zellisolations- und Reinigungstechniken, was ihre Verwendung als von der Stange erhältliches therapeutisches Mittel ermöglicht.

Trotz des Potenzials von NK-Zell-basierten Therapien sind die Expansionsprozesse schlecht verstanden und mangelhaft standardisiert. Schnelle Anpassungen im Stoffwechsel der Immunzellen erschweren die Vorhersagbarkeit der Lymphozytenexpansion zusätzlich. Unser Ziel ist es, die Prinzipien der Qualität durch Design zu verwenden, um konsistente qualitative und quantitative Merkmale therapeutischer NK-Zellen sicherzustellen. Durch die Aufklärung der Wechselwirkungen zwischen kritischen Qualitätsattributen und kritischen Prozessparametern streben wir eine gleichbleibende Qualität der Zellen an. Um die Herausforderungen aufgrund der langsamen Wachstumsdynamik von NK-92-Zellen zu bewältigen, verwendet unsere Studie eine pseudo-statische Kultivierungsmethode für die tägliche phänotypische Charakterisierung, Bewertung der Zytokinproduktion und vergleichende Zytotoxizitätsbewertung. Darüber hinaus beabsichtigen wir, ein tieferes Verständnis für die grundlegenden Stoffwechselanforderungen des NK-92-Expansionsprozesses zu gewinnen, indem wir die Nährstoffaufnahme und den Metabolitenausstoß überwachen.

Unsere Untersuchung deckte einen Stoffwechsel-Fingerabdruck der NK-92-Zellen auf, der auf eine intensive Nutzung von L-Serin, L-Arginin, L-Asparagin und L-Glutamin hinweist. Darüber hinaus beobachteten wir die Entwicklung eines dysfunktionalen Phänotyps, der durch verminderte Stoffwechselaktivität, Zytotoxizität, beeinträchtigte Degranulation und Herunterregulierung aktivierender Rezeptoren gekennzeichnet ist. Dies könnte mit Scherstress während der Zellhandhabung oder mit der Erschöpfung des Kulturmediums und der Anhäufung hemmender Metaboliten in Verbindung stehen. Weiterhin hat unsere Forschung gezeigt, dass die Durchflusszytometrie die optimale Methode zur Bewertung

der zellulären Zytotoxizität ist. Dies wird durch ihre überlegene Empfindlichkeit, Anwendbarkeit und Informationsdichte der erhaltenen Daten begründet. Zusammenfassend liefern die Erkenntnisse aus diesem Projekt eine wertvolle Grundlage für zukünftige Experimente, die es uns ermöglichen werden, den Herstellungsprozess therapeutischer NK-Zellen zu verstehen und zu verbessern.

Table of Contents

CHAPTER 1

Introduction

1.1 The Role of NK Cells in the Immune System

Natural killer (NK) cells are specialized effector cells of the innate immune system, accounting for about 5-20% of peripheral blood lymphocytes[1]. These cells exhibit potent cytotoxicity, cytokine production, and immunomodulatory activities[2, 3]. In humans, NK cells are divided into two main subsets based on the surface expression of neural cell adhesion molecule 1, also known as CD56*[1]. These distinct subsets comprise $CD56^{dim}$ and $CD56^{bright}$ cells, each characterized by unique phenotypic and homing properties[5, 6]. Furthermore, the complexity of NK cell biology expands on the fact that circulatory NK cells also differ in their expression profile and proliferative capacity from those found in secondary lymphoid organs[7]. The predominant subset (90%) of NK cells found in the peripheral blood and spleen is characterized by the $CD56^{dim}CD16^{+}$ phenotype[8]. This subset expresses perforin, exhibits cytotoxicity, and produces IFN-γ upon interaction with tumor cells *in vitro*[8]. Conversely, the majority of NK cells residing in the lymph nodes are characterized by the $CD56^{bright}CD16^{-}$ and lack perforin expression[8]. Despite this, these cells display significant cytokine production in response to stimulation by various interleukin (IL), such as IL-12, IL-15, or IL-18[8].

NK cells predominantly reside in the peripheral blood, spleen, and bone marrow. However, they can also migrate to inflammatory tissues in response to chemoattractants[9]. Primarily tasked with eliminating malignant and virus-infected cells, they also orchestrate immunomodulatory responses[9, 10]. Upon activation, the release of chemokines and cytokines not only modulates hematopoiesis, but also influences the function and growth

*The clusters of differentiation (CD) classification system, initially formulated during the International Workshop and Conference on Human Leukocyte Differentiation Antigens in Paris in 1982, is a nomenclature for standardized clustering of monoclonal antibodies reacting to specific cellular-differentiation patterns. To date, the CD classification system has been expanded to a total of 371 different CD markers (CD1 - CD371)[4].

of monocytes and granulocytes. Consequently, NK cells regulate subsequent adaptive immune responses[9, 10].

1.1.1 The NK Cell Receptor Repertoire

A fundamental characteristic of NK cells is their ability to distinguish between abnormal and healthy cells based on the expression pattern of major histocompatibility complex (MHC) class I molecules[11]. In humans, MHC molecules are also referred to as the human leukocyte antigen (HLA)[12]. Alterations in HLA expression are commonly observed in virus-infected or malignant cells[11, 13]. A summary of the receptors involved in target recognition by NK cells is presented in figure 1.1. NK cells express two main classes of HLA-specific inhibitory receptors: the killer-cell immunoglobulin-like receptor (KIR) family and the CD94/NKG2A heterodimer. KIRs are type I transmembrane receptors and recognize polymorphic HLA-A, B, and C molecules. In contrast, CD94/NKG2A is a type II transmembrane receptor specific for non-classical HLA molecules with limited polymorphism, e.g., HLA-G[11].

These inhibitory receptors harbor immunoreceptor tyrosine-based inhibitory motifs (ITIMs) that initiate inhibitory signaling cascades upon phosphorylation[11]. In addition to inhibitory KIRs, activating KIR receptors, such as CD94-NKG2C and CD94-NKG2E, has also been reported[11]. These lack the ITIMs but carry motifs facilitating the association with immunoreceptor tyrosine-based activation motif (ITAM)-carrying co-stimulatory molecules[11]. Furthermore, NK cells express the inhibitory receptor CD85j, which belongs to the Ig-like receptor superfamily, interacting with classical HLA-A, B, C, and non-classical HLA-G molecules[11]. Immune checkpoints are another essential regulator in maintaining immune homeostasis. Key immunomodulatory receptors in this context comprise T-cell immunoreceptor with immunoglobulin and immunoreceptor tyrosine-based inhibition motif domain (TIGIT), programmed cell death protein 1 (PD-1), lymphocyte-activation gene 3 (LAG-3), CD96, and T cell immunoglobulin and mucin domain-containing protein 3 (TIM-3)[11]. While absent under healthy physiological conditions, these receptors become upregulated under pathological conditions[11]. Their corresponding ligands are frequently overexpressed on tumor cells and modulate NK-cell function upon receptor engagement[11].

In contrast, NK cells express activating receptors known as natural cytotoxicity receptors (NCRs). This receptor class comprises CD335 (NKp46)[15], CD336 (NKp44)[16] and CD337 (NKp30)[17]. CD335 and CD337 are expressed on nearly all resting NK cells and are upregulated upon activation[11]. On the other hand, CD336 is constitutively expressed only on $CD56^{bright}$ NK cells but is induced on almost all subsets upon activation[11]. The transmembrane domain of these receptors contains positively charged amino acids that facilitate the association with TCR-ζ and/or FcεRI-γ for CD335 and CD337 or DAP12 for CD336[11]. This interaction is crucial for both NCR surface expression and activation. Here, reduced surface expression of CD335 and CD337 has been linked to the absence of FcεRI-γ expression[11, 18].

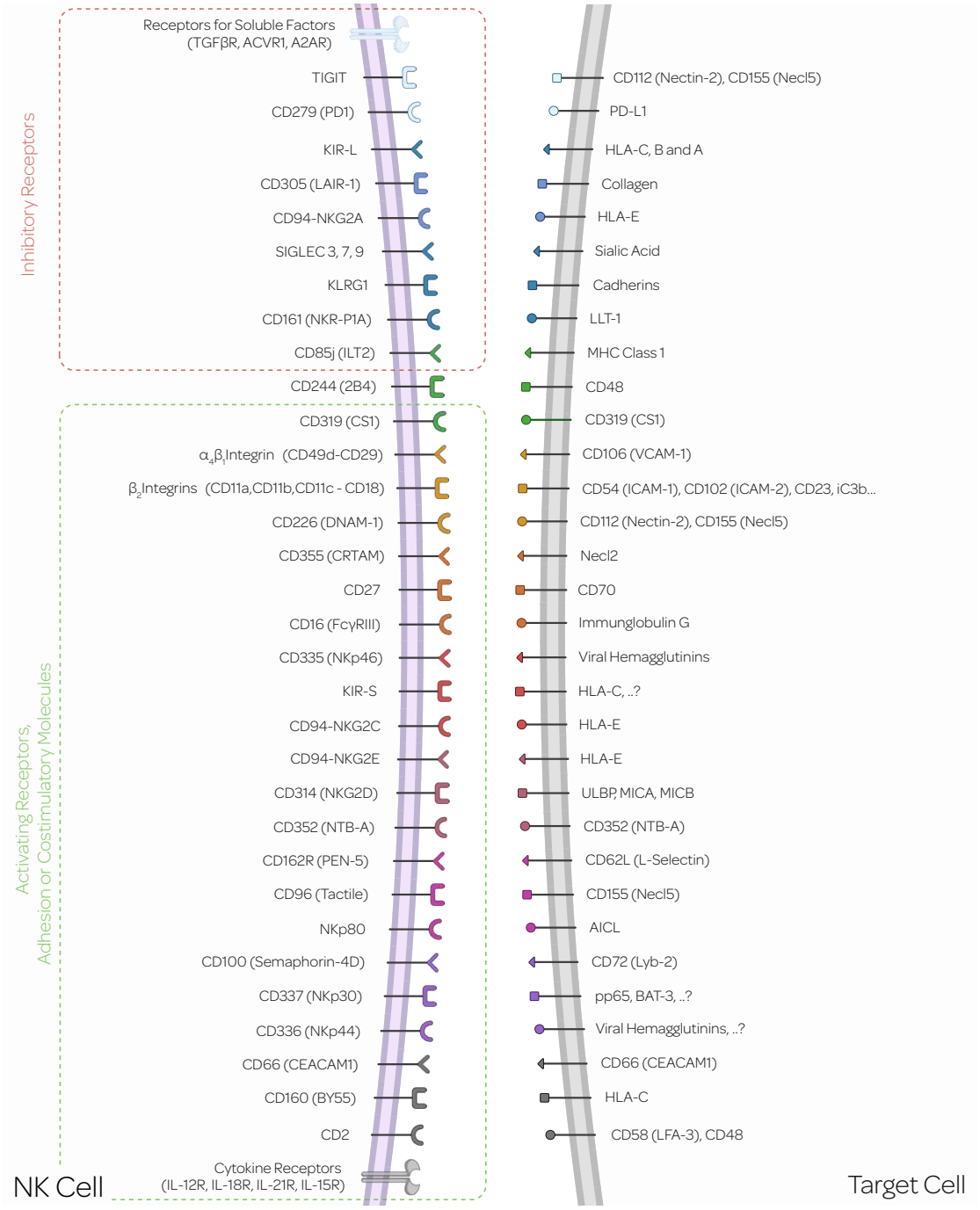

Figure 1.1: Overview of activatory and inhibitory NK-cell receptors. Illustrated is an overview of activating and inhibitory receptors of NK cells and their respective ligands. Notably, CD244, also known as 2B4, can exert both activating and inhibiting signals. This figure was created with Biorender.com and adapted from reference[8, 14].

The extracellular domain of these NCRs interacts with various molecules. For example, CD335 and CD336 recognize viral hemagglutinins but can also recognize stress-induced inhibitory signals such as pp65[19]. Other ligands include HLA-B-associated transcript 3 (BAT3), the mixed lineage leukemia 5 (MLL5) protein, and proliferating cell nuclear antigen (PCNA). Some of these ligands are intracellular proteins but translocate to the cell surface under conditions of cellular stress or during tumor formation[11]. Importantly, research has demonstrated that tumors employ mechanisms to impair the function of NCRs. Hypoxia or soluble factors such as transforming growth factor-β (TGF-β)[20], prostaglandin E2[20], or the soluble form of BAT3[21] have been identified as inhibitors of NCR function and expression. Another crucial NK cell receptor is CD314 (NKG2D), which recognizes UL16 binding proteins (ULBPs) and MHC class I chain-related protein A (MICA) or MICB[22]. These structural MHC class I homologs are upregulated post-infection, under stress, or tumor formation[11]. The suppression of CD314 ligand expression has been reported to be a potential mechanism for tumor evasion[11]. CD352 (NTB-A), CD226 (DNAM-1), CD59, NKp80, and CD244 (2B4) are additional co-receptors, mainly amplifying NCR-mediated activating signals[11]. Here, CD244 can generate both inhibitory and activating signals[23, 24]. Finally, NK cells express the Fcγ receptor CD16, recognizing the Fc region of IgG antibodies. This enables NK cells to eradicate antibody-opsonized target cells, a process known as antibody-dependent cell-mediated cytotoxicity (ADCC)[11].

1.1.2 NK-Cell Target Recognition and Elimination

Contrary to T and B cells, NK cells lack the clonogenic receptor formed through gene rearrangement during cell development and maturation[25]. Instead, they are equipped with the germline-encoded activating and inhibitory receptors mentioned above, for constant immune surveillance of potential threats. The sensitive balance between these signals governs NK-cell function, allowing them to distinguish between healthy and abnormal cells[26].

This selective mechanism results in three possible outcomes, illustrated in figure 1.2. The first one is a hallmark of the immune system itself and involves self-tolerance. In the presence of healthy cells that express normal levels of self-MHC class I, NK cells remain inactive, as inhibitory signals counterbalance the activating signals. In contrast, dysregulated MHC class I expression on target cells releases NK cells from inhibitory constraints and triggers target cell lysis. This process is termed as missing self-recognition. Additionally, viral infection or cellular transformation can alter the expression pattern of stress-related ligands, leading to either overexpression or *de novo* expression of activatory ligands. This disruption of the activation balance leads to lysis of the target cell, a phenomenon known as induced self-recognition[27].

NK cells employ two main mechanisms to mediate cellular cytotoxicity and eliminate target cells, as illustrated in figure 1.3. These mechanisms include receptor-mediated induction of apoptosis and the release of lytic granules loaded with granzymes and perforin[28]. Granzymes are a family of serine proteases that are expressed in NK and

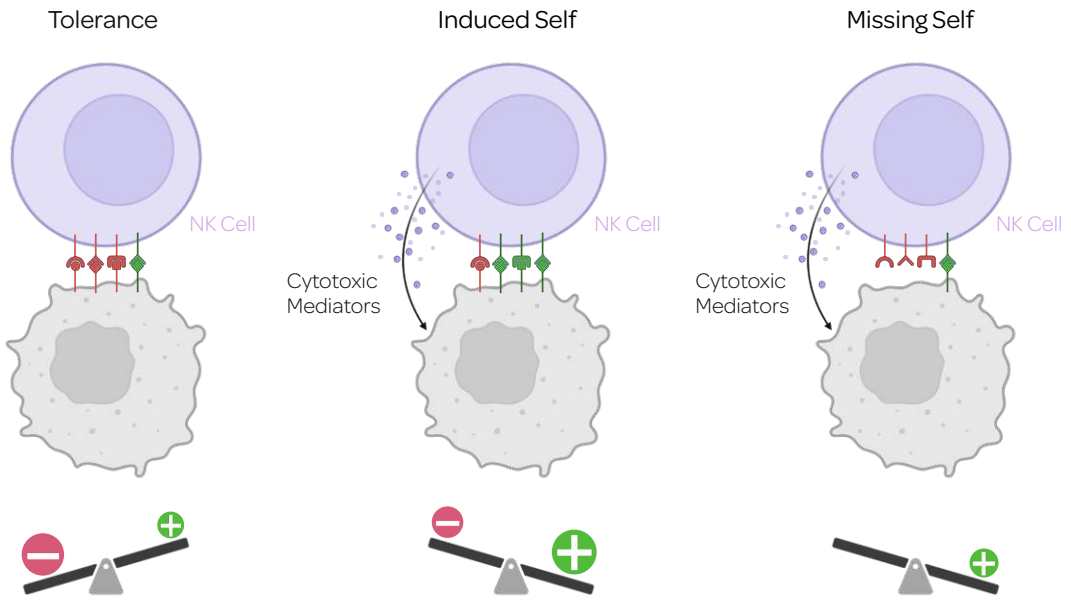

Figure 1.2: Schematic mechanism of NK cell recognition and response. In the presence of healthy cells expressing normal levels of self-MHC class I molecules, NK cells remain inactive and exhibit self-tolerance as inhibitory signals predominate. Conversely, interaction with target cells exhibiting reduced MHC class I expression triggers missing-self recognition, where activating signals become predominant, leading to target cell lysis by releasing cytotoxic mediators. Additionally, the upregulation of stress-induced activatory ligands results in induced self-recognition and target cell lysis. This figure was created with Biorender.com and adapted from reference[26].

cytotoxic T cells, which include five distinct members: granzyme A, B, H, K, and M. Each variant is characterized by its unique substrate specificity and mode of action[28]. Granzyme B is the best-studied variant and is expressed as a zymogen harboring an inhibitory peptide at its N-terminal end. This inactive proenzyme of granzyme B is stored in secretory granules, where it is cleaved by cysteine proteases such as cathepsin C or H and converted into its active form[28]. In the lytic granules, granzymes are co-stored with perforin, a pore-forming protein that facilitates the entry of granzymes into the target cell. Upon entry, granzymes induce cell death through caspase cleavage, caspase-independent pathways (generation of ROS[29], DNA fragmentation[30], nucleophosmin degradation[31]), or cleaving the corresponding Bcl2 homology domain 3-interacting domain death agonist (BID) protein[28]. The proteolytically activated protein tBid subsequently relocates to the mitochondria, where it engages pro-apoptotic factors and thereby disrupts the integrity of the mitochondrial membrane. This disruption leads to the release of pro-apoptotic factors from the mitochondrion, which ultimately leads to the induction of apoptosis and cell death[28].

The second mechanism of cellular-mediated cytotoxicity involves the receptor-mediated induction of cell death via Fas ligand (FasL) and tumor necrosis factor-related apoptosis-

inducing ligand (TRAIL). Both ligands belong to the tumor necrosis factor superfamily and trigger pro-apoptotic programs in the target cell upon engagement with the receptor FAS and TRAIL-R, respectively[28]. Briefly, FasL is translocated to the cell surface through the process of degranulation. Once on the surface, FasL engages its receptor Fas (CD95), which results in receptor oligomerization on the target cell, assembly of the death-inducing signaling complex (DISC), and activation of caspase 8 and 10. This, in turn, induces apoptosis of the target cell. Moreover, FasL on the cell surface can be cleaved by metalloproteases, yielding its soluble form. However, unlike its membrane-bound variant, soluble FasL does not trigger pro-apoptotic programs[28].

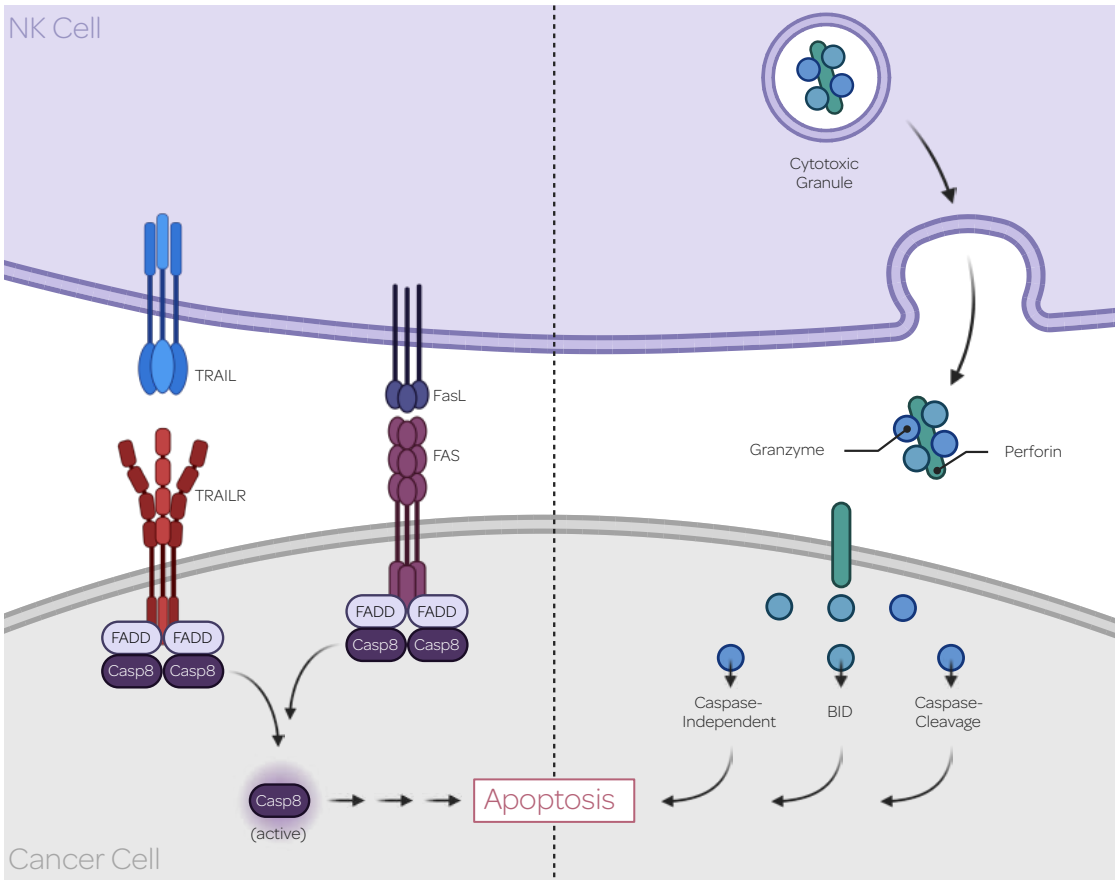

Figure 1.3: Mechanisms of NK cell-mediated cytotoxicity. NK cells employ two mechanisms to lyse abnormal cells: the targeted release of lytic granules (right) and the receptor-mediated induction of apoptosis (left). The latter involves the engagement of FasL or TRAIL with their respective receptors on the target cell that activates pro-apoptotic pathways. This activation leads to the assembly of the DISC complex, which activates caspase 8 or 10, resulting in apoptosis of the target cell. The second pathway involves the release of lytic granules filled with granzymes and perforin. Perforin facilitates the entry of granzymes into the target cell, inducing apoptosis either through caspase cleavage, BID cleavage, or caspase-independent. This figure was created with Biorender.com and adapted from reference[32, 33].

TRAIL is shuttled to the cell membrane with CD107a positive vesicles, where it can bind to one of four different receptors on the target cell. Among these, only TRAIL-R1 and

TRAIL-R2 facilitate the assembly of the DISC complex, thereby triggering apoptosis through caspase 8 activation[28]. This pathway is very similar to FasL-mediated cell death. The remaining receptors activate the NF-κB pathway upon engagement. TRAIL can be cleaved by proteases to generate its soluble form. However, soluble TRAIL retains the ability to induce apoptosis on target cells, even on cells proximal to TRAIL-secreting NK cells[28].

1.2 Principles of Adoptive Cell Therapy

The idea of utilizing the immune system's potential to combat different diseases was recognized early on in the field of personalized medicine. Adoptive cell therapy (ACT) was first described in 1988[34] and gained considerable attention with the development of chimeric antigen receptor (CAR)-T cell therapy to treat hematological malignancies[35]. In contrast to conventional cancer treatments such as chemotherapy or radiation therapy, ACT involves the administration of a living therapeutic agent. This approach involves the administration of either autologous or allogeneic immune cells that are harvested, expanded *ex vivo*, and potentially genetically modified[35]. A variety of cell types and genetic modifications are utilized in ACT. The most important of these include tumor-infiltrating lymphocyte (TIL) therapy, engineered T cell receptor (TCR) therapy, and CAR-T cell therapy. TIL therapy focuses on the *ex vivo* expansion and reinfusion of lymphocytes, capable of penetrating solid tumors, thereby directly attacking cancer cells or recruiting bystander immune cells[36]. In contrast, TCR and CAR T-cell therapy aims to genetically modify T cells to express tumor-specific receptors, that facilite the efficient and specific elimination of tumor cells[36]. Although T-cell-based therapies show promising results and have received U.S. Food and Drug Administration (FDA) approval, they also come with potentially life-threatening side effects, including on-target-off-tumor cytotoxicity, cytokine release syndrome, and neurological complications[36].

1.2.1 NK Cell-Based Immunotherapy

The intrinsic limitations of autologous T-cell therapies, such as challenges associated with individualized autologous cell production, high production costs, and time-intensive manufacturing processes, have intensified the research of NK cell-based therapies[37]. This is mainly due to their improved safety profile, relatively short lifespan, and innate ability to attack cancer cells[37]. NK-based therapies offer an increased safety profile, as clinical studies[38] have revealed that they do not trigger graft-versus-host disease (GvHD) in the allogeneic setting due to the lack of the TCR[39]. Furthermore, NK cells are able to eliminate tumor cells independently of artificial CAR receptors or prior antigen sensitization, utilizing their innate receptors[39]. This is particularly important in the treatment of solid tumors, which are often characterized by antigen heterogeneity and thus evade immune surveillance[39, 40]. Finally, the limited *in vivo* persistence of NK cells can be both an advantage and a disadvantage. On the one hand, the short lifespan facilitates high antitumor activities with minimized long-term consequences of the therapy,

such as cytopenia[37]. On the other hand, it correlates with a short-term clinical benefit, ultimately leading to relapse, which was attributed to the limited persistence of NK cells[41]. In contrast, the superior persistence of CAR-T cells for several months up to years has been recognized as a key factor for sustained therapeutic responses[42]. In addition, NK cells can eliminate cancer cells opsonized by antibodies through the expressed CD16 receptor. This mechanism, known as ADCC, highlights the synergistic potential between NK cells and tumor-specific monoclonal antibodies in cancer therapy. For example, NK cell-mediated ADCC is proposed to improve the efficacy of therapeutic antibodies such as the CD20-targeting monoclonal antibody rituximab in leukemia treatment[42, 43].

NK cells can be obtained from peripheral blood, cord blood, immortalized cell lines, or differentiated from haematopoietic stem and progenitor cells (HSPCs) or induced pluripotent stem cells (iPSCs). Each source offers clinically reasonable cell doses; however, each source comes with distinct advantages and drawbacks[44]. Generally, these doses range from 1-10 $\cdot$ 10^7 NK cells per kg, which has been shown to be an effective and safe dose in clinical trials. However, given their limited *in vivo* lifespan, repeated administrations are necessary, with regimens of 1-4 $\cdot$ 10^7 NK cells per kg infused three times a week[45].

The different sources of NK cells vary not only in yield but also in phenotypic and functional properties. Cord blood-derived NK cells are characterized by high proliferative potential and good accessibility due to cord blood banks, but require long *ex vivo* expansion times (2 weeks) and come with donor-to-donor variability[44]. NK cells from iPSCs are also characterized by high proliferative capacity and produce a homogeneous cell product. However, they exhibit an immature phenotype and require genetic manipulation for CD16-mediated ADCC and extensive culture conditions[44]. Peripheral blood NK cells, in contrast, are characterized by high cytotoxicity, functionality, and a mature phenotype, but require high *ex vivo* expansion rates and suffer from donor-to-donor variability, as well as availability limitations[44].

Clonal NK cell lines such as NK-92, KHYG-1, and YT cells are commonly investigated for their therapeutic potential. However, due to their aneuploid nature, these cell lines are genetically unstable and require irradiation prior to administration to the patient. Irradiated NK-92 cells exhibit a limited *in vivo* persistence of approximately 48 hours, representing a notable disadvantage compared to therapy utilizing primary NK cells in the autologous and allogeneic setting[46].

1.2.2 NK-92 Cells as Therapeutic Agent

NK-92 is a NK cell line that express a large spectrum of activating receptors, with inhibitory receptors limited to CD94/NKG2A and CD85j. Interestingly, inhibition of CD85j does not alter NK-92 cytotoxicity, implying that inhibitory pathways play a minimal role in their cytotoxic function[47]. Remarkably, this cell line lacks most of the receptors of the KIR family, except KIR2DL4, known to inhibit cytotoxicity upon engagement with HLA ligands, thereby preventing functional shutdown upon engagement with unrelated allogeneic cells[48]. NK-92 cells are assigned to the $CD56^{bright}$ phenotype,

which is considered an early and immature stage of NK cell maturation. They highly express various cell adhesion molecules (CD54, CD43, CD48, CD44H) and integrins (CD49d, CD18, CD11a), facilitating effective interaction with tumor cells[49]. Moreover, activating NCRs expressed on NK-92 include CD314, CD337, and CD335, however, they lack CD336[47]. Furthermore, NK-92 cells express elevated levels of granzyme compared to IL-2-dependent blood-derived NK cells, resulting in high cellular cytotoxicity at lower E:T ratios[48]. In addition, NK-92 cells maintain functionality when exposed to the hypoxic tumor microenvironment. Here, oxygen deprivation has been shown to reduce NK cell function[48, 50]. Notably, NK-92 cells also demonstrated superior serial killing abilities compared to blood-derived NK cells[48, 51].

However, the effective use of NK-92 cells in immunotherapy raises two critical questions that need to be clarified. First, given their malignant origin from a patient with lymphoma, there is a potential risk that the recipient develops lymphoma as well[48]. Second, the allogeneic nature of NK-92 cells may lead to their rejection by the patient's immune system[48]. To mitigate the risk of lymphoma development, NK-92 cells are irradiated with 1000-1500 cGy before infusion, effectively stopping their proliferative capacity[48]. In terms of immunogenicity, studies have demonstrated that allogeneic donor T cells do not exhibit increased proliferation or IFN-γ production when exposed to NK-92 cells[48]. Moreover, clinical phase 1 studies have further validated the safety of NK-92 cells in humans[52, 53]. According to a study conducted in Toronto[53], only 6 out of 12 patients developed HLA-specific antibodies after multiple infusions of NK-92 cells[48].

With rapid growth characteristics (T_d = 24-36 h), high cytotoxicity, and easy genetic modification capabilities, the NK-92 platform offers a promising approach to generate off-the-shelf NK cells for ACT[48]. Nevertheless, the requirement for multiple treatments per week, with doses up to $3.2 \cdot 10^9$ NK-92 cells for an 80 kg individual, places considerable demands on the development and control of the process. These cells must be rapidly expanded at high rates, while simultaneously ensuring that quality attributes, such as cytotoxicity, remain consistent.

CHAPTER 2

Aims of my Thesis

The production of therapeutic NK cells currently lacks a defined and standardized process, often involving intensive manual steps. Applying QbD principles is crucial to establishing a standardized framework for GMP-compliant NK-cell manufacturing. This necessitates a profound understanding of the expansion process, particularly the interplay between CQAs and CPPs. Generating detailed time-resolved data is challenging due to the slow growth kinetics of NK-92 cells, resulting in maximized sampling intervals. Nevertheless, obtaining highly time-resolved data is essential for a comprehensive understanding of the NK-cell expansion process.

To overcome these challenges, we employed a pseudo-static cultivation method for NK-92 cells, which was established at the Vienna University of Technology[54]. This approach involved daily sampling and medium replacement for functional assessment and metabolic profiling of NK-92 cells. Given the scope of the practical work, the pseudo-static culture was conducted in collaboration with another student, who also conducted independent analyses for a separate thesis. Although these independent analyses are not included in this thesis, a joint database of the NK-92 pseudo-static experiment was created. This database formed the foundation of at least the fundamental part of this thesis, including nutrient uptake and metabolite release, as well as the cytotoxicity assessment. However, the corresponding data analysis and interpretation were carried out independently.

In the first part of this thesis, the objective was to elucidate the metabolic profile of NK-92 cells. This involved quantifying the biomass, nutrient concentrations, metabolite release, and subsequent rate calculations. The primary objective was to identify the metabolic prerequisites that could affect the growth and functionality of NK-92 cells and to establish a correlation between the observed process parameters and the corresponding quality attributes identified in subsequent parts of this work.

The second part evaluated the process output, specifically by identifying CQAs. To achieve this, the cytotoxicity of cultured NK-92 cells was investigated using three different

methods. This approach not only allowed the assessment of the expected *in vivo* efficacy (i.e., cytotoxicity) of NK cells as CQAs but also facilitated a comparative analysis of the methodologies used to determine this CQA. Additionally, the functionality of NK-92 cells was evaluated by flow cytometry, which involved the study of degranulation and cytokine production when co-cultured with MHC class 1-deficient K-562 target cells. The aim was to identify potential changes induced by the CPPs.

The third part of the thesis extended the flow cytometric analysis of NK-92 cells by a phenotypic characterization. This involved staining cells from the pseudo-static culture with a panel of fluorochrome-conjugated antibodies reactive against functional NK-cell markers and subsequent spectral flow cytometric analysis. This experimental design facilitated the assessment of receptor expression dynamics during the cultivation period, both without and post-stimulation with K-562 cells. The aim was to investigate how the cultivation process affects the phenotypic characteristics of NK-92 cells over time.

CHAPTER 3

Materials and Methods

3.1 Reagents and Consumables

Table 3.1: Reagents and consumables used throughout the experiments

Name	Source	Identifier
3-Mercaptopropionic acid (MPA)	Sigma-Aldrich (St. Louis, MO, USA)	63768-25ML
Acetic acid, 100%	Carl Roth (Karlsruhe, Germany)	6755.3
Acetonitrile, HPLC grade	AppliChem (Darmstadt, Germany)	221881
AdvancedBio AAA UHPLC Guard 3PK	Agilent (Santa Clara, CA, USA)	823750-946
Agilent AdvanceBio AAA LC column	Agilent (Santa Clara, CA, USA)	695975-322
Ala-Gln Bio HT	Roche Diagnostics (Basel, Switzerland)	8056943001
Amino Acid Standard 18AAS	Sigma-Aldrich (St. Louis, MO, USA)	AAS18-5ML
BD Cytofix/Cytoperm	BD Biosciences (Franklin Lakes, NJ, USA)	554714
BD GolgiPlug	BD Biosciences (Franklin Lakes, NJ, USA)	51-2301KZ
BD GolgiStop	BD Biosciences (Franklin Lakes, NJ, USA)	51-2092KZ
Brilliant Stain Buffer	BD Biosciences (Franklin Lakes, NJ, USA)	563794
Calcein AM - Green	Invitrogen (Waltham, MA, USA)	C3100MP
Chromafil RC-20/15 MS	Macherey-Nagel (Düren, Germany)	729036
Dimethyl sulphoxide (DMSO)	Carl Roth (Karlsruhe, Germany)	A994.2
Disodium tetraborate decahydrate	Carl Roth (Karlsruhe, Germany)	T880.1
Fetal bovine serum (FBS)	ATCC (Manassas, VA, USA)	30-2025
Glucose Cedex Bio HT	Roche Diagnostics (Basel, Switzerland)	6608418001
Glutamate V2 Bio HT	Roche Diagnostics (Basel, Switzerland)	7395566001
GlutaMAX™ Supplement	Thermo Fisher Scientific (Waltham, MA, USA)	35050061
Glutamine V2 Bio HT	Roche Diagnostics (Basel, Switzerland)	7395612001
GolgiPlug - Protein Transport Inhibitor	BD Biosciences (Franklin Lakes, NJ, USA)	555029
GolgiStop - Protein Transport Inhibitor	BD Biosciences (Franklin Lakes, NJ, USA)	554724
Human interleukin-2 (IL-2) IS Premium grade	Miltenyi Biotec (Bergisch Gladbach, Germany)	130-097-749
Hydrochloric acid (HCl), 37%	Carl Roth (Karlsruhe, Germany)	9277.3
Iscove's Modified Dulbecco's Medium (IMDM)	Thermo Fisher Scientific (Waltham, MA, USA)	12440046
Ionomycin	Cayman Chemical (Ann Arbor, MI, USA)	10004974
K-562 Cells	ATCC (Manassas, VA, USA)	CCL-243
L-Asparagine monohydrate	Carl Roth (Karlsruhe, Germany)	HN23.1
L-Glutamine	Carl Roth (Karlsruhe, Germany)	HN08.3
L-Tryptophane	TCI Chemicals (Tokyo, Japan)	T0541
Lactate Bio HT	Roche Diagnostics (Basel, Switzerland)	6608485001
LDH Cedex Bio HT	Roche Diagnostics (Basel, Switzerland)	6608493001

Table 3.1: Reagents and consumables used throughout the experiments - continued

Name	Source	Identifier
Live or Dead Fixable Dead Cell Staining Kit	AAT Bioquest (Sunnyvale, USA)	22600
Methanol, HPLC grade	AppliChem (Darmstadt, Germany)	221091
NH3 Bio HT	Roche Diagnostics (Basel, Switzerland)	6608515001
NK-92 Cells	ATCC (Manassas, VA, USA)	CRL-2407
Ortho-phthalaldehyde (OPA)	Sigma-Aldrich (St. Louis, MO, USA)	P0657-1G
Perchloric acid ($HClO_4$), 70%	Carl Roth (Karlsruhe, Germany)	HN51.1
Phorbol-12-myristate-13-acetate (PMA)	Cayman Chemical (Ann Arbor, MI, USA)	10008014
Pyruvate Bio HT	Roche Diagnostics (Basel, Switzerland)	7299818001
Stem Cell Growth Medium (SCGM)	CellGenix (Freiburg, Germany)	20802-0500
Sodium dihydrogen phosphate monohydrate	Carl Roth (Karlsruhe, Germany)	T878.1
Sodium hydroxide (NaOH)	Sigma-Aldrich (St. Louis, MO, USA)	1064691000
UltraComp eBeads™ Plus Compensation Beads	Thermo Fisher Scientific (Waltham, MA, USA)	01-3333-41

Table 3.2: Antibodies used for flow cytometry analysis

Reactivity / Fluorophore	Clone	Source	Identifier	Lot
CD11a - PerCP/Cyanine 5.5	TS2/4	BioLegend (San Diego, CA, USA)	350614	B325240
CD25 - APC/Fire 750	M-A251	BioLegend (San Diego, CA, USA)	356136	B330219
CD49d - Super Bright 600	9F10	Thermo Fisher Scientific (Waltham, MA, USA)	63-0499-42	2308019
CD56 - PE-cF594	NCAM16.2	BD Biosciences (Franklin Lakes, NJ, USA)	564849	2192145
CD69 - BUV737	FN50	Thermo Fisher Scientific (Waltham, MA, USA)	367-0699-42	2560256
CD107a - PE-Cyanine5	eBioH4A3	Thermo Fisher Scientific (Waltham, MA, USA)	15-1079-42	2380466
CD244 - PE	C1.7	BioLegend (San Diego, CA, USA)	329508	B377962
CD314 - BV785	1D11	BioLegend (San Diego, CA, USA)	320830	B367221
CD335 - BV711	9E2	BioLegend (San Diego, CA, USA)	331936	B378731
CD337 - BUV395	p30-15	BD Biosciences (Franklin Lakes, NJ, USA)	743173	3027814
IFN-γ - BV510	B27	BioLegend (San Diego, CA, USA)	506540	B357871
TNF-α - PE-Vio 770	cA2	Miltenyi Biotec (Bergisch Gladbach, Germany)	130-120-492	5221103017
Phosphatidylserine - AF-488	1H6	Merck Millipore (Burlington, VT, USA)	16-256	3849118

3.2 Cell Maintenance

NK-92 and K-562 cells were purchased from the American Type Culture Collection (ATCC). NK-92 cells were cultivated in SCGM medium (CellGenix) supplemented with 5% heat inactivated FBS (ATCC), 2.5 mM GlutaMAX (Thermo Fisher Scientific), 500 IU/mL premium grade IL-2 (Miltenyi Biotec) and maintained between 0.7-1.2 $\cdot 10^6$ cells/mL. The medium was fully exchanged every second day. K-562 cells were maintained in IMDM medium (Thermo Fisher Scientific) supplemented with 10% heat inactivated FBS, and 2.0 mM GlutaMAX. The K-562 cells were split every second day at a ratio of 1:5. All cells were cultivated at 37°C and 5% CO_2 in a humidified atmosphere.

3.3 Pseudo-Static Culture

3.3.1 Culturing Process

In order to investigate the NK-92 cell expansion, including growth, morphology, functionality, and cytotoxicity against K-562 cells, we utilized a pseudo-static cultivation

procedure following the methodology previously described by Aponte et al[54]. The adapted protocol involved daily disruption of cell aggregates, medium replacement, and systematic sampling for a detailed analysis of nutrient and metabolite concentrations, NK-cell phenotype, and functionality. An overview of the daily workflow is illustrated in figure 3.1.

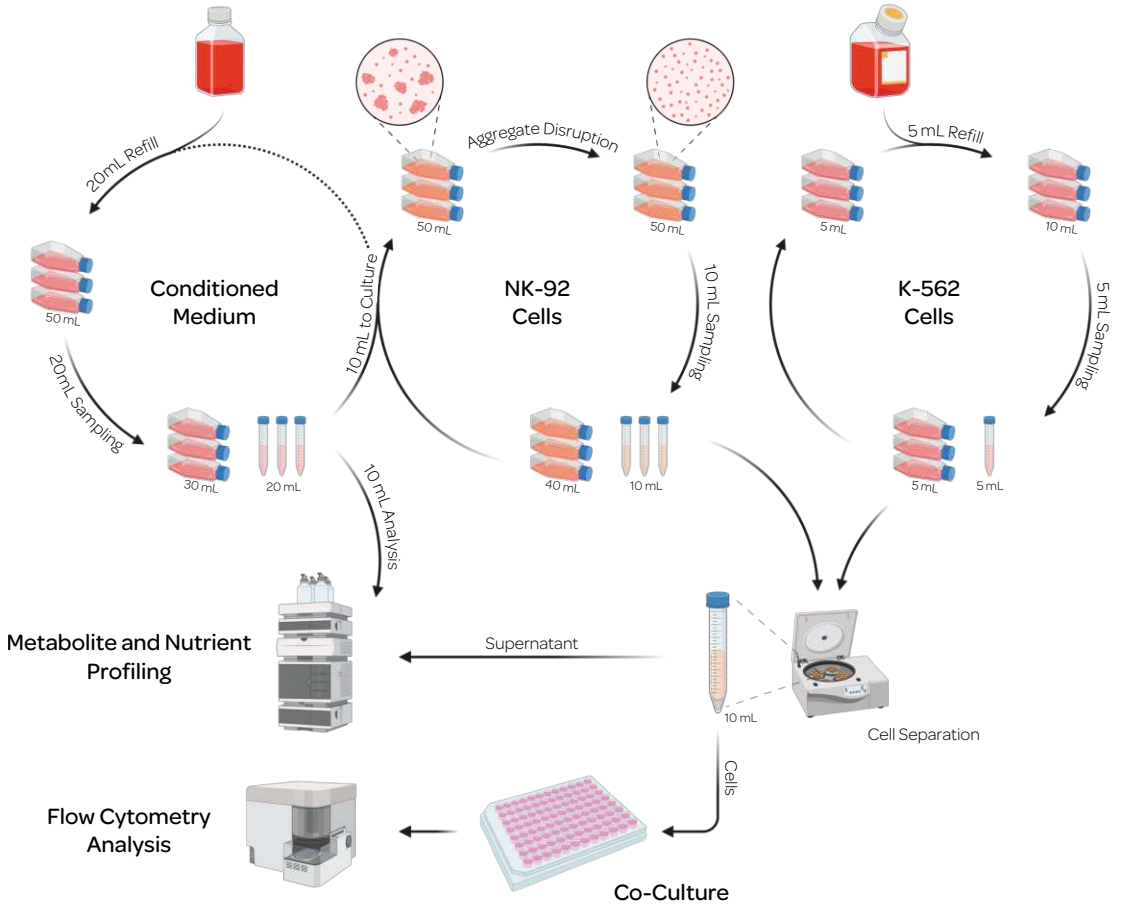

Figure 3.1: Illustration of the pseudo-static cultivation workflow. The NK-92 cells were cultured in triplicates in vented T-175 flasks. The daily routine involved disrupting cell aggregates, replacing the culture medium with conditioned medium, and sampling for nutrient and metabolite analysis, NK-cell phenotype, and functionality assessment. Functionality was determined by conducting cytotoxicity assays using LDH-release, calcein-release, and flow cytometry. Additionally, functional markers and cytokine production were evaluated daily using spectral flow cytometry.

Initially, NK-92 cells were seeded in triplicates into vented T-175 flasks containing 60 mL of SCGM medium, resulting in a final concentration of $1.0 \cdot 10^5$ cells/mL. The corresponding conditioned flasks were filled with 50 mL of SCGM medium. K-562 target cells were seeded in triplicates into 10 mL of IMDM medium, resulting in a final concentration of $2.0 \cdot 10^5$ cells/mL. Phase-contrast images were collected daily to evaluate the general morphological state of the NK-92 culture. However, they were omitted for clarity since they are not part of this thesis. Following the imaging procedure, the culture and conditioned flasks were weighed. Subsequently, 10 mL samples were drawn from all flasks, which included careful disruption of cell aggregates. After the sample collection, the culture and sample flasks were re-weighed to verify accurate liquid handling. To obtain the required K-562 target cells, 5 mL of a single K-562 culture flask was harvested and replenished with 5 mL of fresh IMDM stock medium to maintain the culture volume and cell viability. The collected samples were then centrifuged at 300 g for 5 minutes at room temperature to isolate the cells, which were subsequently utilized for the cytotoxicity assays. The supernatant from the NK-92 culture samples and conditioned flasks was collected, and 300 µL aliquots were used to measure the pH and quantify the concentrations of D-glucose, ammonia, lactate, L-glutamine, L-glutamate, and lactate dehydrogenase (LDH) activity using a Cedex Bio HT instrument (Roche). The remaining supernatant was stored at -20°C until it was subjected to high performance liquid chromatography (HPLC) analysis. To maintain culture volumes, 10 mL of the conditioned medium was transferred to the culture flask (except for day 0) to restore the initial volume. Additionally, IL-2 was added to the NK-92 culture flasks to obtain a final biological activity of 500 IU/mL. The conditioned flasks were replenished with 20 mL of fresh SCGM stock medium, followed by re-incubation of all flasks.

3.3.2 Growth Characteristics and Rate Calculations

To calculate the specific growth rates within the 24-hour sampling intervals, the equation shown in equation (3.1) was used, with the variables defined as follows: μ is the specific growth rate (h^{-1}) within the time interval Δt (h), c_x, t is the viable cell concentration (VCC) (cells/L) at the specific timepoint, and $c_x, 0$ is the initial VCC (cells/L).

$$\mu = \frac{1}{\Delta t} \ln \left(\frac{c_x, t}{c_{x,0}} \right) \tag{3.1}$$

However, to avoid overestimating or underestimating cell growth in longer time frames when using equations applicable to continuous or batch processes, the mean value of two 24-hour intervals was calculated as an approximation using equation (3.2).

$$\mu_{48h} = \frac{\mu_{\text{0-24h}} + \mu_{\text{24-48h}}}{2} \tag{3.2}$$

The volumetric production rates of metabolites were calculated by the general mass balance provided in equation (3.3), with the variables defined as follows: V is the volume

added to the flask or removed by sampling (L), c_i is the concentration of component i (µM), V_R is the reactor volume (L) and r_i is the reaction rate (µM/h).

$$V_{\text{in}}c_{i,\text{in}} + V_{\text{out}}c_{i,\text{out}} + r_i V_R = c_i \frac{\partial V_R}{\partial t} + V_R \frac{\partial c_i}{\partial t} \tag{3.3}$$

In this analysis, it was partially assumed that the concentrations of metabolites and nutrients remained constant in the conditioned flasks. Consequently, most of the rates were calculated using the mean concentrations from the 21 sampling points of the conditioned flask. However, due to time-dependent changes in L-glutamine, total L-glutamine, L-glutamate, L-alanine, pH, and ammonium concentrations in the conditioned flasks caused by the medium composition, the daily value was used for these calculations. After obtaining the volumetric rates, the specific rates were calculated using equation (3.4), with variables as follows: q_i is the specific reaction rate (nmol/10^6cells/h), r_i is the volumetric reaction rate (µM/h) and c_X the viable cell concentration (cells/L). To approximate the VCC in the respective time period, the mean value of the viable cell concentration was calculated. In addition, q_i was calculated per $1.0 \cdot 10^6$ cells to obtain reasonable values.

$$q_i = \frac{r_i}{c_x} \cdot 10^9 \tag{3.4}$$

3.4 Amino Acid Analysis

For precise quantification of primary amino acids in the cell culture supernatant, a HPLC-based approach was utilized. To enhance the resolution and sensitivity of the method, a crucial step involved derivatizing the amino acids with 3-mercaptopropionic acid (MPA) and ortho-phthalaldehyde (OPA). This derivatization process resulted in a product characterized by increased retention during reverse-phase HPLC, attributed to reduced polarity. In addition, this derivatization converts non-fluorescent amino acids into fluorescent isoindole derivatives, as shown in figure 3.2. This derivative is excited at 340 nm and emits fluorescence with a wavelength of 450 nm[55].

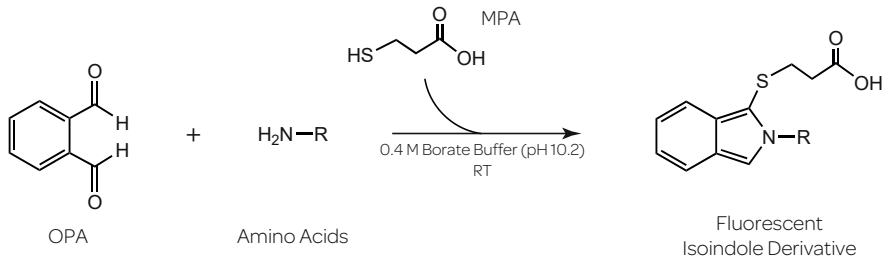

Figure 3.2: Derivatization of primary amino acids with OPA and MPA. The non-fluorescent OPA reacts with primary amino acids in the presence of a free thiol group under basic conditions to form an isoindole derivative. This reaction scheme was adapted from[56].

In this analytical approach, a standard operating procedure was adopted, using an in-needle derivatization routinely employed at the Vienna University of Technology. Initially, the samples obtained from the pseudo-static culture were thawed, and 500 µL was carefully transferred to 1.5 mL tubes. Subsequently, 10.8 µL of 70% (w/w) perchloric acid (final 0.25 mM) was added to the samples to precipitate the proteins, which would reduce the durability of the HPLC column and pre-column, respectively. Following the precipitation, the samples were centrifuged at 14000 g for 10 minutes. The supernatant was filtered through a 0.2 µm cellulose membrane. An aliquot (190 µL) of the deproteinized sample was combined with 10 µL of the internal standard (25 mM L-norvaline in 0.1 M HCl). Furthermore, 1 mL of a 2.5 mM amino acid standard (Sigma-Aldrich) was supplemented with 1 mL of a 2.5 mM pre-dilution of L-asparagine, L-tryptophan, and 5 mM L-glutamine in 0.1 M HCl, to obtain a 1.25 mM extended amino acid analytical standard. This extended standard was serial diluted 1:2, 1:4, 1:10, 1:40, and 1:100 and supplemented with L-norvaline to a final concentration of 1.25 mM. The pre-processed samples (1 µL) were diluted with 5 µL borate buffer (400 mM H_3BO_3 in Milli-Q water, pH 10.2) using an automated injection program. Subsequently, in-needle derivatization was done by drawing 1 µL of the derivatization reagent (37 mM OPA and 115 µM MPA in borate buffer) followed by nine needle pump cycles. The sample was allowed to react for 80 seconds before adding 0.4 µL of 0.1 M acetic acid. The resulting mixture was combined with 32 µL of buffer A, mixed by nine needle pump cycles, and subsequently injected into the column. The derivatized samples were separated by an AdvanceBio AAA column (Agilent) connected to an AdvanceBio AAA guard column (Agilent) on an UltiMate 3000 HPLC instrument (Thermo Fisher Scientific). The column temperature was set to 40°C and the flow rate to 1.2 mL/min. The samples were resolved with a gradient of mobile phase A (10 mM Na_2HPO_4, 10 mM $Na_2B_4O_7$, pH 8.2) and mobile phase B (45% acetonitrile, 45% methanol, 10% water; v/v/v) shown in table 3.3. The amino acid derivatives were excited at 340 nm and detected at 450 nm with an FLD-3400RS detector (Thermo Fisher Scientific). Data analysis was done with Chromeleon software version 7.2.10 (Thermo Fisher Scientific).

Table 3.3: Gradient to resolve the amino acids

Time [min]	-1.0	0.0	0.2	6.8	7.0	9.0	9.0	13
Mobile phase A [%]	98	98	98	43	0	0	98	end
Mobile phase B [%]	2	2	2	57	100	100	2	

3.5 Cytotoxicity Assays

Cytotoxicity assays are fundamental tools in cell biology and pharmacology and represent essential techniques to evaluate the toxic effects of various compounds on viable tissue. One remarkable discovery in this context was the observation that sensitized lymphoid cells can effectively target and destroy cells *in vitro*. This provided the opportunity to

study tumor immunity and investigate the mechanisms of cell-mediated cytolysis. To do so, Brunner et al.[57] developed an assay based on the release of radioactive chromium-51 (^{51}Cr). In this methodology, the target cells were pre-labeled with ^{51}Cr sodium chromate and subsequently exposed to effector cells. Subsequently, the cytolysis-induced release of ^{51}Cr was detected in the supernatant with high sensitivity and reliability[57]. Due to its reproducibility, reliability, and sensitivity, the ^{51}Cr-release assay has long been used to assess cytotoxicity[58]. However, this assay also comes with certain limitations. Specifically, cytotoxicity assays longer than 8 hours may result in the diffusion of ^{51}Cr from viable cells, leading to a high signal-to-noise ratio[58]. In addition, the use of isotopes with short half-live times poses a practical challenge, especially concerning the handling and disposal of the material. Therefore, alternative assays have been described using reporter enzymes, non-radioactive compounds such as 3-(4,5-dimethylthiazol-2-yl)-2,5-diphenyl tetrazolium bromide (MTT), or fluorophores such as calcein, which circumvent the need for radioactive isotopes[59].

3.5.1 Calcein Acetoxymethylester-Release Assay

Calcein acetoxymethyl ester (AM) has emerged as a good choice for cytotoxicity assays due to good retention in target cells. Calcein AM is a non-fluorescent, lipid-soluble derivative of calcein, which can freely diffuse across the cell membrane. Inside the cell, it becomes a substrate for intracellular esterases, which catalyze the hydrolysis of ester bonds, forming the polar, lipid-insoluble, and fluorescent product known as calcein. This newly formed product can no longer diffuse across the cell membrane and is thus metabolically trapped inside the cell. Upon lysis of labeled cells, the entrapped fluorescent calcein is released into the extracellular medium. A representative illustration of the mechanism is provided in figure 3.3[59].

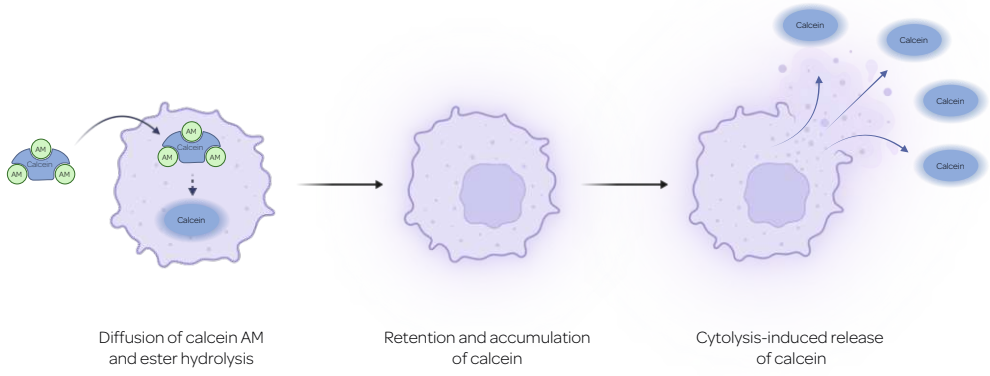

Figure 3.3: Illustration of the mechanism of calcein AM in cytotoxicity assays. Calcein AM is a non-fluorescent, lipid-soluble compound that easily crosses the cell membrane. Inside the cell, it becomes a substrate for intracellular esterases, leading to the hydrolysis of ester bonds. This process yields the polar and fluorescent product calcein, metabolically trapped within the cell. Upon cell lysis, calcein is released into the extracellular medium, enabling the detection in the supernatant. This figure was created with BioRender.com.

K-562 cells ($2.0 \cdot 10^6$) were harvested from one replicate flask and subsequently centrifuged at 300 g for 5 minutes. The supernatant was carefully aspirated, and the cell pellet was resuspended in 200 µL calcein staining solution (15 µM calcein green in serum-free SCGM medium). The cells were stained for 30 minutes at 37°C in the dark. Following incubation, the cells were washed twice with 1xPBS and resuspended in 3.8 mL of serum-free IMDM medium. NK-92 effector cells were harvested in two different quantities: (i) $8.8 \cdot 10^5$ cells for an effector-to-target (E:T) ratio of 1:1, and (ii) $2.2 \cdot 10^6$ cells when sufficient for E:T of 5:1. The effector cells were centrifuged at 300 g for 5 minutes, and the supernatant was discarded. The cell pellet was resuspended in 1518 µL (1:1) or 759 µL (5:1) SCGM medium. The co-culture was set up by combining 115 µL of effector and target cell suspension on a 96-well V-bottom plate. Control wells were prepared with 115 µL of either target or effector cells alone. To maintain a consistent 50/50 (v/v) mixture of IMDM and SCGM medium, control wells were replenished with 115 µL of SCGM or IMDM. K-562-only wells were seeded in duplicates, with one set at the same cell concentration (115 µL) and another set using twice the amount of cells (230 µL).* The loading scheme of the 96-well plate is shown in figure 3.4.

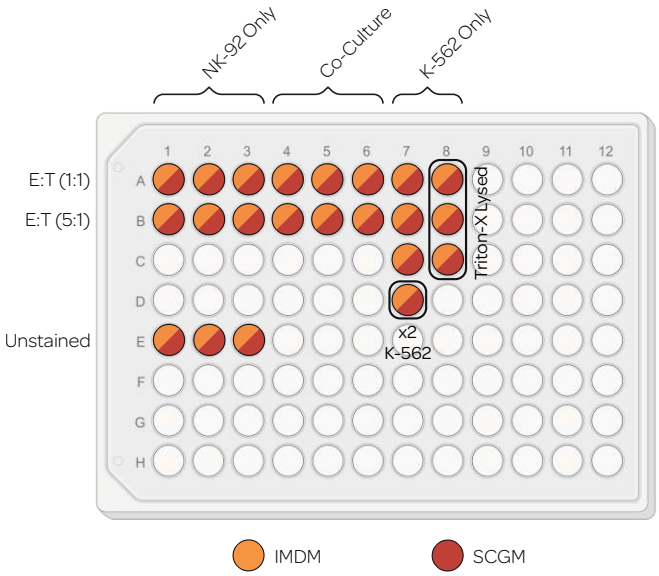

Figure 3.4: Loading scheme for the LDH and calcein-release assay. K-562 cells were stained with calcein AM and combined with NK-92 effector cells at different E:T ratios (1:1 and 5:1). Control wells contained either target ($6.6 \cdot 10^4$ cells) or effector cells ($6.6 \cdot 10^4$ cells) alone. To quantify the total input of calcein and LDH, cells in K-562 control wells were lysed with Triton-X. To remain above the detection limit of calcein and LDH in the spontaneous-release control wells, 2x K-562 ($1.3 \cdot 10^5$ cells) was used as an additional control. Cells in all wells were incubated in a 50/50 (v/v) mixture of SCGM and IMDM medium.

*To ensure the detection of LDH activity in effector-only controls, it is recommended to seed $>6.5 \cdot 10^5$ cells/mL. LDH activity may fall below the detection limit of the Cedex LDH kit if the cell concentration is lower.

The plates were incubated for 3 hours and 15 minutes at 37°C in a humidified atmosphere. Subsequently, 9.2 µL of lysis buffer (5% Triton-X in 1xPBS; v/v) was added, followed by re-incubation for 45 minutes. After incubation, the plate was centrifuged at 300 g for 5 minutes. The supernatant was collected, and 200 µL was transferred to a new 96-well V-bottom plate. The plate was centrifuged at 300 g for 5 minutes to ensure complete cell removal. Subsequently, 150 µL of the supernatant was transferred to a 96-flat bottom plate. The fluorescence of the supernatant was quantified using a Tecan Spark microplate reader instrument. Calcein green was excited at a wavelength of 485 nm, and the corresponding fluorescence was measured at 520 nm. The same supernatant was used to quantify the LDH activity. The specific lysis of K-562 cells was calculated using equation 3.5, with the variables defined as follows: $F_{Calcein}$(Exp.) represents the experimental fluorescence quantified in the supernatant of the co-culture, $F_{Calcein}$(K562, spont.) account for the background or spontaneous release of calcein observed in the K-562 control wells, and $F_{Calcein}$(Total) corresponds to the fluorescence derived from Triton-X lysed K-562 target cells, i.e. the total input of calcein green.

$$\%\ specific\ lysis = \frac{F_{Calcein}\ (Exp.) - F_{Calcein}\ (K562, spont.)}{F_{Calcein}\ (Total) - F_{Calcein}\ (K562, spont.)} \cdot 100 \tag{3.5}$$

3.5.2 Lactate Dehydrogenase-Release Assay

Enzyme release assays, initially described for alkaline phosphatase, encountered limitations when assessing the cytotoxicity of effector cells, as their target cells typically exhibit low levels of alkaline phosphatase. To address this challenge, Carol Korzeniewski and Denis M. Callewaert described a novel assay based on the release of LDH[60]. LDH is a ubiquitous cytosolic enzyme that plays a central role in cellular metabolism by mediating the interconversion of pyruvate and lactate. Upon disruption of the integrity of the cell membrane, LDH is released into the medium, where the enzymatic activity can be reliably quantified. The analytical concept is based on the conversion of lactate to pyruvate, thereby reducing the cofactor nicotinamide adenine dinucleotide (NAD^+) to $NADH/H^+$. The resulting NADH can be quantified using various photometric methods[61].

In this study, the LDH-release assay was coupled with the calcein-release assay, as elaborated in section 3.5.1. A total of 150 µL of the supernatant collected from the co-culture was carefully transferred to 1.5 mL tubes. The LDH activity of the sample was quantified on a Cedex Bio HT instrument (Roche). The specific lysis was calculated using the equation 3.6, with the variables defined as follows: A_{LDH}(Exp.) represents the experimental LDH activity quantified in the supernatant of the co-culture, while A_{LDH}(NK92, spont.) and A_{LDH}(K562, spont.) account for the background or spontaneous LDH-release observed in the control wells. Additionally, A_{LDH}(Total) corresponds to the LDH activity derived from Triton-X lysed K-562 target cells, i.e., the total input of LDH.

$$\%\ specific\ lysis = \frac{A_{LDH}\ (Exp.) - A_{LDH}\ (NK92, spont.) - A_{LDH}\ (K562, spont.)}{A_{LDH}\ (Total) - A_{LDH}\ (K562, spont.)} \cdot 100 \tag{3.6}$$

3.5.3 Flow Cytometry-Based Cytotoxicity Assay

Flow cytometry is a powerful technique for analyzing cells and particles for their physical and chemical properties. A more detailed description and the analysis protocol are provided in section 3.6. The evaluation of cytotoxicity via flow cytometry is based on upregulation of specific markers associated with apoptosis and cell death. Our analytical approach employed reagents compatible with the permeabilization and fixation steps. Specifically, a fixable Alexa Fluor-488-labeled antibody reactive against phosphatidylserine and the fixable amine-reactive dye Live or Dead (LD) with blue fluorescence were used. Viable cells maintain a distinct membrane asymmetry, with different phospholipids segregated into specific leaflets of the cell membrane[62]. Choline-containing phospholipids, such as phosphatidylcholine, are predominantly localized on the outer leaflet, while aminophospholipids like phosphatidylserine (PS) and phosphatidylethanolamine are restricted to the inner leaflet[62]. However, when a cell undergoes apoptosis, the membrane asymmetry is disrupted, leading to the exposure of PS on the outer leaflet of the cell membrane[62]. In this altered state, PS becomes accessible for recognition and binding by specific antibodies or proteins, such as annexin-V. Therefore, analysis of PS surface expression provides a reliable measurement of apoptosis[62]. The gating strategy to obtain the corresponding cytotoxicity values is shown in figure 3.5.

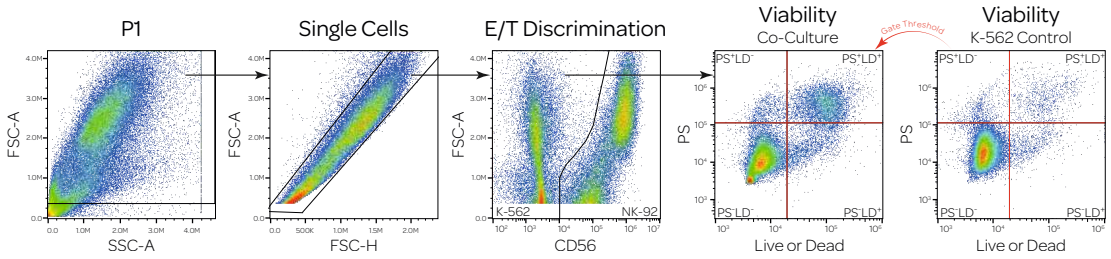

Figure 3.5: Gating strategy to quantify cytotoxicity using flow cytometry. Initially, a P1 gate was defined to include all events except very small debris, based on the area signals of the forward scatter (FSC) and side scatter (SSC). Subsequently, the doublets of these events were excluded by gating on the area and height signals of the forward scatter. The resulting single events were further categorized based on CD56 expression, distinguishing K-562 target cells ($CD56^-$) and NK-92 effector cells ($CD56^+$). Within the K-562 cell population, viability was analyzed by gating on PS and LD. To set the gating thresholds, the K-562-only controls were used and applied to the co-culture samples.

Using this gating strategy, the specific lysis of K-562 cells was calculated using equation 3.7, with the variables defined as follows: $\%_{\mathrm{VC}}$ (K562, spont.) represents the percentage of viable K-562 cells in the K-562 control wells, $\%_{\mathrm{VC}}$ (Exp.) represents the percentage of viable K-562 cells observed in the co-culture. Our analysis identifies viable cells as negative for PS and LD staining (PS^-LD^-).

$$\%\ specific\ lysis = \frac{\%_{VC}\ (K562, spont.) - \%_{VC}\ (Exp.)}{\%_{VC}\ (K562, spont.)} \cdot 100 \tag{3.7}$$

3.6 Flow Cytometry Analysis of NK-Cell Functionality

3.6.1 Basics of Flow Cytometry

Flow cytometry is a single-cell technique that enables the analysis of single cells by evaluating their light scattering and fluorescence patterns. During the analysis, cells are focused within a fluidic stream to ensure separation and individual exposure to one or more laser beams. A detector is positioned either in the path of the laser beam or at an angle of 1 to 2 degrees to measure the light scattering in the forward direction. This forward scatter (FSC) follows the principles of Mie scattering and depends – for spheres – on the particle size. Another detector measures the side scatter (SSC) orthogonal to the laser beam, which provides insights into the internal composition of particles. For example, granulocytes, characterized by their high granularity and intracellular complexity, produce strong side scatter signals[63].

These two non-fluorescent scatter parameters are sufficient to identify distinct subpopulations of leukocytes based on their fundamental morphological characteristics, such as cell size and granularity. However, fluorescence detection is the main strength of flow cytometry and allows the simultaneous examination of multiple intracellular and extracellular markers. Here, the traditional method of using bandpass and dichroic filters in polychromatic flow cytometers has several limitations. It requires assigning a specific bandpass filter to each detector, which limits the number of fluorophores that can be used simultaneously. Additionally, only a fraction of the entire spectrum is captured, resulting in a loss of information. Moreover, the intensity of a fluorophore in the designated bandpass filter section is crucial for an accurate measurement[63].

Spectral flow cytometry emerged as a solution to overcome the challenges posed by traditional flow cytometry in scientific research. This approach measures the entire fluorescence spectrum and analyzes the spectral fingerprint of one fluorophore or the combination of different fluorophores. Here, the fluorescence spectrum is measured using a detector array with up to 64 individual channels as for the Cytek Aurora instrument. Although the intensity of the fluorophores is still important for spectral flow cytometry, the focus shifts to the spectral signature of the fluorophore, eliminating the need for bandpass filters. Furthermore, spectral flow cytometry distinguishes fluorophores with overlapping fluorescence, that faciliate the straightforward use of over 35 fluorophores simultaneously[63].

3.6.2 Workflow for Experimental Flow Cytometry Analysis

The analysis of NK-92 cells by flow cytometry involved the use of two distinct antibody panels. The first panel comprised antibodies targeting the surface markers PS, CD11a, CD25, CD49d, CD56, CD69, CD244, CD314, CD335, CD337, and the viability dye LD. This panel was used to phenotyping NK cells and quantifying NK cell-mediated cytotoxicity. The second panel contained antibodies reactive against the intracellular cytokines TNF-α and IFN-γ, alongside the extracellular markers CD56, PS, CD107a, and

LD. Analysis of the cytokines TNF-α, IFN-γ, and the degranulation marker CD107a, required the addition of protein transport inhibitors (PTI), namely monensin and brefeldin A. However, these inhibitors could affect the expression patterns of surface markers and cell-mediated cytotoxicity. To mitigate this, two separate co-culture plates for each panel were seeded to ensure precise analysis.

Cell seeding was performed simultaneously with the calcein- and LDH-based cytotoxicity assay as indicated in section 3.5.1. K-562 cells ($2.6 \cdot 10^6$) were harvested and centrifuged at 300 g for 5 minutes. The supernatant was carefully aspirated and the cell pellet was resuspended in 4.55 mL of IMDM medium. NK-92 cells were harvested in two different quantities: (i) $8.8 \cdot 10^5$ cells for a 1:1 E:T ratio, and (ii) $2.2 \cdot 10^6$ cells when sufficient for E:T of 5:1. The effector cells were centrifuged at 300 g for 5 minutes and the supernatant was discarded. The cell pellet was resuspended in 1518 µL (1:1) or 759 µL (5:1) SCGM medium. The co-culture was set up by combining 115 µL of effector and target cell suspension on a 96-well V-bottom plate. The control wells were prepared with 115 µL of either target or effector cells alone. To maintain a consistent 50/50 (v/v) mixture of IMDM and SCGM medium, the control wells were replenished with 115 µL of SCGM and IMDM, respectively. As a control, NK-92 cells were activated with 3 µL of a stimulant pre-dilution containing 310 nM phorbol-12-myristate-13-acetate (PMA), and 51 nM ionomycin in SCGM medium. Furthermore, 3 µL of a PTI mix containing 0.16 µL CD107a-PE-Cyanine5 (2.75 µg/mL), 0.20 µL GolgiPlug and 0.13 µL GolgiStop was added to the wells of the cytokine co-culture plate. The co-culture plates were incubated for 4 hours at 37°C in a humidified atmosphere. The loading scheme for the flow cytometry-based cytotoxicity assay is illustrated in figure 3.6

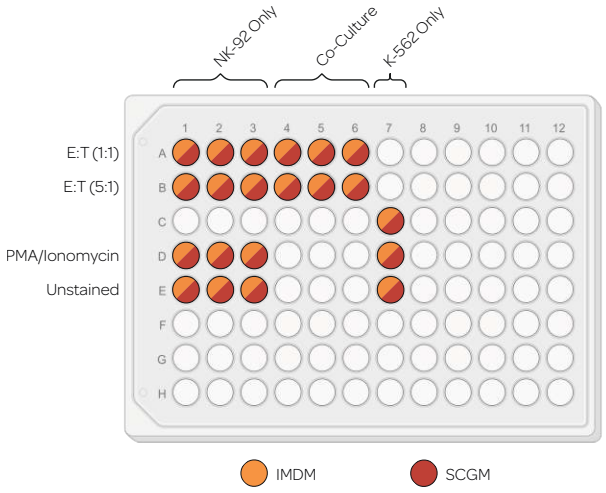

Figure 3.6: Loading scheme for the flow cytometry analysis. K-562 cells were combined with NK-92 effector cells at different E:T ratios (1:1 and 5:1). Control wells contained either target or effector cells alone. As a positive control, cells were activated with PMA and ionomycin. The setup for the surface and cytokine plates was similar, except for the addition of the PTIs monensin and brefeldin A to the cytokine plate to facilitate the analysis of CD107a, TNF-α, and IFN-γ.

After incubation, the plates were centrifuged at 300 g for 5 minutes to pellet the cells. The supernatant was discarded and the cells were washed once with 150 µL of 1xPBS. To evaluate the viability, the cells were resuspended in 25 µL Live or Dead staining solution (0.1 µL Live or Dead in 1xPBS) and stained for 30 minutes at 37°C in the incubator. For treating the unstained controls, 25 µL of 1xPBS was added to the corresponding wells. Afterwards, the cells were washed twice with 150 µL staining buffer (1xPBS supplemented with 1% v/v FBS). For extracellular marker staining, the cell pellet was resuspended in the antibody mix and incubated on ice for 30 minutes.

The corresponding staining mixtures contained: i) 0.05 µL CD56-PE-cF594 (0.11 µg/mL), 0.18 µL PS-Alexa-Fluor-488 (3.59 µg/mL), 0.15 µL CD11a-PerCP/Cyanine-5.5 (0.29 µg/mL), 0.15 µL CD25-APC/Fire-750 (0.59 µg/mL), 0.15 µL CD49d-Super-Bright-600 (0.29 µg/mL), 0.15 µL CD69-BUV737 (0.07 µg/mL), 0.06 µL CD244-PE (0.12 µg/mL), 0.15 µL CD314-BV785 (0.59 µg/mL), 0.15 µL CD335-BV711 (0.59 µg/mL), and 0.52 µL CD337-BUV395 (4.17 µg/mL) in Brilliant Stain Buffer for the phenotyping and cytotoxicity plate and, ii) 0.05 µL CD56-PE-cF594 (0.11 µg/mL), 0.18 µL PS-Alexa-Fluor-488 (3.59 µg/mL) in 1xPBS for the surface stains of the cytokine plate. After staining on ice, the cells were washed twice with 150 µL of staining buffer. Subsequently, the supernatant was removed and the cells were fixed in 100 µL fixation/permeabilization solution (BD Biosciences) containing 4.2% (w/w) formaldehyde on ice for 20 minutes. The plates were centrifuged at 300 g for 5 minutes, and the fixation buffer was discarded. To maintain permeabilization of the cells, the fixed cells were washed twice with 150 µL Wash/Perm buffer. The cell pellets on the phenotyping and cytotoxicity plate were resuspended in 150 µL staining buffer and kept on ice until flow cytometry measurement. Cell pellets from the cytokine plate were resuspended in 25 µL antibody pre-dilution containing 0.12 µL IFN-γ (0.47 µg/mL) and 0.08 µL TNF-α (1:305) in Wash/Perm buffer, and stained on ice for 30 minutes. The stained cells were washed twice with 150 µL Wash/Perm buffer and subsequently resuspended in 150 µL staining buffer. Analysis was done on a Cytek Aurora instrument with SpectroFlo software version 3.0.3. Subsequent data analysis was performed using FlowJo software version 10.9.

3.6.3 Gating Strategy to Evaluate NK-Cell Functionality

The gating strategy used to analyze the phenotype of NK cells and cytokine production is outlined in figure 3.7. This approach follows essentially the same strategy as for the flow cytometry-based quantification of the cytotoxicity. Here, the focus was on the NK-92 cell population, which is subdivided into two distinct subsets based on the FSC properties: a NK-92 subset with high FSC representing healthy NK-92 cells (termed Quali-NK) and an NK cell population with reduced FSC. The total NK-cell population (Total-NK) is obtained by combining both subsets. Dead cells were excluded from both subsets via LD and PS gating. The mean fluorescent intensity (MFI) values of the surface markers from the LD^-PS^- Quali-NK population were calculated and used for subsequent analysis.

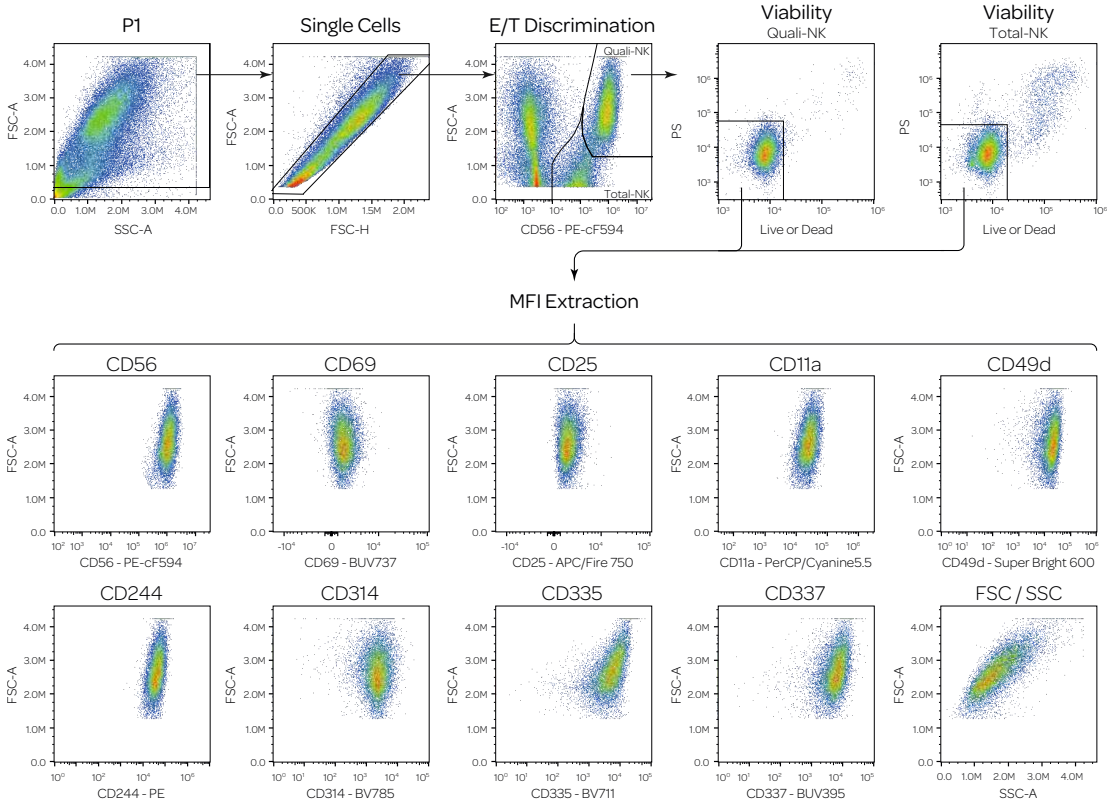

Figure 3.7: Gating strategy to evaluate NK-cell phenotype. Initially, a P1 gate was defined to include all events except very small debris, based on the area signals of the forward scatter and side scatter. Subsequently, the doublets of these events were excluded by gating on the area and height signals of the forward scatter. The remaining single events were further categorized based on CD56 expression. The respective NK-cell population ($CD56^{+}$) was subdivided into a population with high FSC (quali-NK) and a population with a decreased FSC. The combination of both subpopulations is referred to as Total-NK. From these subsets, the viable cells were extracted by LD and PS gating. Ultimately, the MFI of each channel was calculated for the respective viable quali-NK and Total-NK populations and used for subsequent analysis.

The gating strategy used to analyze the cytokine production and degranulation was similar to that used for NK cell phenotyping. Initially, the viable (LD^-PS^-) quali-NK subpopulation was identified according to the strategy depicted in figure 3.7. Within this viable quali-NK subpopulation, degranulated and non-degranulated NK cells were distinguished based on CD107a expression. An unstimulated NK-only control was used as a reference to establish the fluorescence threshold for the gate. Next, a gate was established on the degranulated and non-degranulated subsets to evaluate the production of cytokines using the fluorescence of IFN-γ versus TNF-α. The percentage of cells in the respective quadrant gate (figure 3.8) was used for subsequent calculations. Finally, the corresponding cytokine production levels were calculated using equation (3.8).

$$\%\ cytokine\ expression = \frac{\%_{Cells}\ (\text{Co-Culture}) - \%_{Cells}\ (\text{NK-Control})}{1 - \%_{Cells}\ (\text{NK-Control})} \cdot 100 \qquad (3.8)$$

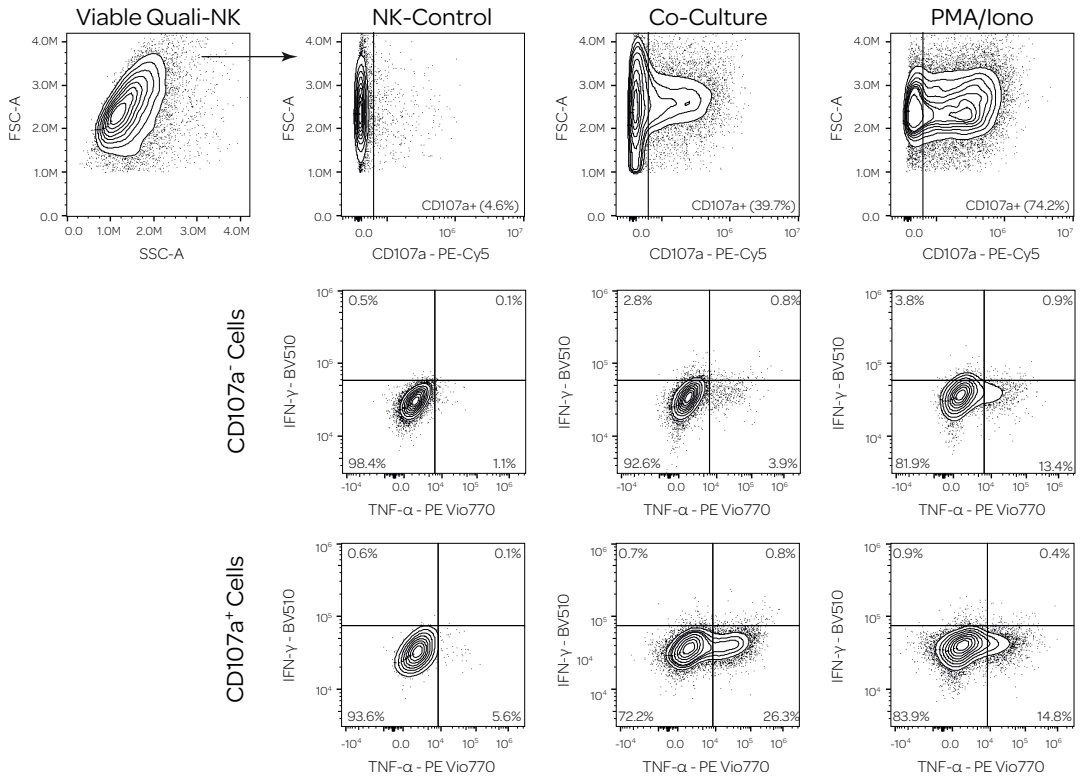

Figure 3.8: Gating strategy to evaluate NK-cell cytokine production. Starting with the viable quali-NK subpopulation (as outlined in figure 3.7), degranulated NK cells ($CD107a^+$) and non-degranulated NK cells ($CD107a^-$) were identified by their CD107a expression. The non-stimulated NK-only control was used as a reference to set the fluorescence threshold for the gate. The gate was adjusted to minimize the percentage of $CD107a^+$ cells in the reference. Following this classification, cytokine production was assessed by applying a quadrant gate for IFN-γ versus TNF-α.

CHAPTER 4

Results and Discussion

4.1 Metabolic Flux of NK-92 Cells

4.1.1 Temporal Dynamics of Nutrient and Metabolite Concentrations

The metabolic activity of immune cells plays a crucial role in driving immune responses. These cells exhibit remarkable metabolic adaptability to fulfill the demands of their biological functions. This study focuses on the expansion process of NK-92 cells and aims to develop a method to generate highly functional NK cells. In this work, NK-92 cells were cultured using a pseudo-static method that involved daily disruption of cell aggregates, medium replacement, and regular sampling to assess nutrient and metabolite concentrations. This approach facilitated close monitoring of the culturing process to identify the general metabolic requirement for the expansion of NK cells. The results of the nutrient analysis are shown in figure 4.1, which depicts the time-resolved concentration data collected at 24-hour intervals. However, every second sampling day was omitted for clarity. On day 8, the viability of the cells decreased, resulting in stagnant viable cell concentration (VCC). Here, the Countess II instrument used for cell counting exhibited insufficient accuracy and precision, affecting the reliability of viability, total cell count, and viable cell count assessments. Notably, the cell count data from the technical replicates displayed a high standard deviation, particularly evident at lower cell concentrations (data not shown).

The process was divided into two distinct phases to streamline subsequent correlation analysis. It is striking that the ammonium concentration reaches its maximum precisely at the phase boundary (day 8), which coincides with a drop in cell viability. All other parameters do not appear limiting, as they continue to decrease in the second process phase. Similarly, inhibitory metabolites, such as lactate, continue to increase in the second phase of the cultivation. These findings align with existing research indicating that ammonium negatively affects the cytotoxicity of NK cells against K-562 target

cells in a concentration-dependent manner after short-term exposure[64]. Specifically, the cytotoxicity of NK cells treated with 3 mM ammonium has already been reduced by 80% compared to untreated cells. However, the ammonium concentration did not influence the viability of NK cells when cultured in ammonium-containing media for 4 hours[64]. Nevertheless, considering the prolonged exposure to 3 mM ammonium during the culturing process, potential toxic effects might impact the viability, growth rate, cytokine production, and cytotoxicity of the NK-92 cells.

The D-glucose concentration gradually decreased until process day 12, ultimately stabilizing at 12 mM. The concentration of the alternative energy source, pyruvate, increased until the phase transition of the cultivation on day 8. Subsequently, the pyruvate concentration reached a plateau shortly after reaching phase 2, except for replicate 3, where the concentration decreased again. This discovery is significant, suggesting that NK-92 cells excrete pyruvate during the exponential growth phase instead of utilizing it.

The time course of the amino acid concentrations varied considerably between the individual amino acids. Concentrations of asparagine (Asp), serine (Ser), glutamine (Gln), arginine (Arg), isoleucine (Ile), and leucine (Leu) decreased significantly, while those of glutamate (Glu), glycine (Gly), and alanine (Ala) increased over time. However, other amino acids showed less consistent patterns, making it difficult to identify clear trends. Interestingly, no limitations were observed during the cultivation process for any monitored nutrient. Nonetheless, very low concentrations of serine and asparagine were found at the end of the process. At the end of phase 2, the concentration of serine and asparagine in the medium had reduced to 17% and 39% of their initial concentrations. These were the only amino acids to fall below half of their initial concentration by the end of the experiment.

The quantification of glutamate and glutamine using HPLC and enzymatic methods resulted in comparable patterns; however, their absolute values differ. It is essential to note that these parameters are influenced by the analytical technique as well as the sampling process. The samples analyzed by enzyme assays on the Cedex Bio HT instrument were measured immediately after sampling, whereas HPLC samples were initially collected and stored at -20°C as outlined in chapter 3. The measurement of glutamine specifically refers to the free glutamine in the medium, which also contains the supplement GlutaMAX. The latter is an L-alanyl-L-glutamine dipeptide, not directly measurable by either HPLC or the standard Cedex Bio HT glutamine kit. Therefore, a separate kit was used that cleaves the dipeptide and quantifies the glutamine. The resulting glutamine + GlutaMAX value is referred to as total glutamine. Furthermore, increasing trends in glutamate, glutamine, and alanine were observed to a lesser extent in the conditioned flask, even in the absence of any cells. Likewise, the pH in the conditioned flask demonstrates a consistent decrease throughout the entire process time (data not shown).

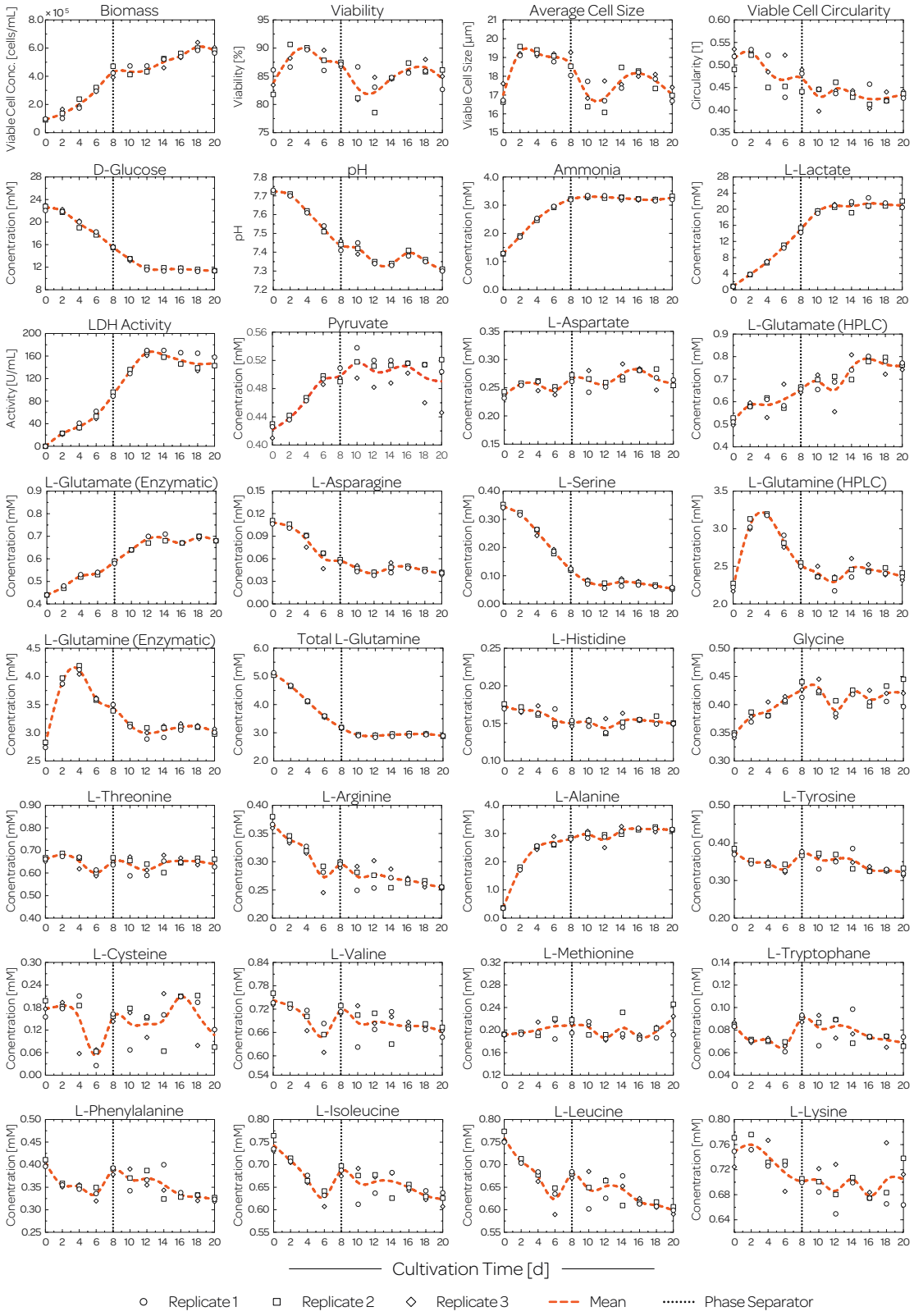

Figure 4.1: Time course of metabolite and nutrient concentrations.

4.1.2 Correlations Analysis of Metabolite and Nutrient Concentrations

To provide an objective and quantitative analysis of the observed visual trends, the Pearson correlation coefficient (P) was calculated for each pair of parameters shown in figure 4.1. This involved calculating the coefficients for the entire process and each specific cultivation phase. The resulting P values are depicted in the matrices shown in figure 4.2 and figure 4.3, respectively. The findings reveal strong correlations between the VCC and specific amino acids such as glutamine, glycine, alanine, asparagine, serine, arginine and leucine throughout the entire cultivation period.

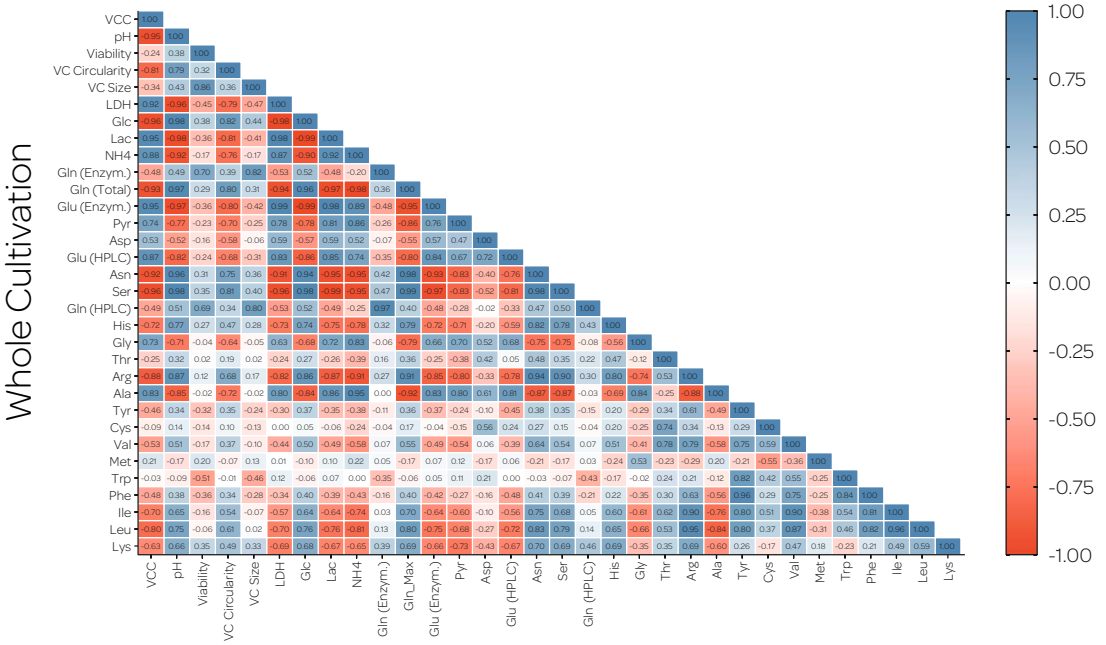

Figure 4.2: Correlation analysis of concentration changes in the cultivation process. Depcited are the Pearson correlation coefficients for all data pairings, comprising the overall process (top) and distinct process phases (bottom). The main diagonal axis of the matrix represents the boundary between the two process phases. The P values were calculated using two-tailed analysis with GraphPad Prism software.

In particular, all of these amino acids, except alanine and glycine, exhibit negative Pearson coefficients, indicating an inverse relationship between their concentration and VCC. The positive correlation for alanine might be attributed to the use of GlutaMAX as a source of glutamine. As mentioned above, GlutaMAX is a dipeptide of L-alanyl-L-glutamine which, upon hydrolysis, releases both glutamine and alanine. This increase is also observed in the conditioned flask, albeit to a much lesser extent. Therefore, it is assumed that the GlutaMAX hydrolysis is not only autocatalytic but also, at least partly, cell-mediated through enzymes or acidification of the medium. However, another possibility for the positive correlation of the alanine concentration could be the metabolism of NK-92 itself.

Alanine can be synthesized from pyruvate via transamination. This reaction results in the formation of α-ketoglutarate, which is subsequently fed into the tricarboxylic acid cycle[65]. A detailed description of the metabolic characteristics of NK cells is outlined in section 4.1.5. Yet, it remains elusive whether alanine originates from GlutaMAX hydrolysis or is produced via metabolic pathways of the NK-92 cells.

One possible approach to address the issue of spontaneous GlutaMAX hydrolysis in the medium is to adjust the alanine or glutamine rate based on the corresponding GlutaMAX hydrolysis rate of the conditioned flasks. However, it is important to note that the samples associated with these rates are not directly comparable due to variations in the sampling procedure. Specifically, different parameters, such as glutamine (enzym.), glutamine (HPLC), glutamine (total), and alanine, were conducted at different time points, i.e., with different numbers of freeze-thaw cycles. Since GlutaMAX has been shown to be sensitive to freeze-thaw cycles, the inclusion of the hydrolysis rate would lead to an overestimation of the corresponding rates.

Strong positive correlations ($P > 0.80$) through the entire cultivation time were observed between the VCC and LDH-activity, ammonium, lactate, and glutamate concentration. In contrast, significant negative correlations ($P < -0.80$) were found between VCC and pH, viable cell circularity, D-glucose, and total glutamine concentration.

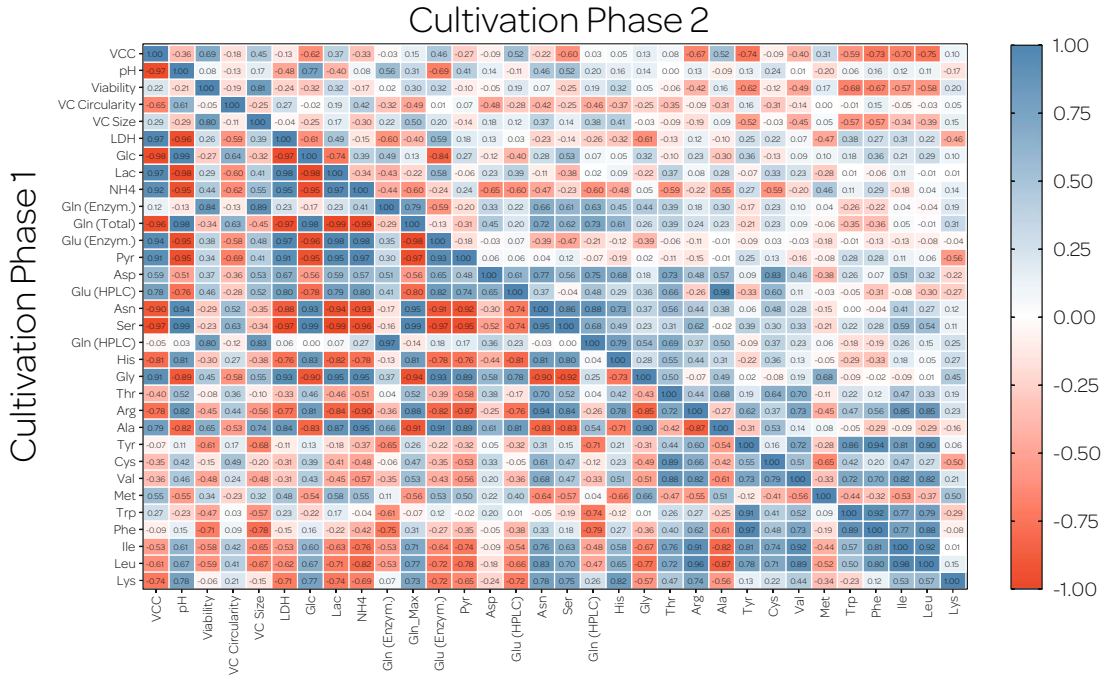

Figure 4.3: Correlation analysis of concentration changes in the process phases. Depcited are the Pearson correlation coefficients for all data pairings, comprising the overall process (top) and distinct process phases (bottom). The main diagonal axis of the matrix represents the boundary between the two process phases. The P values were calculated using two-tailed analysis with GraphPad Prism software.

During cultivation phase 1 which is characterized by elevated cell growth, similar correlations were observed to those in the entire process, although with some variations. For example, a substantial increase in the correlation between the VCC and pyruvate was found in phase 1. This is expected as pyruvate levels stabilize during the second phase of cultivation. Furthermore, it supports the hypothesis that NK-92 cells sustain a different metabolic program in the exponential growth phase, where pyruvate is released into the medium rather than consumed.

Interestingly, during the second cultivation phase, only a small number of strong correlations with the VCC were observed. This can be attributed to the fact that metabolic activity is generally reduced during this phase. However, robust negative correlations ($P < -0.60$) of the VCC with the concentration of glucose, serine, arginine, tyrosine, phenylalanine, leucine and isoleucine were determined.

4.1.3 Metabolic Uptake and Production Rates

Throughout the cultivation process, the culture medium is partly exchanged, biomass accumulates, and culture volume decreases due to media evaporation. Furthermore, the concentrations of glutamate, total glutamine, alanine, and the pH in the conditioned flask change over time, thus also altering the amount of nutrients added to the NK-92 culture flasks. To avoid potential misinterpretations caused by changes in the concentration of nutrients, the volumetric and specific reaction rates, specific growth rate (μ) and the doubling time (T_d) were calculated as shown in figure 4.4 and figure 4.5, respectively.

The initial process phase exhibits significantly higher specific growth rates compared to the subsequent phase. Notable variations in μ among the biological replicates were apparent in the first phase but converged and became more consistent in the second phase. This is attributed to the inaccurate and imprecise counting method. As already mentioned earlier, the error is particularly high for low cell concentrations. To illustrate the growth rate, T_d was calculated, showing an average of approximately 49 hours during the initial culturing phase. However, the second phase of the experiment demonstrates a significant increase in the doubling time to 60 hours.

Due to low basal uptake rates and significant biological variance, volumetric and specific metabolic rates were calculated over 48-hour intervals to improve the signal-to-noise ratio. As volumetric production and uptake rates do not account for biomass growth, it is crucial to focus on the specific rates. These rates normalize the volumetric reaction rates to the cell concentration, providing an interpretable value for the actual consumption and production rates per cell. The corresponding specific rates are shown in figure 4.5.

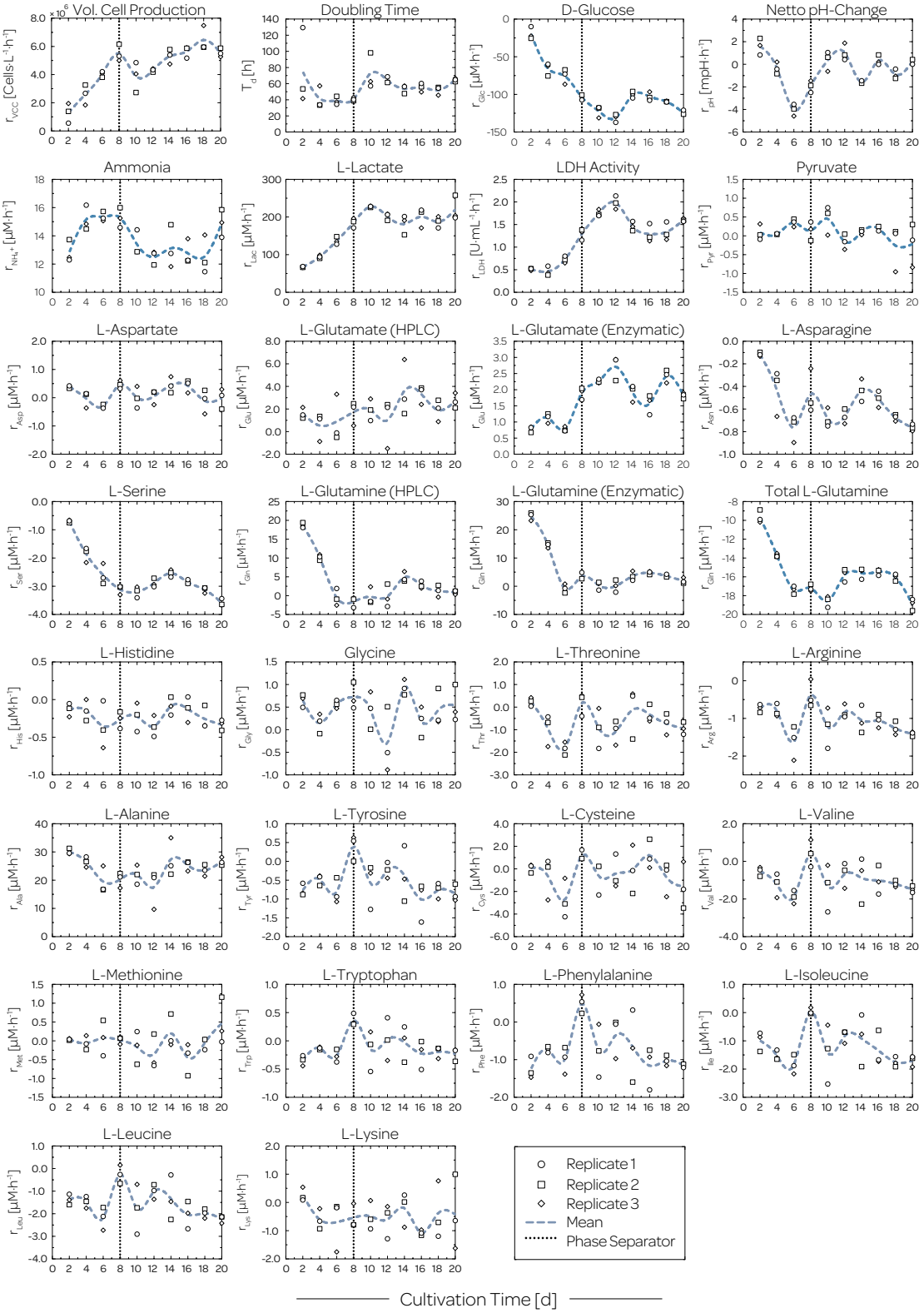

Figure 4.4: Time course of volumetric metabolic reaction rates.

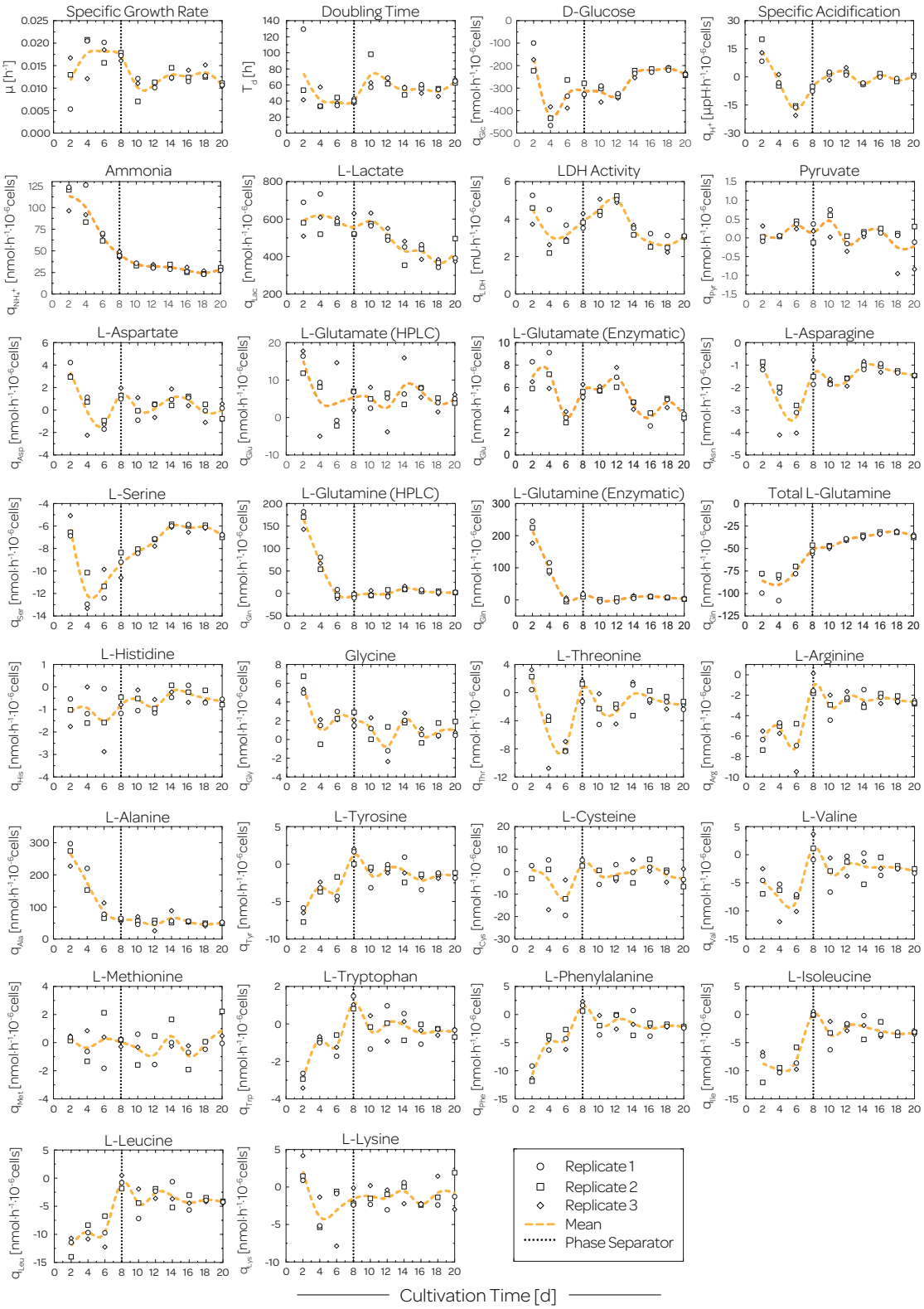

Figure 4.5: Time course of specific metabolic reaction rates.

In the first phase of the experiment, nutrient uptake was significantly higher compared to the second phase, primarily due to exponential cell growth during this period. Concurrently, there was substantial lactate production, suggesting that the cells were using Warburg metabolism.

The availability of ATP is crucial to maintain rapid cell proliferation. As a result, cells utilize kinetically favored anaerobic glycolysis for ATP production over the more efficient but slower oxidative phosphorylation. This metabolic process involves the transformation of cytosolic pyruvate into lactate, which is then released from the cell, a phenomenon recognized as the Warburg effect[66]. The rapid supply of ATP is essential to support the anabolic processes required for cell growth. Furthermore, pyruvate production was observed in the first phase, which supports the hypothesis that the cells undergo Warburg metabolism and bypass oxidative phosphorylation.

In the second phase of the cultivation, the uptake rates of most amino acids remain relatively stable, except glutamate (enzymatic), total glutamine, and serine. This observation is attributed to the substantial decrease in nutrient levels in the medium. Furthermore, a gradual reduction in D-glucose uptake was evident in this phase. Interestingly, after adaptation (days 14-20), cells exhibited lower glucose consumption rates compared to the adaptation phase (days 8-12), despite significantly higher growth rates.

The specific lactate production decreases throughout the entire process, while the specific production rate of ammonium decreases in the first phase but stabilizes from the phase transition until the end of the second phase. The pattern for q_{LDH} is inverse to the cell viability. This is hardly surprising, as LDH is released from damaged, non-viable cells.

Remarkably, the specific rates of most amino acids are negative throughout the cultivation time, except glutamate, glutamine, alanine, and glycine. Consequently, these amino acids are released into the medium instead of being consumed. Nevertheless, glutamine is consumed, as evidenced by the negative rates of total glutamine. The positive rates for glutamine, as measured by both HPLC and enzymatic methods, can be attributed to the release of glutamine from GlutaMAX through the freezing and thawing cycles.

An overview of the minimum, maximum and mean specific rates in each phase and initial medium concentration is presented in table 4.1. In phase 1 and phase 2, the highest specific uptake rates were observed for serine, asparagine, total glutamine, and arginine, in descending order when normalized by their initial concentrations. These findings are further explored and summarized in section 4.1.5, which discusses the utilization of these amino acids by NK cells.

Table 4.1: Overview of the specific rates as well as the initial medium concentration.

Compound	Specific rates [nmol/h/10^6cells]				Concentration [mM]
	q_{max}	q_{min}	$\overline{q}_{i,phase1}$	$\overline{q}_{i,phase2}$	
D-Glucose	-165 ± 50.5	-427 ± 34.1	-308 ± 103	-260 ± 49.8	22.6 ± 0.399
Pyruvate	1.50 ± 0.307	-0.491 ± 0.939	0.710 ± 0.907	0.090 ± 0.868	0.422 ± 0.009
L-Aspartic acid	3.41 ± 0.580	-1.30 ± 0.309	0.850 ± 1.96	0.320 ± 0.778	0.237 ± 0.005
L-Glutamate (HPLC)	15.3 ± 2.52	2.61 ± 4.58	7.17 ± 7.10	5.33 ± 3.72	0.512 ± 0.013
L-Glutamate (Enzym.)	7.41 ± 1.31	3.36 ± 0.539	5.84 ± 1.80	4.80 ± 1.33	0.440 ± 0.000
L-Asparagine	-1.01 ± 0.144	-3.31 ± 0.522	-2.12 ± 1.12	-1.39 ± 0.306	0.108 ± 0.002
L-Serine	-5.98 ± 0.105	-12.1 ± 1.42	-9.72 ± 2.52	-6.78 ± 0.852	0.345 ± 0.006
L-Glutamine (HPLC)	163 ± 16.1	-4.53 ± 8.30	54.7 ± 69.1	4.02 ± 5.55	2.22 ± 0.042
L-Glutamine (Enzym.)	216 ± 28.5	-1.07 ± 2.66	81.6 ± 87.1	4.97 ± 5.24	2.80 ± 0.042
Total L-Glutamine	-31.3 ± 0.619	-90.2 ± 12.5	-75.6 ± 17.1	-37.6 ± 5.60	5.09 ± 0.037
L-Histidine	-0.202 ± 0.220	-1.51 ± 1.15	-1.09 ± 0.774	-0.51 ± 0.350	0.173 ± 0.003
Glycine	5.69 ± 0.767	-0.734 ± 1.54	2.83 ± 1.89	0.83 ± 1.25	0.346 ± 0.004
L-Threonine	1.98 ± 1.17	-7.87 ± 0.643	-2.84 ± 4.60	-1.54 ± 1.59	0.660 ± 0.007
L-Arginine	-1.07 ± 0.862	-7.05 ± 1.92	-4.91 ± 2.59	-2.52 ± 0.655	0.369 ± 0.008
L-Alanine	266 ± 29.2	44.4 ± 13.7	147 ± 84.6	53.0 ± 12.0	0.354 ± 0.008
L-Tyrosine	1.23 ± 0.876	-6.69 ± 0.779	-3.04 ± 2.97	-1.38 ± 1.01	0.377 ± 0.006
L-Cysteine	3.59 ± 1.12	-11.8 ± 6.42	-2.77 ± 8.31	-0.78 ± 3.52	0.177 ± 0.018
L-Valine	1.31 ± 1.86	-8.20 ± 1.34	-4.84 ± 4.34	-2.43 ± 1.71	0.743 ± 0.013
L-Methionine	0.888 ± 0.973	-0.943 ± 0.711	0.060 ± 0.974	-0.170 ± 1.05	0.192 ± 0.001
L-Tryptophan	1.11 ± 0.282	-3.00 ± 0.321	-0.980 ± 1.49	-0.280 ± 0.574	0.085 ± 0.001
L-Phenylalanine	1.55 ± 0.692	-10.8 ± 1.18	-4.61 ± 4.50	-1.84 ± 1.23	0.405 ± 0.006
L-Isoleucine	0.152 ± 0.297	-9.88 ± 0.351	-6.62 ± 4.23	-2.91 ± 1.36	0.743 ± 0.015
L-Leucine	-0.704 ± 0.949	-12.0 ± 1.42	-7.98 ± 4.57	-3.80 ± 1.47	0.759 ± 0.011
L-Lysine	2.18 ± 1.44	-3.96 ± 1.85	-1.61 ± 3.16	-1.17 ± 1.46	0.748 ± 0.019
Lactate	622 ± 88.0	365 ± 17.0	592 ± 67.3	459 ± 83.0	0.857 ± 0.038
Ammonia	113 ± 12.1	24.4 ± 1.72	81.5 ± 29.1	29.6 ± 3.82	1.29 ± 0.009
LDH*	5.06 ± 0.142	2.61 ± 0.376	3.67 ± 0.870	3.58 ± 0.954	0.000 ± 0.000

* LDH is given in [U/h/10^6cells] and [U/L], respectively

4.1.4 Correlations Analysis of Metabolic Rates

The Pearson coefficients for the volumetric and specific metabolic reaction rates were calculated to obtain a statistical value of the metabolic requirements for the growth of NK cells. The correlation matrices are shown in figure 4.6 and figure 4.7, respectively. The correlations observed between the specific growth rate (μ) and the uptake rates were found to be notably lower compared to those between VCC and concentration data. This decreased correlation may be attributed to significant biological variability and a lack of precision and accuracy in the cell counting method. The susceptibility of the Pearson correlation analysis to outliers is a key factor that could result in low values of the correlation analysis.

Throughout the entire cultivation, strong correlations were identified between the average cell size and $q_{Gln(Total)}$ (-0.70) and $q_{NH_4^+}$ (+0.73). Furthermore, $q_{Gln(Total)}$ exhibited strong positive correlations with the VCC (+0.95), q_{Ile} (+0.76), q_{Leu} (+0.76), q_{Arg} (+0.73) and strong negative correlations with VC circularity (-0.76), q_{Lac} (-0.80), q_{Ala} (-0.83), $q_{NH_4^+}$ (-0.95), and $q_{Gln(Enzym.)}$ (-0.71). These findings align with the literature, which reports that dividing cells are larger than non-dividing cells[67]. On average, cultures with fast-proliferating cells contain many dividing cells, thus increasing the

average cell size. Furthermore, these cells require a certain size threshold to divide. In a state of nutrient deficiency, cells maintain this size threshold by slowing down cell cycle progression and, consequently, proliferation[67]. Cell size has also been reported to be correlated with mitochondrial mass, a critical site for lipid biosynthesis of the cell membrane, and other molecules of the energy metabolism[68]. Since mitochondria are the main consumers of oxygen in the cell and are crucial for their functionality, studies on mitochondrial mass, transmembrane potential, and oxygen uptake rate could be beneficial. Hypothetically, oxygen uptake rates could provide information on metabolism and functionality, potentially serving as a soft sensor for process control.

Interestingly, this pattern did not apply to the volumetric rates. As mentioned earlier, volumetric rates are not normalized for biomass and can thus be significantly influenced by cell density. This suggests that these findings are indeed metabolically linked and are not caused by cell density or volumetric effects.

The specific rates q_{Ser} and q_{Glc} exhibited a strong correlation (+0.76) throughout the process, which was consistent with the corresponding volumetric rates. Here, r_{Glc} is also strongly correlated with $r_{Gln(HPLC)}$ (+0.81), $r_{Gln(Enzym.)}$ (+0.86), $r_{Gln(Total)}$ (+0.81), $r_{Glu(Enzym.)}$ (-0.81), and r_{Lac} (-0.92). This suggests that serine is strongly required for cell growth. Hypothetically, serine could be supplemented in addition to or alongside D-glucose in the cultivation process as a potential feeding strategy.

Analyzing each cultivation phase independently reveals consistent correlations both in individual phases and in the overall cultivation process. However, these correlations were more pronounced during the first phase, characterized by rapid growth and increased metabolic activity. Here, a strong negative correlation (-0.72) of q_{Glc} with μ was observed. In the second phase, a decrease in the availability of nutrients leads to reduced cell growth, metabolic activity, and declining correlation coefficients.

According to Monod kinetics, growth depends on the concentration of the substrate (c_S) and the Monod saturation constant (K_S), which represents the affinity of the organism to a specific substrate[69]. This relationship is highly sensitive, particularly when $c_S \approx K_S$. Therefore, if the availability of nutrients decreases in the second phase, this could explain the observed reduction in proliferation, lower metabolic rates, and weaker correlations. Moreover, during the second phase, a steady-state condition is reached where the specific uptake rates remain relatively constant. The observed fluctuations of q_i could result from the addition of fresh medium to the exhausted medium. The resulting variation might explain the low correlations in the second cultivation phase. Nonetheless, q_{Ser} displayed a strong negative correlation with q_{Lac} (-0.90), $q_{NH_4^+}$ (-0.82), and q_{LDH} (-0.80) in the second cultivation phase.

Furthermore, q_{LDH} was found to be strongly correlated with cell viability, which was not evident in phase 1 or throughout the whole process. This finding is expected, as LDH is released into the culture medium only upon cell death, correlating with reduced viability.

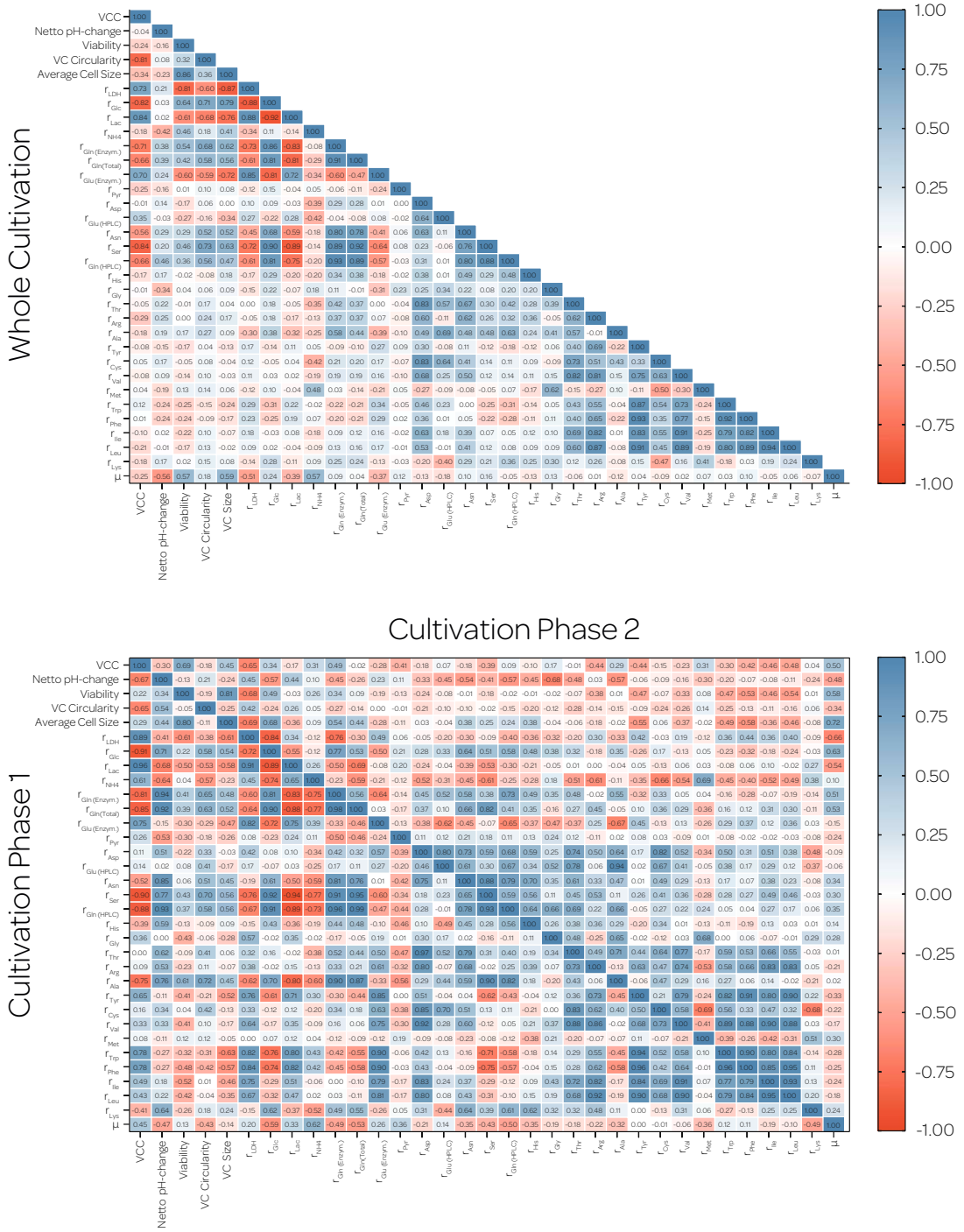

Figure 4.6: Correlation analysis of the volumetric reaction rates. Depcited are the Pearson correlation coefficients for all data pairings, comprising the overall process (top) and distinct process phases (bottom). The main diagonal axis of the matrix represents the boundary between the two process phases. The P values were calculated using two-tailed analysis with GraphPad Prism software.

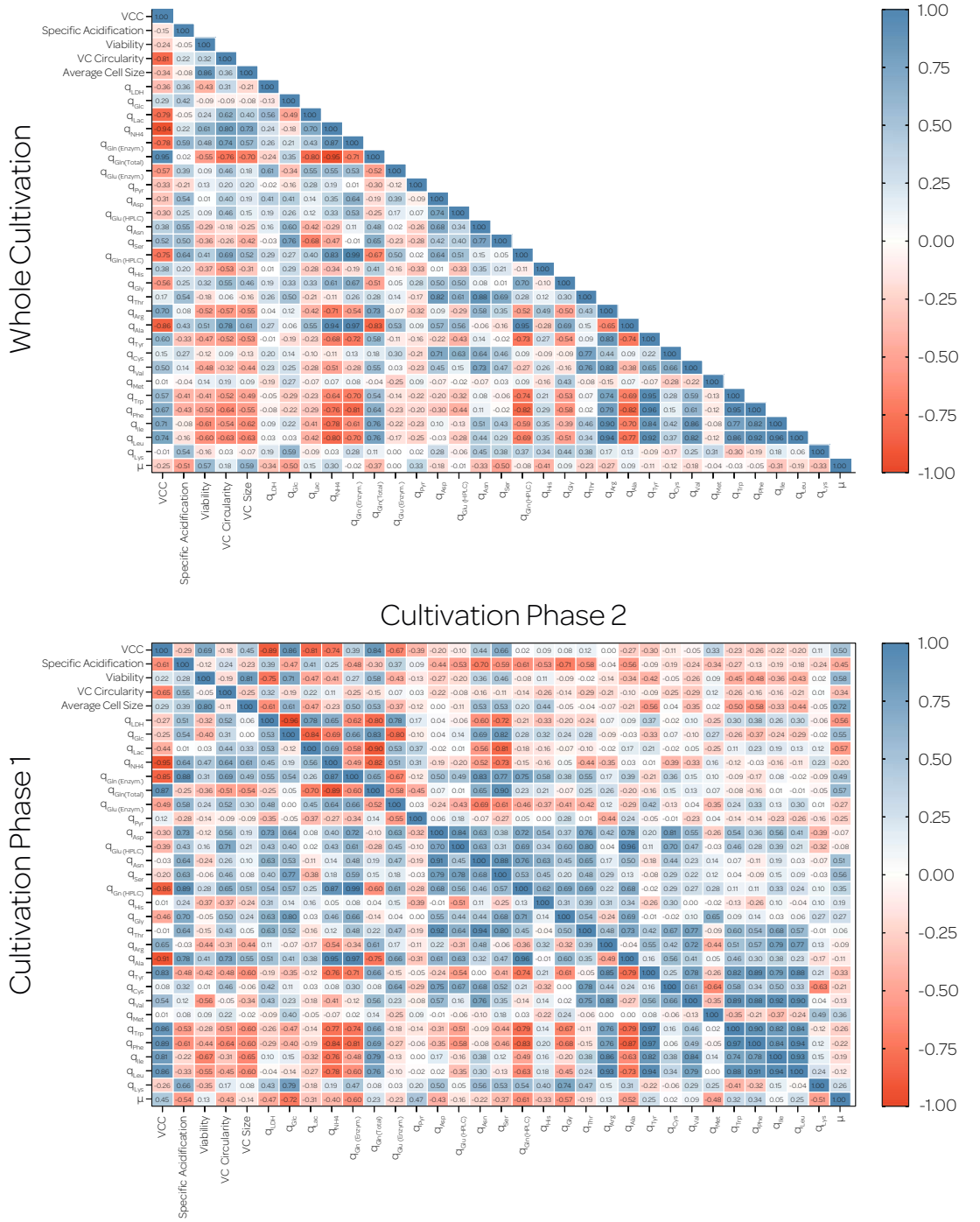

Figure 4.7: Correlation analysis of the specific reaction rates. Depcited are the Pearson correlation coefficients for all data pairings, comprising the overall process (top) and distinct process phases (bottom). The main diagonal axis of the matrix represents the boundary between the two process phases. The P values were calculated using two-tailed analysis with GraphPad Prism software.

4.1.5 NK-92 Cells Display a Clear Metabolic Fingerprint

Figure 4.8 provides an overview of metabolic pathways, illustrating how glucose and amino acids are metabolized in immune cells. This illustration is not intended to be complete, but rather to provide an overview of how nutrients are fueled into different metabolic pathways.

Following glucose uptake, it is converted into pyruvate by glycolytic enzymes. Subsequently, pyruvate is converted into lactate by LDH and is either excreted from the cell or retained within the cytosol. In cytokine-stimulated NK cells, pyruvate is mainly converted into cytosolic citrate, fueling oxidative phosphorylation (OXPHOS) and ATP synthesis via the citrate-malate shuttle (CMS) rather than entering the tricarboxylic acid (TCA) cycle[70, 71]. Citrate, also serve as a precursor for *de novo* lipid biosynthesis, crucial for many aspects of cellular functionality. These processes are regulated by the master regulator sterol regulatory element-binding protein (Srebp), whose activity is essential for NK-cell proliferation, effector function, and maintenance of the CMS[70, 71].

Throughout the cultivation process, a reduction of the specific uptake rate of glucose and other amino acids was observed, accompanied by a decline in NK-92 cell cytotoxicity, particularly their degranulation when co-cultured with K-562 cells (see section 4.3.2). The latter decreases towards the phase boundary, with a brief recovery that does not reach the initial level. This trend supports the hypothesis linking NK-cell functionality to their metabolic activity. Leptin stimulation, for example, has been shown to increase mitochondrial metabolic activity, improve cytotoxicity and expression of the receptors CD335 and CD337 on NK-92 cells[72]. Furthermore, mitochondrial fitness and polarization have been identified as essential prerequisites for NK cell function, emphasizing the importance of cultivating strategies to preserve mitochondrial fitness[73, 74].

Normalized to the initial concentration in the medium, serine is the most heavily consumed amino acid. Unlike glucose, serine is linked to a different metabolic node. Although serine can be metabolized to pyruvate, recent studies have demonstrated that effector T cells predominantly utilize serine for one-carbon metabolism[75]. In this process, the enzyme serine hydroxymethyltransferase (SHMT) transfers a methyl group from serine to the methyl carrier tetrahydrofolate (THF), producing glycine and 5,10-methylene THF (MTHF). The resulting MTHF is then fed into the folate cycle and used for purine and pyrimidine biosynthesis. Furthermore, the folate cycle is linked to the methionine cycle, which yields amino acids, lipids, and S-adenosyl methionine and is also linked to the trans-sulphuration pathway. The latter produces glutathione and thus regulates the redox balance within the cell[75].

Effector T cells and NK cells are two cytotoxic effector cells of the immune system that use lytic granules to eliminate target cells. Although they share some similarities, they differ significantly in terms of sensitivity, specificity, and signaling events upon activation[76]. However, considering the massive consumption of serine and the concomitant production of glycine, it can be hypothesized that NK cells (specifically NK-92 cells) also utilize serine through one-carbon metabolism rather than converting it to pyruvate.

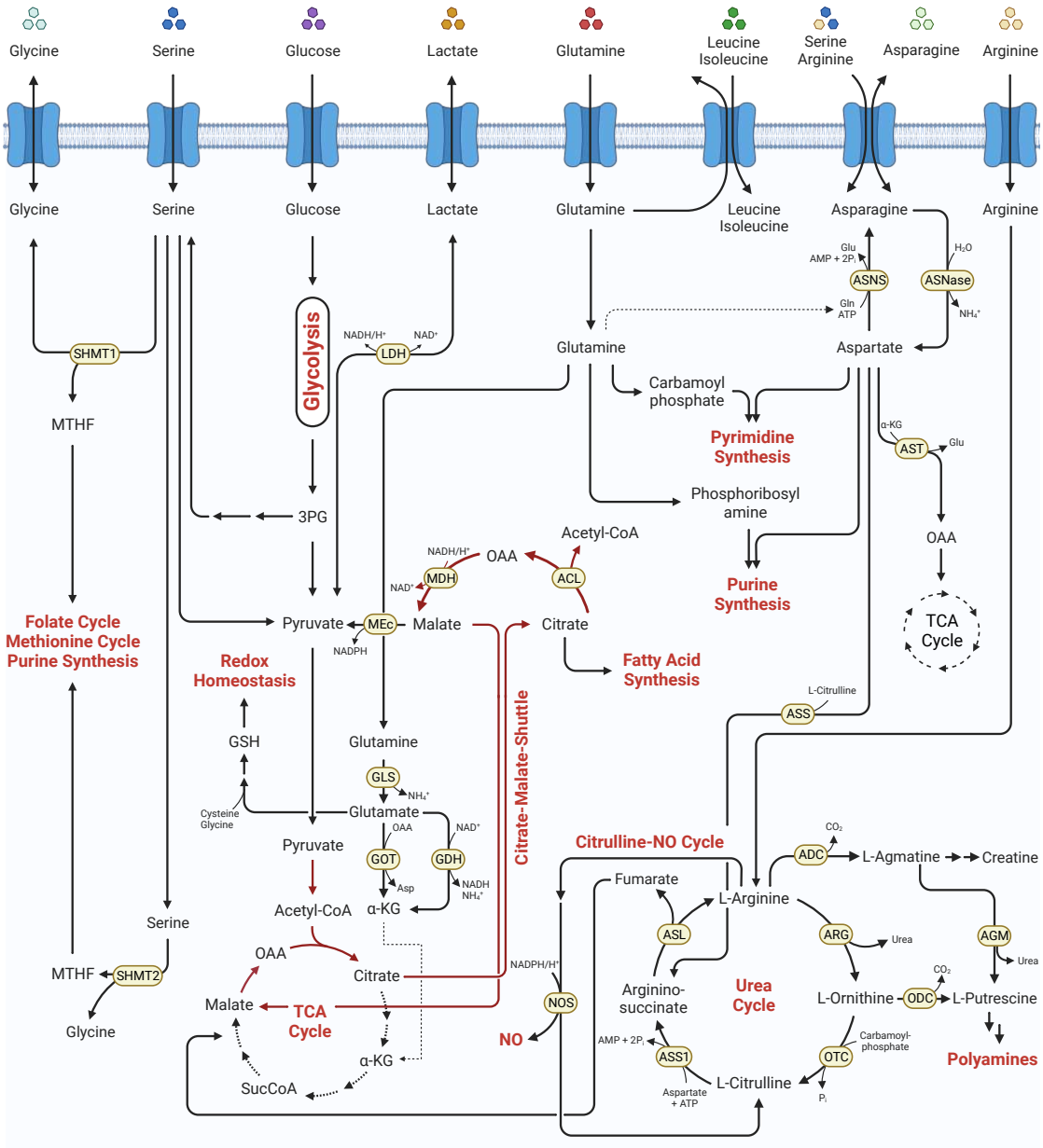

Figure 4.8: Metabolic pathways of NK cells and other immune cells. Abbreviations are: serine hydroxymethyltransferase (SHMT), glutaminase (GLS), asparagine synthetase (ASNS), asparaginase (ASNase), aspartate transaminase (AST), citrate lyase (ACL), malate dehydrogenase (MDH), malic enzyme (MEc), glutaminase (GLS), glutamate oxaloacetate transaminase (GOT), glutamate dehydrogenase (GDH), nitric oxide synthase (NOS), argininosuccinate lyase (ASL), argininosuccinate synthetase 1 (ASS1), ornithine transcarbamylase (OTC), ornithine decarboxylase (ODC), L-arginine amidinohydrolase (ARG), arginine decarboxylase (ADC), agmatinase (AGM). This figure was created with Biorender.com and adapted from [70, 75, 77–83].

Therefore, supplementing cell culture media with nucleosides might relieve the purine and pyrimidine biosynthesis pathway, resulting in enhanced cell growth.

Glutamine is an essential component of energy metabolism and is heavily metabolized, by rapidly proliferating cells. Through glutaminolysis, glutamine converts into glutamate, which then enters the TCA cycle to support energy production. However, the uptake rates of glutamine vary greatly between different cell types. In NK cells, cytokine stimulation upregulates the bidirectional amino acid transporter CD98. This nutrient transporter facilitates the efflux of intracellular glutamine and the import of essential amino acids such as leucine or isoleucine. Subsequently, these amino acids activate mTORC1, a crucial metabolic regulator. Blocking of CD98 inhibits IFN-γ production, highlighting its importance for NK-cell functionality[79]. Interestingly, studies indicate that NK cells incorporate only minimal quantities of glutamine into the TCA cycle via glutaminolysis. Therefore, glutamine only contributes to a minor fraction of total OXPHOS rates. NK cells utilize glutamine primarily as a signaling molecule to regulate cMyc expression. It has been shown that glutamine withdrawal, rather than the inhibition of glutaminolysis, results in cMyc loss, reduced cell growth, and impaired NK-cell functionality[81]. Therefore, it is suggested to reduce glutamine concentration in subsequent experiments. Using 5 mM total glutamine is already twice the standard concentration of 2.5 mM for cell culture applications. Furthermore, a strong correlation was observed between $q_{Gln(total)}$ and $q_{NH_4^+}$ throughout the entire process (P = -0.95), indicating that the generated ammonium in the culture medium is primarily derived from glutamine. Hence, a decrease in glutamine concentration could consequently result in a reduction in ammonia production.

Arginine is also a key player in immune responses. Once internalized, it is metabolized into L-ornithine and urea by intracellular arginases. The resultant L-ornithine is then used to synthesize polyamines, which are essential factors required for mammalian cell proliferation. Altered arginine metabolism correlates with accelerated tumor growth, attributable to the enhanced polyamine synthesis in malignant cells. Moreover, increased arginase activity reduces arginine levels in the tumor microenvironment, facilitating the escape of immunosurveillance. Interestingly, low arginine has been shown to reduce, but not completely suppress, the cytotoxicity of NK cell lines and primary NK cells. Conflicting results regarding the impact of arginine concentration on NK cell cytotoxicity may stem from the use of different cell lines, such as IL-2-dependent and independent variants[84]. Regardless of this, arginine concentration has been shown to influence the surface expression of CD335 and CD337 on NK-92 cells. Specifically, arginine increases the number of receptor-expressing cells but not the receptor density[84]. Similarly, reduced expression of ζ chain, an essential element of downstream signaling, was observed but not replicated for *ex vivo* expanded primary NK cells. This discrepancy might be due to the fact that NK-92 cells express both endothelial and inducible nitric oxide synthase (eNOS and iNOS), whereas primary NK cells solely express eNOS mRNA. Nitric oxide (NO) plays a role in various signaling pathways and is known to inhibit apoptosis in primary NK cells. However, the mechanism by which NO affects ζ chain expression remains elusive[84]. The findings of this study also reveal a notable decrease in CD335 and CD337

surface expression over time. Statistically, the expression of both receptors is lower during the second cultivation phase compared to the initial one (see section 4.3). This suggests that prolonged arginine depletion during continuous cultivation could reduce the surface expression of CD335 and CD337, and consequently NK cell-mediated cytotoxicity.

In $CD8^+$ T cells, asparagine enhances activation and effector function *in vitro* and *in vivo*. Asparagine acts as a signal molecule, binding to lymphocyte-specific protein tyrosine kinase (Lck) and orchestrates the signaling cascade upon activation of the T cell[85]. Conversely, asparagine has been shown to act as an exchange factor for other amino acids, as already demonstrated for glutamine. Diverging from the latter, which is readily utilized upon internalization, asparagine represents a metabolic dead-end metabolite. Therefore, it is a favored exchange factor for importing amino acids, particularly serine, and arginine, which supports mTORC1 activation and protein synthesis[86].

4.2 Assessing the Cytotoxic Activity of NK-92 Cells

4.2.1 Comparison of the Cytotoxicity Methods

Cytotoxicity is a fundamental benchmark to evaluate the functionality of cultured NK-92 cells. To understand the temporal dynamics of the cytotoxic response of NK-92 cells against K-562 target cells, a comparative approach was employed using flow cytometry, LDH-release, and calcein-release assays. Figure 4.9 illustrates time-resolved cytotoxicity profiles against K-562 target cells at E:T ratios of 5:1 and 1:1. The corresponding sampling days are connected by a cubic spline function (dashed line). Substantial deviations were observed between the assays in both E:T ratios. Furthermore, the visual trends differed markedly, especially in the 5:1 ratio. This is also reflected by the low correlation coefficients ($P < 0.7$) among all methods across all E:T ratios (data not shown).

Importantly, the increase in specific lysis rates with increasing E:T ratios was not consistent between the methods. The most substantial difference between 1:1 and 5:1 was observed in the flow cytometry data, decreasing from the LDH-release to the calcein-release assay. The difference between different E:T ratios may indicate that flow cytometry is the most sensitive approach. Specifically, the flow cytometry-based assay showed a noticeable decline in cytotoxicity at the 1:1 ratio, reaching its lowest point on day 6 before showing a slight upward trend until the end of the culturing process. Although less pronounced, the LDH- and calcein-based assays indicate a minimum around the process phase transition.

Interestingly, there was a significant rise in the proportion of necrotic target cells in the second phase compared to the initial phase (figure 4.9b). During the second phase, the specific lysis of K-562 cells was primarily characterized by necrotic cells, whereas late apoptotic cells dominated in the first phase. Hence, it was proposed that while NK-92 cells are capable of perforating target cells, they fail to trigger apoptosis. One potential

explanation for this finding may be a reduction in granzyme expression, while perforin production remains unaltered.

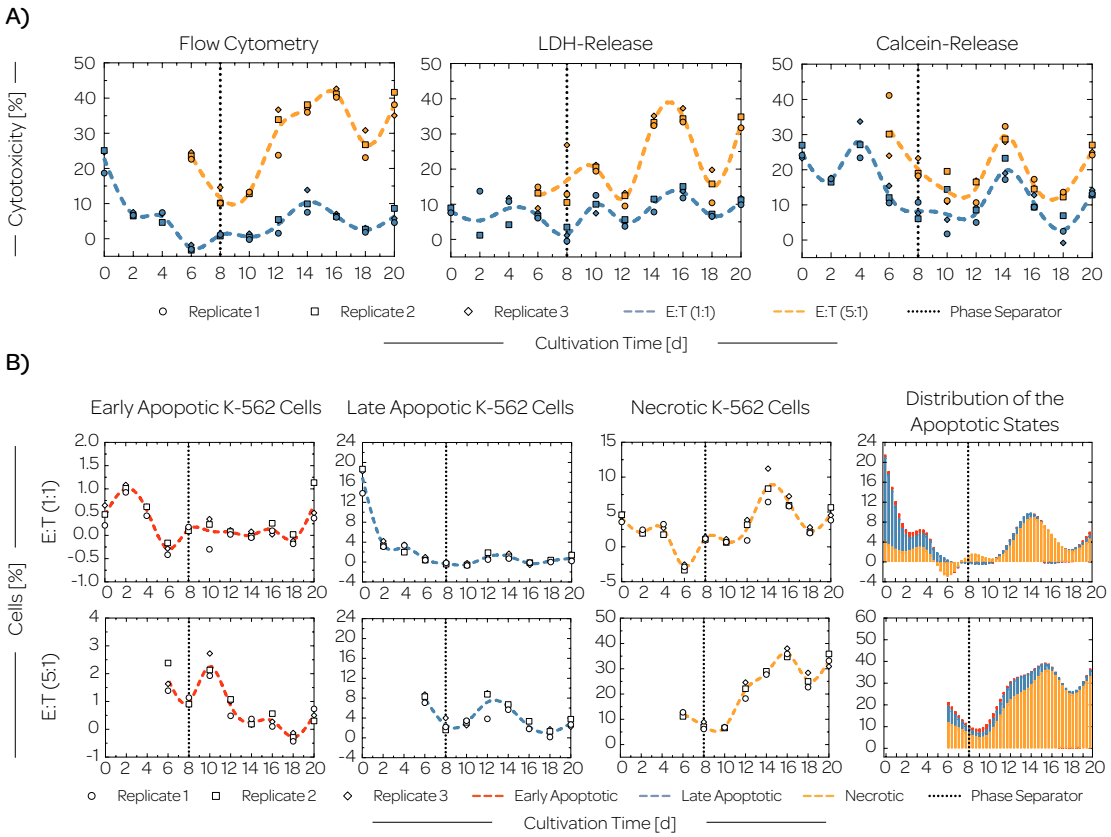

Figure 4.9: Time-resolved comparative cytotoxicity data. NK-92 cells were harvested from the pseudo-static culture and co-cultured daily with K-562 target cells in two distinct E:T ratios for 4 hours and assessed for cytotoxicity via flow cytometry, LDH-release, and calcein-release assay. To improve clarity, the presented data are displayed at 48-hour intervals. A) Data are depicted as biological triplicates, with a cubic spline function (dashed line) connecting corresponding mean values to facilitate comparative cytotoxicity evaluation. B) Depicts the stages of apoptosis of the target cell at an E:T ratio of 1:1 and 5:1 as determined by flow cytometry. Notably, an increase in necrotic cells is observed in the second process phase, while the first phase is primarily characterized by late apoptotic cells.

4.2.2 Statistical Evaluation of NK-Cell Cytotoxicity

In order to demonstrate the variations observed between the cytotoxicity methods, statistical tests were conducted. The values were pooled and analyzed using the Friedman test and Dunn's multiple comparison test. Figure 4.10 illustrates the individual data points, the mean values and the standard deviation. Significant differences in the mean values for the 1:1 ratio were found between all methods. However, only flow cytometry and calcein release exhibited significant differences for the 5:1 ratio. No significant differences were found between LDH- and calcein-release, as well as flow cytometry and LDH-release. However, the cells used for the calcein-release and LDH-release assays were

incubated on a plate different from the one used for flow cytometric analysis. As a result, the comparability of the data is limited to LDH-release and calcein-release. However, it is anticipated that comparable results will be observed in the flow cytometric analysis, as the underlying cell handling and protocol were similar.

The smaller difference in specific lysis rates with increasing E:T ratio, observed in both calcein-release and LDH-release, may suggest a lower test sensitivity. Additionally, a higher cell number for the spontaneous release control was employed to avoid values below the detection limit for fluorescence and LDH activity, respectively. However, this methodology assumes a linear correlation between the spontaneous release of the analyte and the cell concentration, which the findings suggest is not accurate.

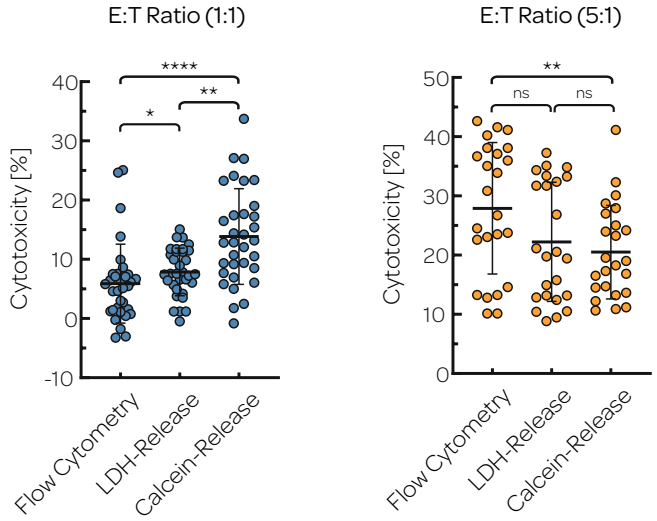

Figure 4.10: Statistical comparison of cytotoxicity methods. To assess the comparability of the cytotoxicity results obtained from the different methods, the respective values of the entire culturing period were pooled and tested using a Friedman test followed by Dunn's multiple comparison test. All methods exhibited significant differences, except for LDH/calcein-release and flow cytometry/LDH-release in the 5:1 ratio. Mean values are represented by horizontal bars with error bars indicating the standard deviation. Statistical significance levels are denoted as follows: ns (not significant, $P > 0.1234$), * ($P < 0.0332$), ** ($P < 0.0021$), *** ($P < 0.0002$), and **** ($P < 0.0001$).

An additional explanation for the observed differences in the lysis rates between the methods could be attributed to the specific timing of cell death. LDH activity is detectable in the supernatant only when the cell membrane is compromised enough to allow the release of LDH. Given its smaller molecular weight, calcein (0.62 kDa) may escape the cell earlier or more rapidly compared to the significantly larger LDH protein (149 kDa). This disparity in molecular size could result in noticeable variations in the observed timing of cell death. This might explain the varying outcomes observed in the different assays. In addition, premature leakage of calcein, in general, could lead to unreliable cytotoxicity results because the measurement is based on the fluorescence of the supernatant. Furthermore, accurate cell separation is crucial to prevent any

contamination with fluorescently labeled cells, which would bias the results. In this study, cells were separated by centrifugation followed by the removal of the supernatant. This method has the potential of cell carryover or cell damage and subsequent calcein release.

During flow cytometric analysis, various markers are examined at single-cell resolution. Here PS exposure is recognized as an early event in apoptosis[87]. Hence, it serves as an appropriate marker to evaluate the cytotoxicity of NK cells.

Furthermore, flow cytometry facilitates the detection of responses in specific cell populations. Within a co-culture of K-562 and NK-92 cells, this capability allows for the isolated observation of effects on K-562 cells alone. In contrast, assays such as LDH- and calcein-release are limited to comparative analysis between the co-culture and its corresponding control. Furthermore, should NK cells undergo self-damage by releasing cytotoxic mediators, these would not be detected with LDH- and calcein-release, potentially leading to biased cytotoxicity results. In contrast, flow cytometry enables a detailed cell population-specific analysis, thereby mitigating the influence of this factor. This might also explain why LDH- and calcein-based assays often report higher cytotoxicity values compared to those obtained by flow cytometry. Thus, flow cytometry is the superior technique for assessing cellular-mediated cytotoxicity.

However, for future experiments, it is recommended to incorporate DNA intercalating dyes such as 7-aminoactinomycin D (7-AAD), propidium iodide (PI), or 4',6-diamidino-2-phenylindol (DAPI) in addition to the PS marker. In this study, the use of the fixable Live-or-Dead Blue dye with its narrow emission spectrum was essential for the multicolor analysis of NK-92 cells, enabling their phenotypic characterization.

4.2.3 Advanced Analysis of the Cytotoxic Activity

In a detailed analysis of the flow cytometry results, the reduction in size of K-562 target cells within the co-culture was measured. This shrinkage was calculated using the MFI of the FSC-A and SSC-A of K-562 target cells in the co-culture relative to the K-562 control. Although the reduction of the MFI is more pronounced for FSC than for SSC, it still reflects the temporal dynamics of the cytotoxicity demonstrated in figure 4.9.

This is particularly evident in the flow cytometry-based method, where both E:T ratios display an $R^2 > 0.500$ for FSC-shrinkage and SSC-shrinkage, respectively. This indicates a strong correlation between the altered scatter properties and specific lysis rates. Furthermore, the flow cytometry data include outliers. Omitting these outliers leads to a substantial increase in the R^2 value. In contrast, alternative methods only achieved $R^2 > 0.500$ for FSC-shrinkage and calcein-release. However, this is expected since the LDH and calcein-release assay was seeded on a separate plate, as mentioned above.

Generally, FSC or SSC shrinkage yields values higher than those of the corresponding evaluation using flow cytometric analysis of viability markers. However, there is agreement between the FSC shrinkage and the marker-based assessment of cytotoxicity. However, it is not recommended to reduce resolution and rely solely on non-fluorescent parameters.

Instead, viability can be determined directly with viability dyes such as 7-AAD, PI, or DAPI immediately after addition. These dyes do not require an incubation period or the use of specialized buffers, which eliminates the need for time-consuming staining protocols.

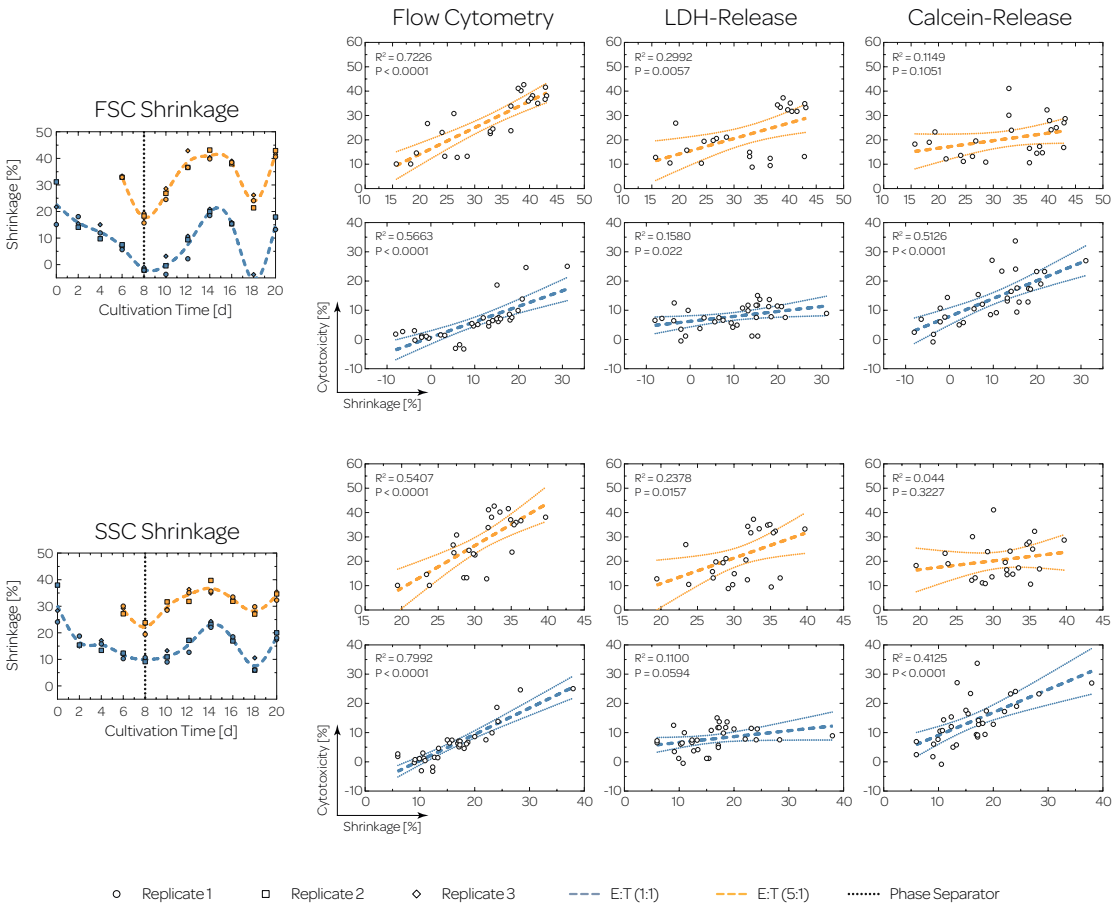

Figure 4.11: Correlation analysis of FSC and SSC shrinkage with specific lysis rates. The advanced analysis of flow cytometric data is depicted, specifically the evaluation of K-562 target cells when co-cultured with NK-92 effector cells. The shrinkage is calculated by comparing the MFI of FSC-A or SSC-A for K-562 in co-culture with the K-562 control (target cells only). Notably, the shrinkage of FSC and SSC strongly correlates with viability marker-based cytotoxicity values obtained by flow cytometry. On the other hand, alternative methods exhibit a weaker correlation with the MFI shrinkage.

4.3 Flow Cytometry-Based Analysis of NK-92 Cells

Flow cytometry-based characterization of NK-92 cells was an essential analytical technique utilized for the pseudo-static culturing experiment. First, we used an antibody panel to investigate various surface markers on NK-92 cells using spectral flow cytometry. Additionally, we employed a second antibody panel to assess the degranulation and cytokine production of NK-92 cells.

4.3.1 NK-92 Cells Develop Toward a Dysfunctional Phenotype

To evaluate the surface expression of functional markers, NK-92 cells were harvested from the pseudo-static culture and co-cultured with K-562 cells for 4 hours. Following the co-culture, the cells were stained with the antibody panel containing fluorescently labeled antibodies reactive against CD56, CD69, CD25, CD11a, CD49d, CD244, CD314, CD335, CD337, PS, and a viability dye. Subsequently, cells were fixed with paraformaldehyde and analyzed on a Cytek Aurora instrument with a 5-laser configuration. The data was analyzed, employing the gating strategy outlined in figure 3.7. The MFI of the viable part of the quali-NK and total-NK populations was calculated and used for further analysis.

The total NK population was omitted for clarity, as trends mirrored those observed in the quali-NK population. The temporal changes of the MFI are depicted in figure 4.12. Furthermore, the fold change in surface marker expression was determined by dividing the individual MFI measured in the quali-NK population from the co-culture by the MFI of the same population in the NK-only control. Interestingly, the surface expression of CD69 and CD25 increases over the cultivation time. However, upregulation of CD69 and CD25 was observed only in phase 1. Conversely, CD11a, CD335, and CD337 showed a visual decrease of the MFI over time, although fold-change values generally remained at approximately 1. This indicates no substantial upregulation of the marker expression. Moreover, periodic fluctuations of the MFI are evident for CD49d, CD335, and CD244.

Remarkably, the MFI from PS experiences a significant increase prior to the phase transition, followed by a continuous decrease until the end of the cultivation process. This is particularly noteworthy as PS^+ and LD^+ cells were excluded from the analysis. Consequently, these observed changes in the MFI correspond to the background expression or basal PS exposure at the cell surface. The mechanisms underlying the exposition of PS at the cell surface are not yet fully understood. However, apoptotic cell death is linked to mitochondrial processes. Depending on the organism, PS exposure occurs either before, during, or after mitochondrial damage[88].

However, basal exposure can indicate mitochondrial stress, as the ability to maintain the membrane asymmetry of the cell is disrupted. This phenomenon might be associated with the mitochondrial transmembrane potential $\Delta\Psi_m$, which is a driving force for OXPHOS[88]. Hence, it is plausible that basal PS exposure could serve as an indicator or soft sensor for NK cell expansion protocols.

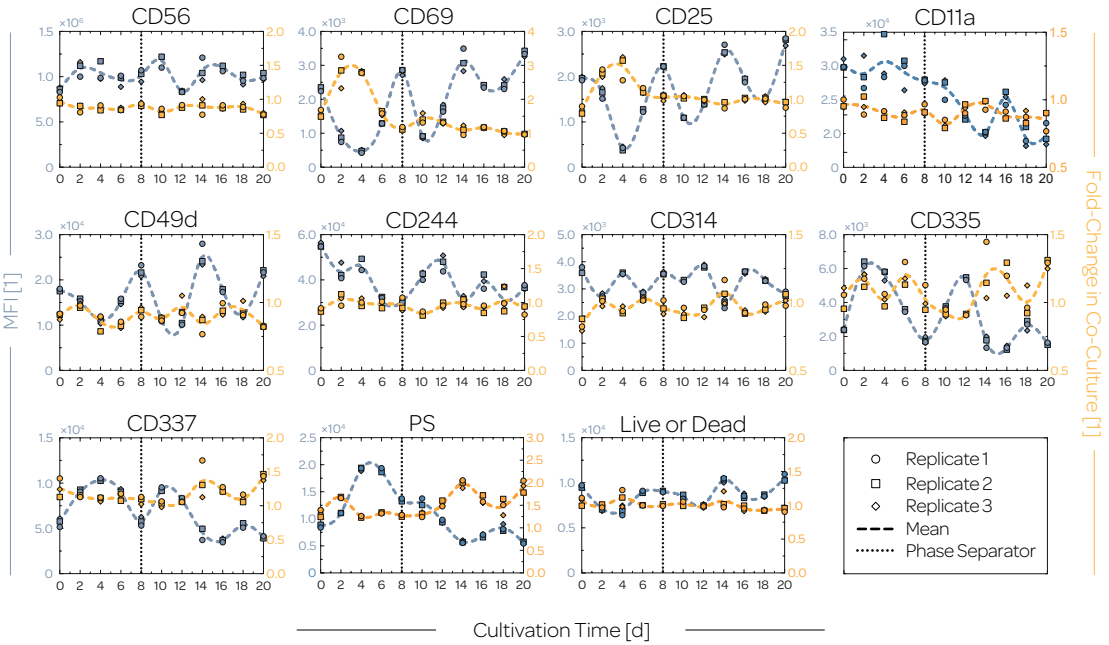

Figure 4.12: Time course of surface marker expression and upregulation. NK-92 cells were harvested from the pseudo-static culture and co-cultured daily with K-562 target cells for 4 hours. Subsequently, the cells were stained with fluorophore-conjugated antibodies reactive against human CD56, CD69, CD25, CD11a, CD49d, CD244, CD314, CD335, CD337, PS, and a viability dye and analyzed by flow cytometry. Surface marker expression is depicted as the MFI of the corresponding fluorophore-labeled antibody in the NK-only samples (blue). The fold-change (yellow) is calculated by dividing the MFI obtained from the co-culture by the corresponding NK-only control. All MFIs were extracted from the viable quali NK population.

Significant changes of the surface expression between cultivation phases 1 and 2 are evident for CD69, CD11a, CD244, CD335, CD337, and PS, as illustrated in figure 4.13. The decreased expression of CD335 and CD337 may result from the absence of FcεRI-γ and/or TCR-ζ expression. In particular, studies indicate that arginine deficiency can lead to a reduction in TCR-ζ expression[89]. Furthermore, the study revealed that CD69 and CD25 are substantially more upregulated in the first cultivation phase compared to phase 2, as shown in figure 4.14. The findings demonstrate a significant increase in PS upregulation on NK-92 cells during the second culturing phase when co-cultured with K-562 cells. This could indicate a dysfunctional phenotype, as activating NK-92 cells in the co-culture leads to increased apoptotic programs instead of target cell lysis.

The expression of CD11a showed a profound decrease over the cultivation time. Effective target cell lysis by NK cells relies on the polarization and degranulation of lytic granules, which is regulated by a variety of signals and receptors. The formation of an immunological synapse is an early and crucial event of NK-mediated cytotoxicity. This synapse is a specialized junction between the effector and the target cell that facilitates the delivery of cytotoxic granules and death-inducing ligands[90].

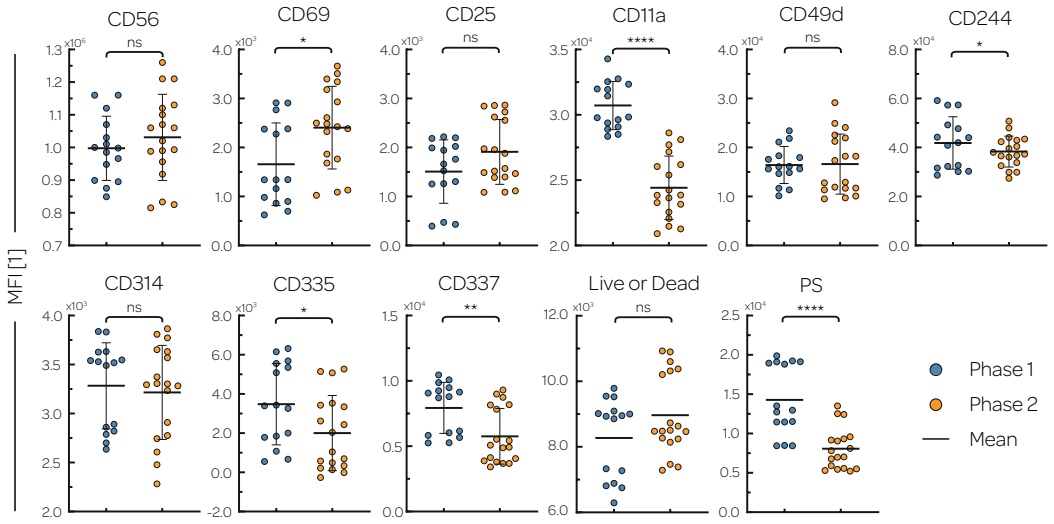

Figure 4.13: Changes of surface marker expression across the process phases. Depcited are the MFI values for the analyzed surface markers of the viable quali-NK population from the NK-only control. Data from the individual process phases were pooled and tested for normality. For parameters passing the normality test (CD56, CD11a, CD244, CD49d), an unpaired t-test was conducted. Alternatively, a Mann-Whitney U-test was employed for those not meeting the normality criteria. Statistical significance levels are denoted as follows: ns (not significant, $P > 0.1234$), * ($P < 0.0332$), ** ($P < 0.0021$), *** ($P < 0.0002$), and **** ($P < 0.0001$).

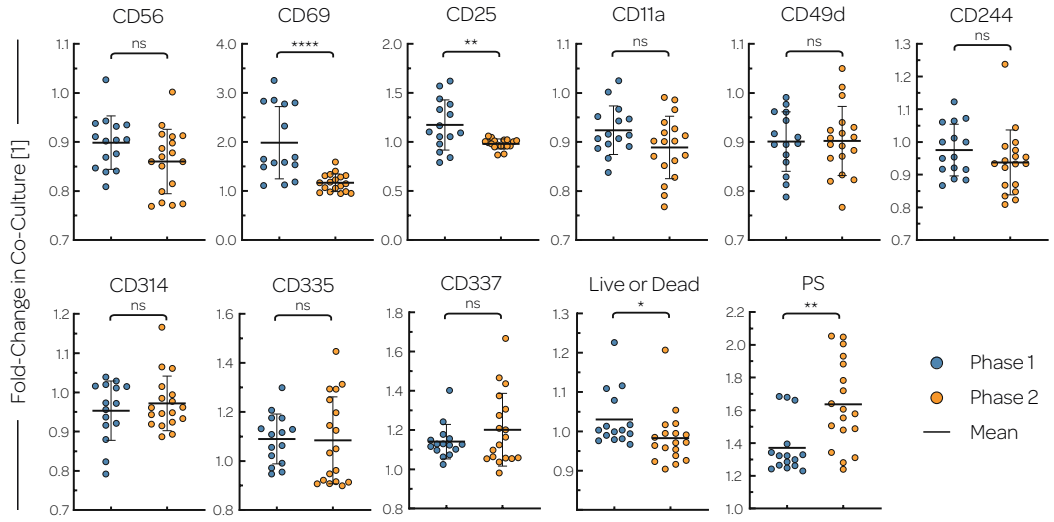

Figure 4.14: Changes of surface marker upregulation across the process phases Depcited are the fold-changes of the MFI of the analyzed surface markers of the viable quali-NK population when co-cultured with K-562 target cells. Data from the individual process phases were pooled and tested for normality. For parameters passing the normality test (CD56, CD11a, CD244, CD69, CD25), an unpaired t-test was conducted. Alternatively, a Mann-Whitney U-test was employed for those not meeting the normality criteria. Statistical significance levels are denoted as follows: ns (not significant, $P > 0.1234$), * ($P < 0.0332$), ** ($P < 0.0021$), *** ($P < 0.0002$), and **** ($P < 0.0001$).

Various receptors are recruited to this synapse, initiating a signaling cascade that leads to the lysis of the target cell[91, 92]. The decision whether the target is lysed depends not only on the balance between activating and inhibiting signals but also on the intensity and duration of the cell-cell contact. Recent studies highlight the role of CD244 in this context[91, 92]. CD244 has been shown to rapidly interact with its ligand on the target cell, leading to a strong increase in the force required to separate the synapse[92]. This intensified contact enhances the cytotoxic activity of the NK cell. Furthermore, CD16-mediated degranulation of NK cells, triggered by saturated IgG on target cells, exhibits a substantial increase (from 60% to 80%) when CD244 is co-recruited to the immunological synapse[91]. Additionally, the enhanced cell adhesion facilitated by CD244 is CD11a dependent. Here, CD11a is not only a cell adhesion molecule but also mediates the polarization of lytic granules required for efficient lytic activity[91]. Despite this cooperativity, neither lytic granule polarization nor degranulation activation alone results in efficient target cell lysis[91]. This underscores the collaborative nature of different NK receptors. Consequently, the observed alterations in CD11a and CD244 surface expressions and the reduction of activating NK receptor expressions such as CD335 and CD337 suggest a shift towards a dysfunctional phenotype.

4.3.2 Temporal Dynamics of NK-Cell Cytokine Produktion

In addition to the phenotypic characterization, the functional evaluation of NK-92 cells was extended by the analysis of degranulation and cytokine production via flow cytometry. Degranulation of NK-92 cells was assessed through the expression of CD107a, while the production of IFN-γ and TNF-α was analyzed using intracellular staining and flow cytometry. For this purpose, cells were stained with a small set of extracellular markers (CD107a, CD56, PS, LD), followed by a fixation step, permeabilization, and staining for intracellular cytokines. Using the gating strategy outlined in section 3.6.3, the proportion of cells expressing CD107a, IFN-γ, and TNF-α was determined. The corresponding cytokine production was then calculated, using equation (3.8).

The time-resolved data are illustrated in figure 4.15. To improve clarity, the cytokine production data at an E:T ratio of 5:1 was omitted, as similar trends were observed but to a lesser extent. This is attributed to a diminished activating stimulus at increased E:T ratios, where each effector cell interacts with fewer target cells. During the co-culturing experiment, PMA/ionomycin-stimulated cells served as positive control. The results showed a preliminary increase in CD107a expression, which subsequently declined on day 4 and reached a minimum at the cultivation phase transition. The expression of CD107a remained low for 4 days before recovering, although it did not reach the initial expression level. This is potentially associated with reduced expression of activating surface markers. The downregulation of CD11a, CD244, CD335, and CD337 expression may lead to impaired activation of NK cells and altered granule polarization and degranulation.

Interestingly, minimal to no expression of IFN-γ was observed. Even the positive control using chemical stimuli PMA and ionomycin demonstrated low rates of $CD107a^{+}TNF\alpha^{-}IFN\gamma^{+}$ (1-4%) and $CD107a^{+}TNF\alpha^{+}IFN\gamma^{+}$ (1-2%) cells. A possible explanation for this phe-

nomenon is that IFN-γ production in NK cells is tightly regulated. Research has shown that primary NK cells require the co-recruitment of more receptors to induce IFN-γ production compared to TNF-α and CD107a, respectively[93]. Moreover, IFN-γ not only has a higher activation threshold but also requires longer stimulation time to induce cytokine production. Specifically, NK cells produce IFN-γ after approximated 5-6 hours upon stimulation, whereas 3 hours seem to be sufficient to trigger the production of TNF-α and CD107a, with the latter being expressed almost immediately at the cell surface[93]. Therefore, given an incubation period of 4 hours, only little IFN-γ production is expected, as the cells are likely at the onset of IFN-γ production.

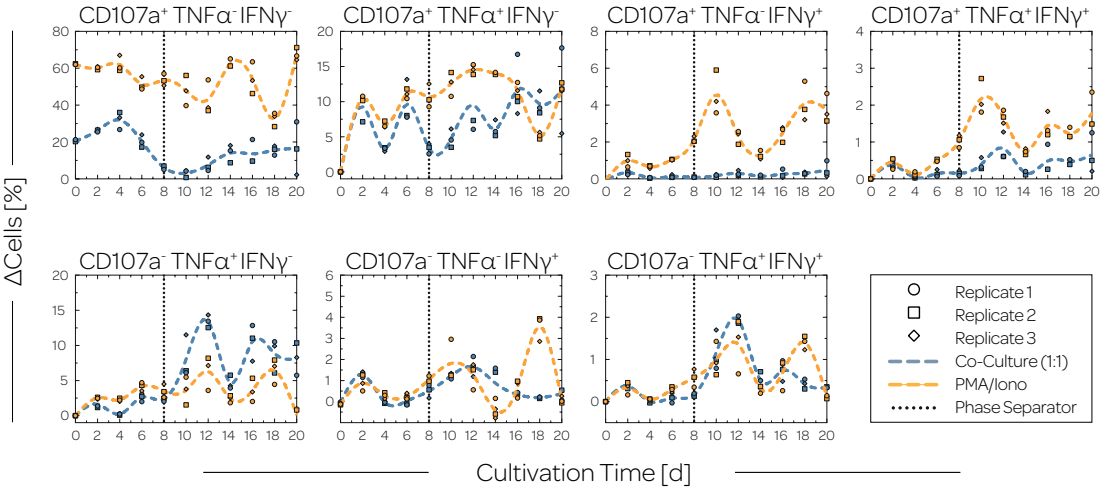

Figure 4.15: Time-resolved analysis of NK-cell cytokine production. NK-92 cells were co-cultured with K-562 target cells in the presence of protein transport inhibitors for 4 hours at 37°C. Following the co-culture, cells were stained with antibodies reactive against CD56, PS, CD107a, IFN-γ, TNF-α, and a viability dye. The figure depicts the calculated cytokine production rates of NK cells when co-cultured with K-562 target cells in a E:T ratio of 1:1 (blue). Additionally, cells were stimulated with PMA/ionomycin as a positive control (yellow). The dashed line represents a cubic spline function for the mean values of the biological triplicates.

Between the positive control and the co-culture with K-562 cells, no significant differences were observed in the $CD107a^{-}TNF\alpha^{-}IFN\gamma^{+}$ and $CD107a^{-}TNF\alpha^{+}IFN\gamma^{+}$ cell populations. The use of PMA and ionomycin as positive controls may not be an appropriate method for exclusively stimulating cytokine production without inducing degranulation.

Interestingly, cells not undergoing degranulation ($CD107a^{-}$) showed no TNF-α expression in the first phase. In the second cultivation phase, however, these cells demonstrated a notable increase in the proportion of $CD107a^{-}TNF\alpha^{+}IFN\gamma^{-}$ cells, accounting for up to 10% of the NK cell population. This suggests that the cells might have adapted during cultivation, reducing their ability to degranulate while simultaneously altering their phenotype to enhance the production of pro-inflammatory cytokines.

Statistical analysis also highlights that the proportion of TNF-α-producing cells is significantly increased during the second phase of cultivation (see figure 4.16). The data

demonstrated a statistically significant decrease of degranulation ($CD107a^+TNF\alpha^-IFN\gamma^-$) in the second culture phase, but a significant increase of TNF-α-producing cells such as $CD107a^+TNF\alpha^+IFN\gamma^+$, $CD107a^-TNF\alpha^+IFN\gamma^-$ and the $CD107a^-TNF\alpha^+IFN\gamma^+$ cell population, as shown in figure 4.16.

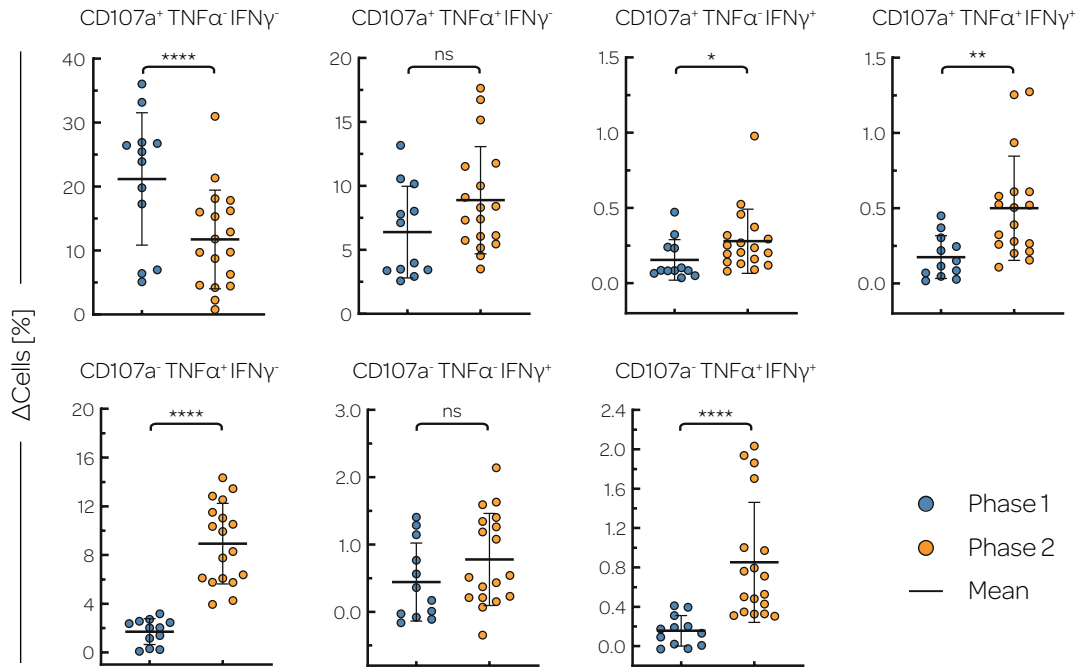

Figure 4.16: Changes of the cytokine production across the process phases. Depcited is the cytokine production and degranulation of NK-92 cells when co-cultured with K-562 target cells at an E:T ratio of 1:1. Data from the individual process phases were pooled and tested for normality. For parameters passing the normality test, an unpaired t-test was conducted. Alternatively, a Mann-Whitney U-test was employed for those not meeting the normality criteria. Statistical significance levels are denoted as follows: ns (not significant, $P > 0.1234$), * ($P < 0.0332$), ** ($P < 0.0021$), *** ($P < 0.0002$), and **** ($P < 0.0001$).

As mentioned above, the altered expression pattern of the activatory receptors might explain the reduced degranulation ($CD107a^+TNF\alpha^-IFN\gamma^-$ cells) observed in the second phase. Additionally, the observed dysfunctionality and diminished expression of CD335, CD337, and CD244 might indicate NK-cell exhaustion, characterized by diminished cytotoxicity, cytokine production, and proliferative capacity. The process of NK cell exhaustion involves both the downregulation of activating receptors and the upregulation of inhibitory or immunoregulatory receptors, including programmed cell death protein 1 (PD-1), T-cell immunoreceptor with immunoglobulin and immunoreceptor tyrosine-based inhibition motif domain (TIGIT), T cell immunoglobulin and mucin domain-containing protein 3 (TIM-3), lymphocyte-activation gene 3 (LAG-3), and CD96[94–96].

To comprehensively characterize the exhaustion status of cultivated NK cells, future experiments should specifically investigate the expression patterns of exhaustion markers.

However, this study demonstrated reduced expression of activating receptors, impaired proliferative capacity, and decreased glucose uptake and extracellular acidification in the second process phase, which fits the exhausting phenotype. An aspect that partially contradicts an exhaustion phenotype is the significantly increased TNF-α production in the second cultivation phase. However, altered expression of activatory markers can plausibly trigger the activation of alternative pathways, thereby amplifying cytokine stimulation. This, coupled with impaired granule polarization and degranulation, provides a potential explanation for the observed results. Specifically, it remains elusive whether the observed dysfunction is due to NK cell exhaustion or factors related to the cultivation process, including mechanical stress or depletion of the medium.

A detailed analysis of the flow cytometry data revealed a significant increase in the number of NK cells that exhibit reduced FSC and SSC properties in the coculture compared to the NK-cell control. This change in the scatter properties was particularly observed in samples used for phenotypic characterization, which were not treated with protein transport inhibitor (PTIs). Figure 4.17a illustrates the dot plots from the flow cytometric analysis demonstrating a significant increase of the anomalous NK cell population in coculture at an E:T ratio of 1:1. Depicted are only viable cells within the total-NK population. Moreover, figure 4.17b depicts histograms comparing the co-culture (red) and NK control (black) in the FSC and SSC channels. In particular, NK cells treated with PTIs exhibited a reduction in the properties of FSC and SSC when cocultured with K-562 cells.

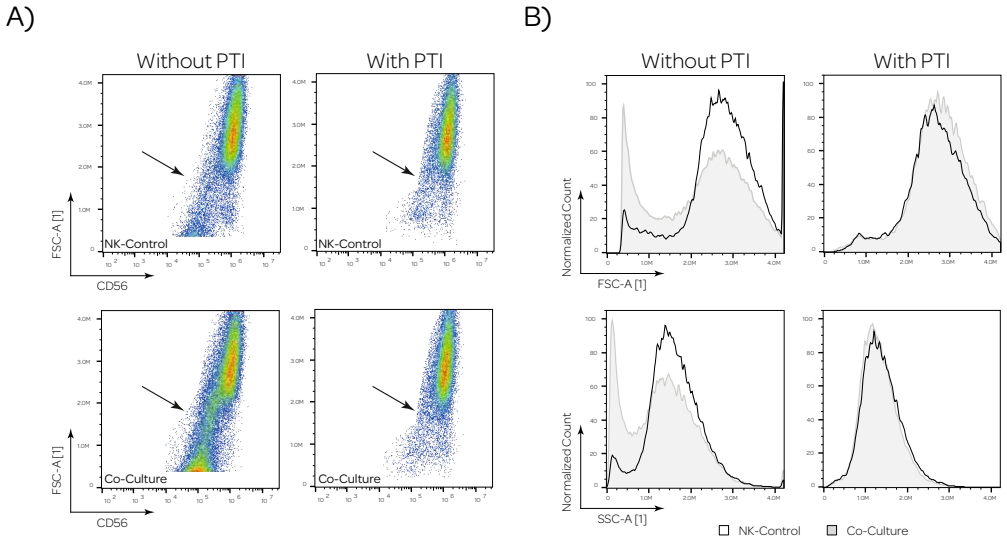

Figure 4.17: Impact of PTIs on NK-cell size when co-cultured with K-562 cells. A) Illustrated are the dot plots of the viable total NK-cell population in the co-culture and NK control, both with and without the presence of PTIs. Notably, cells not treated with PTIs showed an increasing proportion of NK cells with reduced scatter properties (indicated by an arrow). B) Overlay of the histograms of the viable total NK cell population obtained from the co-culture and NK-cell control. Cells not treated with PTIs significantly shifted towards smaller scatter intensities from the NK control (black) to the co-culture samples (red).

Analysis of the resulting diminished FSC and SSC used the corresponding MFI of the viable total NK cell population. This is noteworthy as dying and apoptotic cells exhibit altered FSC and SSC properties, which would bias subsequent results. The time course of the scatter shrinkage is shown in figure 4.18. Evidently, samples treated with PTIs showed a substantial reduction in both FSC and SSC, respectively. As shrinkage could potentially be related to the release of granules or the secretion of cytokines, the correlation coefficient was calculated for these parameters. Interestingly, no strong correlation was identified between cell shrinkage and either degranulation or cytokine production.

However, both FSC and SSC reduction exhibited a negative correlation with degranulation ($CD107a^+TNF\alpha^-IFN\gamma^-$), as indicated by the negative slope of the regression analysis. Regarding cytokine production, R^2 was calculated to be 0.4445 (SSC) and 0.3915 (FSC) for $CD107a^-TNF\alpha^+IFN\gamma^+$ cells, representing the highest correlation between cytokine parameters. Furthermore, R^2 was found to be 0.2354 (SSC) and 0.1059 (FSC) for exclusively TNF-α producing cells ($CD107a^-TNF\alpha^+IFN\gamma^-$).

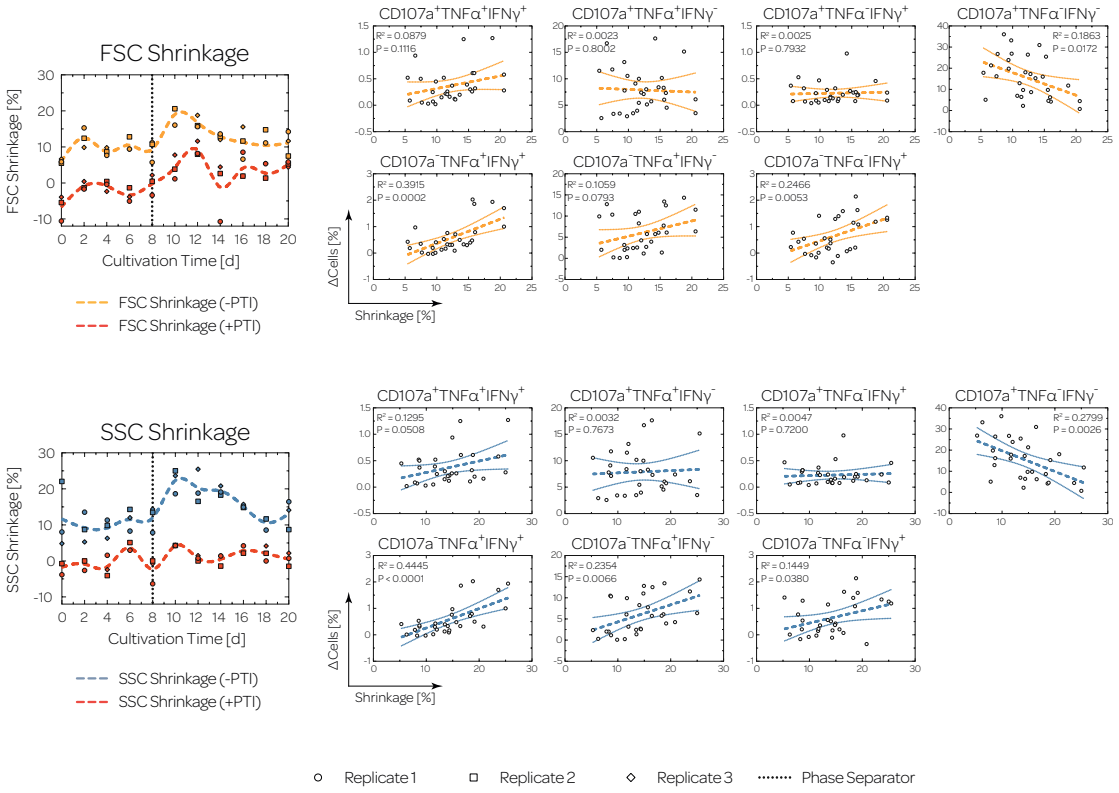

Figure 4.18: Time course of NK-cell shrinkage when co-cultured with K-562 cells. Depicted is the change in FSC and SSC properties of NK-92 cells when co-cultured with K-562 cells for 4 hours. The scatter shrinkage was calculated using the MFI of the corresponding parameter in the co-culture relative to the NK-only control. Additionally, we calculated a linear regression analysis between degranulation, cytokine production, and cell shrinkage.

The observed changes of the SSC and FSC were particularly significant during the second phase of the cultivation. Simultaneously, a significant rise in PS exposure was observed in NK-92 cells when co-cultured with K-562 cells. It is plausible that NK-92 cells become particularly fragile or prone to self-damage during this phase of cultivation. The stress induced by the co-culture, or the release of cytotoxic mediators could trigger apoptosis in NK-92 cells, thus altering their scatter properties.

The addition of PTIs (brefeldin A and monensin) disrupts membrane trafficking between the endoplasmic reticulum and the Golgi apparatus, as well as within the trans-Golgi network and the secretory pathway[97, 98]. Following the addition of these inhibitors, the diminished FSC observed in the co-culture is reduced by 10%, or even disappears for the SSC. Interestingly, cells appear significantly more resistant to these changes during the first cultivation phase. This is critical, as this phase is characterized by rapid proliferation, high viability, as well as high cytotoxicity, and degranulation. These observations support the hypothesis that changes in cell size and granularity, induced by the co-culture, serve as indicators of cellular resilience. This is supported by the observation that these alterations were pronounced only under conditions of reduced cell viability and poor cytotoxicity. Furthermore, these alterations were inhibited by the addition of PTIs suggesting their association with intracellular membrane shuttling or the secretory pathway.

4.4 The interplay of process parameters and quality anttributes

The primary focus of the study was to examine the process parameters and their relationship to the corresponding quality attributes, with the aim of identifying potential critical quality attributes (CQAs) and critical process parameters (CPPs). Although these CQAs have not been defined, they could include aspects such as cell proliferation, viability, and expected *in vivo* efficacy, for instance, cytotoxic effects on cancer cells and cytokine production. To assess these correlations, the coefficients of determination (R^2) were determined using the metabolic reaction rates and parameters obtained by the flow cytometric analysis. The resultant R^2 values for the entire culture are visualized as a heat map in figure 4.19. Heat maps of individual process phases are provided in figure 4.20 and figure 4.21.

Interestingly, a strong correlation was observed between the MFI of PS (basal expression, excluding LD^+ and PS^+ cells from the analysis) and specific metabolic reaction rates, specifically q_{Glc} ($R^2 = 0.46$), q_{Lac} ($R^2 = 0.52$), $q_{Gln(Total)}$ ($R^2 = 0.61$), q_{Asn} ($R^2 = 0.56$) and q_{Ser} ($R^2 = 0.78$) throughout the entire cultivation. In particular, these variables also show the strongest correlation to the VCC and r_{VCC}, respectively. This again emphasizes the potential application of PS background expression as a bioprocess predictor. However, these observations remain to be verified in future experiments.

Moreover, upregulation of CD69 after co-culture with K-562 cells correlated with NK cell degranulation ($CD107a^{+}TNF\alpha^{-}IFN\gamma^{-}$) throughout the whole culture period ($R^2 = 0.41$). When examining only phase 1, this correlation increases to $R^2 = 0.72$. Additionally, the basal expression of CD69 showed strong correlations with CD337 ($R^2 = 0.86$), CD335 ($R^2 = 0.72$), CD49d ($R^2 = 0.60$), and CD25 ($R^2 = 0.82$) throughout the process time. Similar patterns were observed for the basal expression of CD25, which was strongly correlated with CD337 ($R^2 = 0.70$), CD69 ($R^2 = 0.82$), and CD49d ($R^2 = 0.75$).

Furthermore, a strong correlation was found between the upregulation of CD69 and CD25 and glutamine metabolism throughout the cultivation time, specifically fold-change of CD69 with $q_{NH_4^+}$ ($R^2 = 0.88$), $q_{Gln(Enzym.)}$ ($R^2 = 0.75$), $q_{Gln(HPLC)}$ ($R^2 = 0.71$), $q_{Gln(Total)}$ ($R^2 = 0.79$), q_{Ala} ($R^2 = 0.84$) and the fold change of CD25 with $q_{NH_4^+}$ ($R^2 = 0.72$), $q_{Gln(Enzym.)}$ ($R^2 = 0.57$), $q_{Gln(HPLC)}$ ($R^2 = 0.53$), $q_{Gln(Total)}$ ($R^2 = 0.67$), q_{Ala} ($R^2 = 0.64$).

It is recognized that activation of NK cells leads to the upregulation of CD69 and CD25 expression[99, 100]. Therefore, these findings suggest that highly activated NK cells exhibit increased glutamine consumption and simultaneous alanine production, presumably through pyruvate transamination. Furthermore, when evaluating each cultivation phase separately, it is evident that the lactate-per-glucose yield, $Y_{Lac/Glc}$, correlates significantly with the specific growth rate in the first phase ($R^2 = 0.69$), while this is not the case in the second phase. This metabolic profile indicates that these rapidly proliferating and activated NK cells preferentially secrete rather than utilize pyruvate, which highlights the potential of pyruvate as a useful process parameter.

Further analysis revealed correlations between CD11a expression and various parameters throughout cultivation. These include correlation with the specific uptake rate of glutamine, $q_{Gln(Total)}$ ($R^2 = 0.52$), as well as the concentrations of LDH ($R^2 = 0.62$), glucose ($R^2 = 0.64$), lactate ($R^2 = 0.60$), total glutamine ($R^2 = 0.67$), glutamate ($R^2 = 0.67$), asparagine ($R^2 = 0.53$), and serine ($R^2 = 0.55$).

Furthermore, the specific growth rate μ was correlated with $q_{NH_4^+}$ ($R^2 = 0.83$), $q_{Gln(Enzym.)}$ ($R^2 = 0.77$), $q_{Gln(HPLC)}$ ($R^2 = 0.79$), and q_{Ala} ($R^2 = 0.83$) during the first phase of the cultivation.

No robust correlation was observed between cytokine production or the cytotoxicity and the process parameters for the entire cultivation period. However, in the first phase, CD244 expression was correlated with cytotoxicity quantified by flow cytometry ($R^2 = 0.80$) and the degranulation of NK cells ($R^2 = 0.65$). Interestingly, in this phase the volumetric biomass growth r_{VCC} was correlated with the degranulation ($R^2 = 0.59$) and cytotoxicity by flow cytometry ($R^2 = 0.52$), indicating that proliferation is closely related to NK cell functionality.

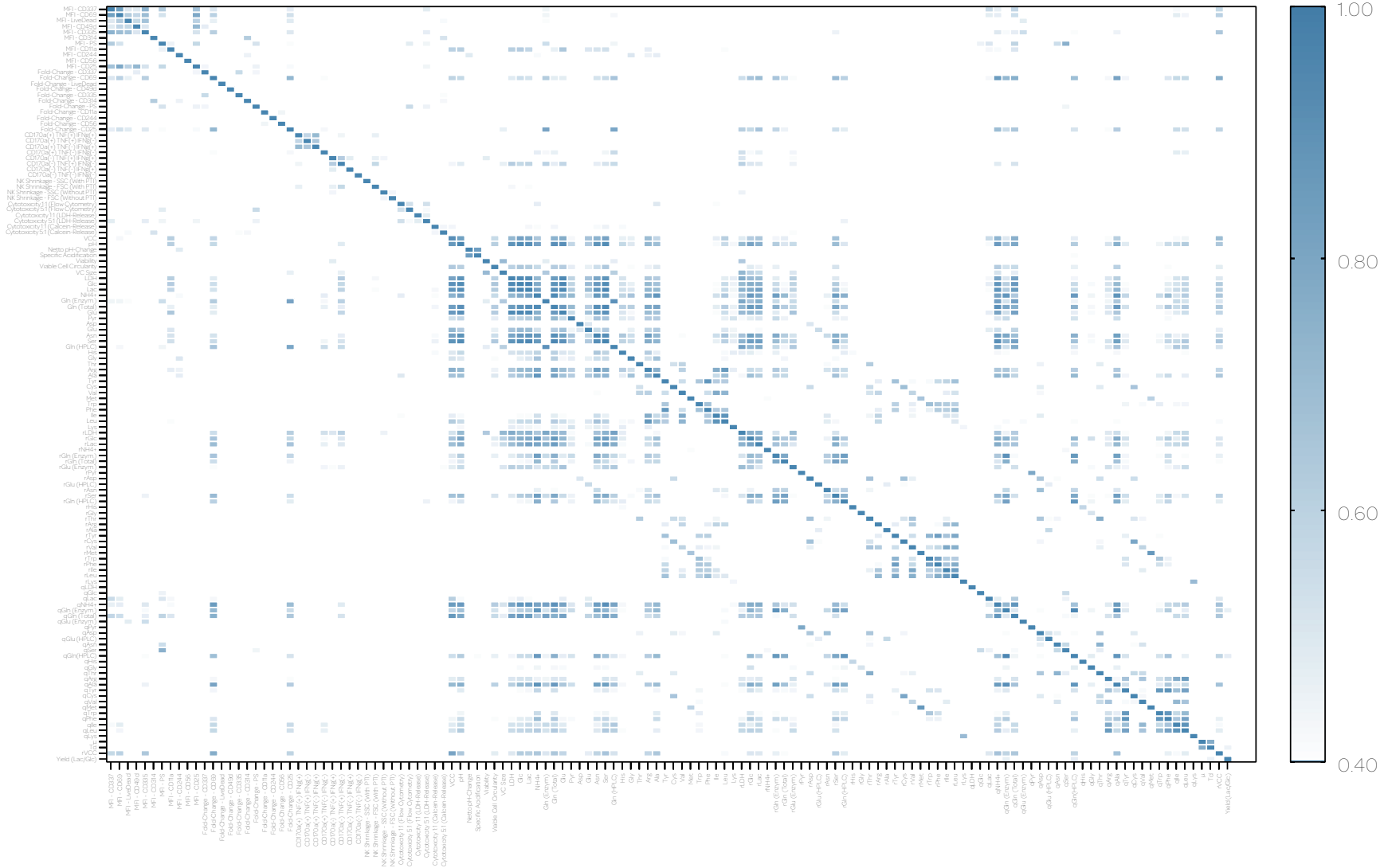

Figure 4.19: Heatmap illustrating the coefficient of determination across the entire process dataset. Depicted are the squared Pearson coefficients (coefficients of determination) representing the correlation of the specific reaction rates with determined parameters, including cytotoxicity, surface marker expression, and cytokine production.

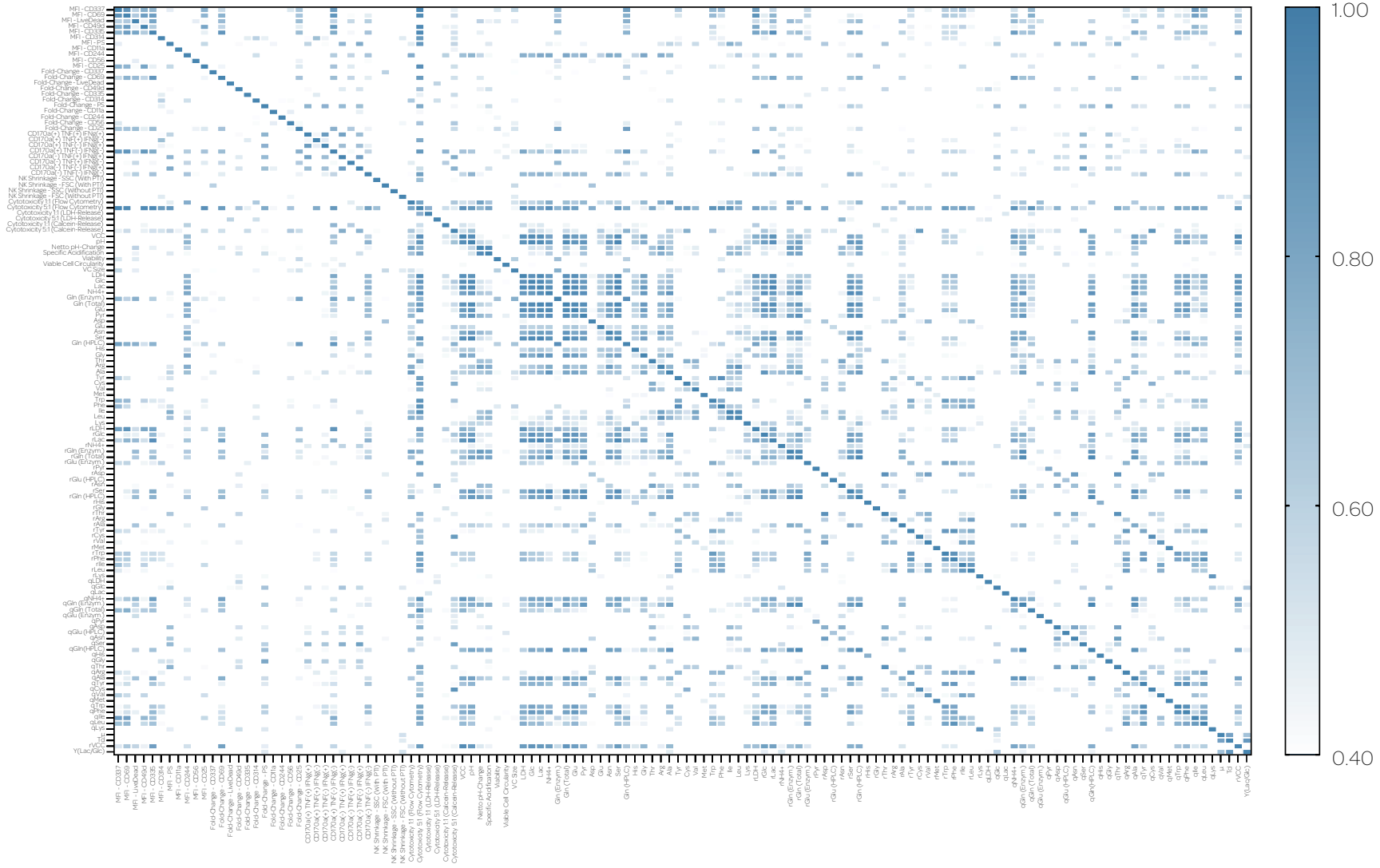

Figure 4.20: Heatmap of the coefficient of determination for phase 1 process data Depcited are the squared Pearson coefficients (coefficients of determination) representing the correlation of the specific reaction rates with determined parameters, including cytotoxicity, surface marker expression, and cytokine production.

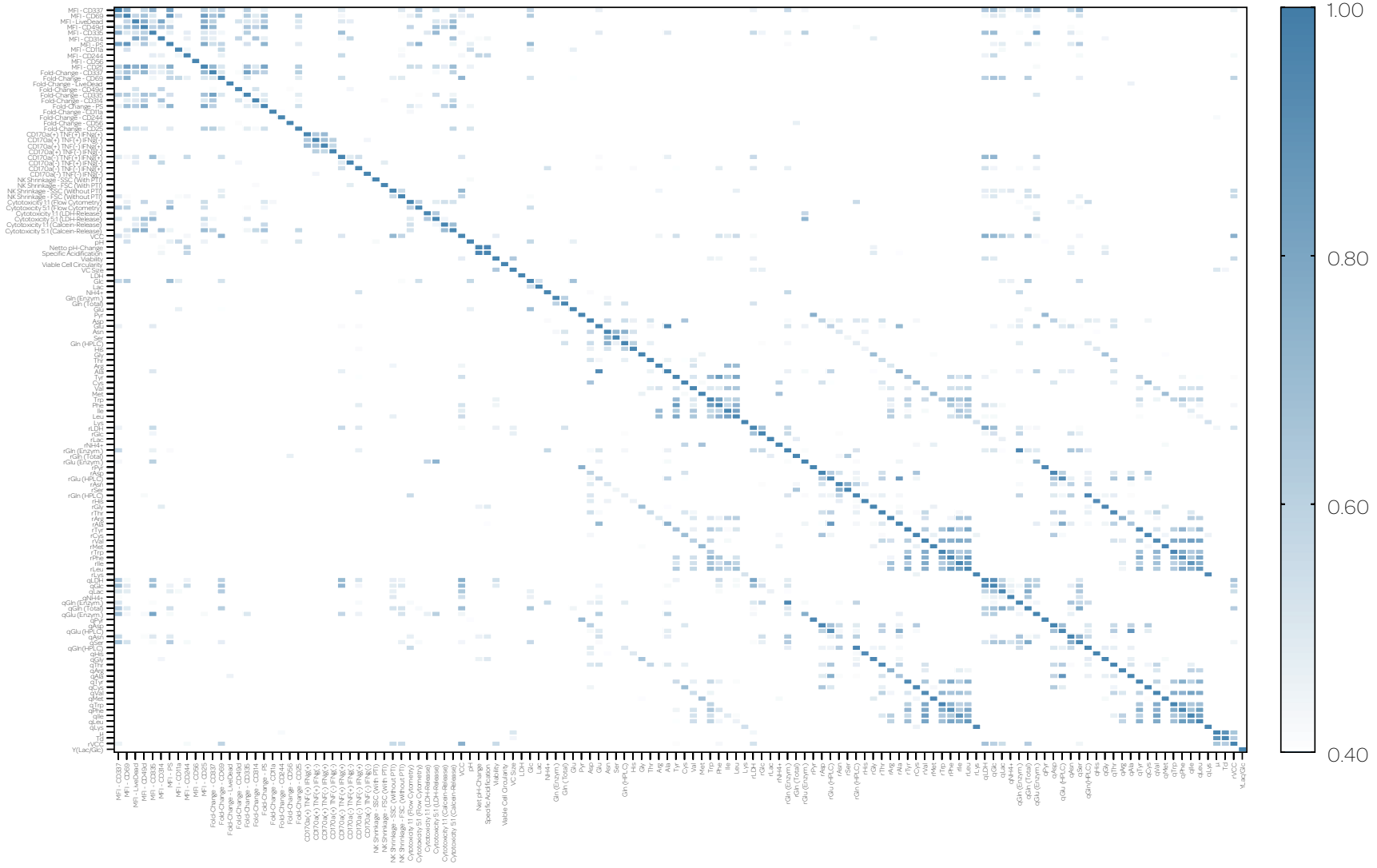

Figure 4.21: Heatmap of the coefficient of determination for phase 2 process data Depcited are the squared Pearson coefficients (coefficients of determination) representing the correlation of the specific reaction rates with determined parameters, including cytotoxicity, surface marker expression, and cytokine production.

CHAPTER 5

Conclusion and Outlook

To standardize the production of therapeutic NK cells, a deep understanding of their expansion process is essential. This requires the generation of detailed, time-resolved data, which is challenging due to the slow growth kinetics of NK-92 cells. To overcome these challenges, we employed a pseudo-static cultivation method, enabling comprehensive data collection on the prerequisites for NK cell proliferation. From these data, we identified a metabolic fingerprint of NK-92 cells. Specifically, the concentrations of L-glutamine, L-alanine, L-asparagine, L-arginine, L-serine, and L-leucine, showed a strong correlation with the viable cell concentration. L-serine was the most utilized amino acid relative to its initial concentration, highlighting its importance for NK-92 metabolism. Moreover, the findings of this thesis align with previous research that indicates that cytotoxic T cells primarily fuel L-serine into the one-carbon metabolism[75]. Given the comparable effector functions of cytotoxic T cells and NK cells, along with our observation of significant glycine release, we propose that NK-92 cells utilize L-serine in a similar manner. The one-carbon metabolism is particularly relevant as it drives both the folate and methionine cycles. These interconnected pathways play a crucial role in the synthesis of purines, pyrimidines, lipids, and maintaining cellular redox balance via glutathione synthesis[75].

Moreover, NK-92 cells released significant amounts of pyruvate into the medium during the exponential growth phase. Typically, NK cells convert glycolysis-derived pyruvate to cytosolic citrate through the citrate-malate shuttle instead of fueling it into the tricarboxylic acid cycle to sustain OXPHOS rates[70, 71]. Cytosolic citrate serves as a precursor for lipid biosynthesis, suggesting that lipid metabolism plays a pivotal role in the function of NK cells. Our findings indicate that NK-92 cells utilize the Warburg metabolic pathway (anaerobic glycolysis) during the exponential phase, resulting in saturated pyruvate utilization. This hypothesis was based on the observation that both pyruvate and lactate were released into the medium during the initial culturing phase. In support of this, the lactate-per-glucose yield ($Y_{Lac/Glc}$) demonstrated a strong correlation

with the specific growth rate in the initial but not in the second cultivation phase. This suggests a change in the metabolic activity of NK-92 cells between the two phases.

After the adapting phase, we observed a significant reduction in metabolic activity, accompanied by a dysfunctional phenotype. The latter was characterized by reduced surface expression of CD11a, CD244, and the NK receptors CD335 and CD337, as well as decreased cytotoxicity and degranulation, but increased TNF-α production. In particular, the upregulation of CD69 and CD25, upon co-culturing with K-562 target cells, was only observed in the first phase of cultivation and was completely absent in the subsequent phase. This decreased expression of activating receptors is linked to reduced cytotoxic activity and degranulation. Previous studies have confirmed the essential role of these receptors in granule polarization and degranulation, which subsequently affects the lytic activity of NK cells[91, 92, 101]. We hypothesized that the reduced expression of these markers was caused by medium depletion, and metabolic adaption.

Furthermore, the NK-92 cells exhibited increased susceptibility to cellular stress during and after the adaptation phase. This was evidenced by the reduction in cell size and granularity, as well as increased exposure of phosphatidylserine following co-cultivation with K-562 target cells, which was not observed before the adaptation phase. Our findings demonstrate that these effects are linked to intracellular protein trafficking, as inhibitors such as brefeldin A and monensin diminished or completely eliminated these effects. Nevertheless, these mechanisms appear to be mitochondrially driven, suggesting that the observed morphological changes of the cells could be attributed to alterations in mitochondrial structures[88, 102]. Furthermore, research indicates that the functionality of NK cells is dependent on mitochondrial fitness and polarization[73, 74, 103]. Therefore, future experiments are planned to evaluate mitochondrial mass and polarization, as well as functionality to refine the cultivation process and ensure the production of functionally optimized NK cells.

Our study used a comparative approach that included three different methods for assessing the cytotoxicity of cultured NK-92 cells. The time-resolved comparative analysis not only assessed the cytotoxicity but also allowed us to compare these methods. Among them, flow cytometry emerged as the most accurate method due to its superior sensitivity, and the information content it provides. The calcein- and LDH-release assays showed lower sensitivity and faced limitations in differentiating between the effects on NK-92 cells and K-562 cells. Hence, it is not possible to track potential off-target effects. The advantage of flow cytometry lies in its ability to provide single-cell resolution and utilize specific markers selectively examined on target cells. This circumvents the above-mentioned effects and biased results. Moreover, the combination of different markers (phosphatidylserine and DNA intercalators) facilitates the differentiation of various stages of cell death, thus providing additional insights into the kinetics of NK-cell-mediated cell lysis.

In summary, this thesis lays a solid foundation for future research aimed at improving and optimizing NK cell expansion processes. The identification of a metabolic fingerprint of NK-92 cells has provided the foundation for the development of media and potential feeding strategies. Furthermore, by identifying the optimal methodology for assessing

cytotoxicity, we have contributed to the enhancement of the therapeutic efficacy and safety of NK cell-based therapies.

List of Figures

List of Tables

Acronyms

NH_4^+ ammonium. 33

µ specific growth rate. 34, 38, 39

7-AAD 7-aminoactinomycin D. 48

ACL citrate lyase. 43

ACT adoptive cell therapy. ix, 7, 9

ADC arginine decarboxylase. 43

ADCC antibody-dependent cell-mediated cytotoxicity. 4, 8

AGM agmatinase. 43

Ala alanine. 30

AM acetoxymethyl ester. 19

ARG L-arginine amidinohydrolase. 43

Arg arginine. 30

ASL argininosuccinate lyase. 43

ASNase asparaginase. 43

ASNS asparagine synthetase. 43

Asp asparagine. 30

ASS1 argininosuccinate synthetase 1. 43

AST aspartate transaminase. 43

ATCC American Type Culture Collection. 14

BAT3 HLA-B-associated transcript 3. 4

BID Bcl2 homology domain 3-interacting domain death agonist. 5

CAR chimeric antigen receptor. 7

CD cluster of differentiation. 1, 14

CMS citrate-malate shuttle. 42

CPPs critical process parameters. 11, 12, 58

CQAs critical quality attributes. 11, 58

DAPI 4',6-diamidino-2-phenylindol. 48

DISC death-inducing signaling complex. 6, 7

DMSO Dimethyl sulphoxide. 13

E:T effector-to-target. 20, 24

FasL Fas ligand. 5, 6

FBS fetal bovine serum. 13, 14

FDA U.S. Food and Drug Administration. 7

FSC forward scatter. 23, 58

GDH glutamate dehydrogenase. 43

Glc D-glucose. 33

Gln glutamine. 30, 33

GLS glutaminase. 43

Glu glutamate. 30, 33

Gly glycine. 30

GOT glutamate oxaloacetate transaminase. 43

GvHD graft-versus-host disease. 7

HLA human leukocyte antigen. 2

HPLC high performance liquid chromatography. 16–18, 30, 37

HSPCs haematopoietic stem and progenitor cells. 8

IFN-γ interferon-γ. 1, 9, 14, 23–25, 27, 44, 53, 54

IL interleukin. 1, 13, 14

Ile isoleucine. 30

IMDM Iscove's Modified Dulbecco's Medium. 13, 14, 16, 20, 24

iPSCs induced pluripotent stem cells. 8

ITAM immunoreceptor tyrosine-based activation motif. 2

ITIM immunoreceptor tyrosine-based inhibitory motif. 2

IU International Unit. 14

KIR killer-cell immunoglobulin-like receptor. 2

Lac lactate. 33

LAG-3 lymphocyte-activation gene 3. 2, 55

Lck lymphocyte-specific protein tyrosine kinase. 45

LD Live or Dead. 22–25, 53

LDH lactate dehydrogenase. 16, 21, 59

Leu leucine. 30

MDH malate dehydrogenase. 43

MEc malic enzyme. 43

MFI mean fluorescent intensity. 25, 48, 50

MHC major histocompatibility complex. 2

MICA MHC class I chain-related protein A. 4

MICB MHC class I chain-related protein B. 4

MLL5 mixed lineage leukemia 5. 4

MPA 3-mercaptopropionic acid. 13, 17, 18

MTHF 5,10-methylene THF. 42

MTT 3-(4,5-dimethylthiazol-2-yl)-2,5-diphenyl tetrazolium bromide. 19

NAD nicotinamide adenine dinucleotide. 21

NCRs natural cytotoxicity receptors. 2, 4, 9

NK natural killer. 1

NO nitric oxide. 44

NOS nitric oxide synthase. 43, 44

ODC ornithine decarboxylase. 43

OPA ortho-phthalaldehyde. 14, 17, 18

OTC ornithine transcarbamylase. 43

OXPHOS oxidative phosphorylation. 42, 44, 50, 63

P Pearson correlation coefficient. 32

PCNA proliferating cell nuclear antigen. 4

PD-1 programmed cell death protein 1. 2, 55

PI propidium iodide. 48

PMA phorbol-12-myristate-13-acetate. 14, 24, 53

PS phosphatidylserine. 14, 22, 23, 25, 48, 53, 54, 58

PTI protein transport inhibitor. 24, 54, 56

Pyr pyruvate. 34

QbD Quality by Design. 11

SCGM Stem Cell Growth Medium. 14, 16, 20, 24

Ser serine. 30

SHMT serine hydroxymethyltransferase. 42, 43

Srebp sterol regulatory element-binding protein. 42

SSC side scatter. 23, 58

T_d doubling time. 9, 34

TCA tricarboxylic acid. 33, 42, 44

TCR T cell receptor. 7

TGF-β transforming growth factor-β. 4

THF tetrahydrofolate. 42

TIGIT T-cell immunoreceptor with immunoglobulin and immunoreceptor tyrosine-based inhibition motif domain. 2, 55

TIL tumor-infiltrating lymphocyte. 7

TIM-3 T cell immunoglobulin and mucin domain-containing protein 3. 2, 55

TNF-α tumor necrosis factor-α. 14, 23–25, 27, 53–57, 64

TRAIL tumor necrosis factor-related apoptosis-inducing ligand. 5, 6

ULBPs UL16 binding proteins. 4

VCC viable cell concentration. 16, 17, 29, 32, 38, 58

Bibliography

1. Cooper, M. A., Fehniger, T. A. & Caligiuri, M. A. The biology of human natural killer-cell subsets. *Trends in Immunology* **22,** 633–640. ISSN: 1471-4906. https://doi.org/10.1016/S1471-4906(01)02060-9 (2001).
2. Brady, J. *et al.* The Interactions of Multiple Cytokines Control NK Cell Maturation. *The Journal of Immunology* **185,** 6679–6688. ISSN: 0022-1767. https://doi.org/10.4049/jimmunol.0903354 (2010).
3. Naranjo-Gomez, M., Cahen, M., Lambour, J., Boyer-Clavel, M. & Pelegrin, M. Immunomodulatory Role of NK Cells during Antiviral Antibody Therapy. *Vaccines* **9,** 137. ISSN: 2076-393X. https://www.mdpi.com/2076-393X/9/2/137 (2021).
4. Engel, P. *et al.* CD Nomenclature 2015: Human Leukocyte Differentiation Antigen Workshops as a Driving Force in Immunology. *The Journal of Immunology* **195,** 4555–4563. ISSN: 0022-1767. https://doi.org/10.4049/jimmunol.1502033 (2015).
5. Stabile, H., Fionda, C., Gismondi, A. & Santoni, A. Role of Distinct Natural Killer Cell Subsets in Anticancer Response. *Frontiers in Immunology* **8.** ISSN: 1664-3224. https://www.frontiersin.org/journals/immunology/articles/10.3389/fimmu.2017.00293 (2017).
6. Cooper, M. A., Fehniger, T. A. & Caligiuri, M. A. The biology of human natural killer-cell subsets. *Trends in Immunology* **22,** 633–640. ISSN: 1471-4906. https://doi.org/10.1016/S1471-4906(01)02060-9 (2001).
7. Ferlazzo, G. & Münz, C. NK Cell Compartments and Their Activation by Dendritic Cells1. *The Journal of Immunology* **172,** 1333–1339. ISSN: 0022-1767. https://doi.org/10.4049/jimmunol.172.3.1333 (2004).
8. Vivier, E., Tomasello, E., Baratin, M., Walzer, T. & Ugolini, S. Functions of natural killer cells. *Nature Immunology* **9,** 503–510. ISSN: 1529-2916. https://doi.org/10.1038/ni1582 (2008).
9. Moretta, A., Bottino, C., Mingari, M. C., Biassoni, R. & Moretta, L. What is a natural killer cell? *Nature Immunology* **3,** 6–8. ISSN: 1529-2916. https://doi.org/10.1038/ni0102-6 (2002).

10. Trinchieri, G. in *Advances in Immunology* (ed Dixon, F. J.) 187–376 (Academic Press, 1989). ISBN: 0065-2776. https://www.sciencedirect.com/science/article/pii/S0065277608606641.

11. Sivori, S. *et al.* Human NK cells: surface receptors, inhibitory checkpoints, and translational applications. *Cellular and Molecular Immunology* **16,** 430–441. ISSN: 2042-0226. https://doi.org/10.1038/s41423-019-0206-4 (2019).

12. Kromer, J. *et al.* Influence of HLA on human partnership and sexual satisfaction. *Scientific Reports* **6,** 32550. ISSN: 2045-2322. https://doi.org/10.1038/srep32550 (2016).

13. Fisher, K., Hazini, A. & Seymour, L. W. Tackling HLA Deficiencies Head on with Oncolytic Viruses. *Cancers (Basel)* **13.** 2072-6694. ISSN: 2072-6694. https://doi.org/10.3390/cancers13040719 (2021).

14. Huntington, N. D., Cursons, J. & Rautela, J. The cancer–natural killer cell immunity cycle. *Nature Reviews Cancer* **20,** 437–454. ISSN: 1474-1768. https://doi.org/10.1038/s41568-020-0272-z (2020).

15. Pessino, A. *et al.* Molecular Cloning of NKp46: A Novel Member of the Immunoglobulin Superfamily Involved in Triggering of Natural Cytotoxicity. *Journal of Experimental Medicine* **188,** 953–960. ISSN: 0022-1007. https://doi.org/10.1084/jem.188.5.953 (1998).

16. Vitale, M. *et al.* NKp44, a Novel Triggering Surface Molecule Specifically Expressed by Activated Natural Killer Cells, Is Involved in Non–Major Histocompatibility Complex–restricted Tumor Cell Lysis. *Journal of Experimental Medicine* **187,** 2065–2072. ISSN: 0022-1007. https://doi.org/10.1084/jem.187.12.2065 (1998).

17. Pende, D. *et al.* Identification and Molecular Characterization of Nkp30, a Novel Triggering Receptor Involved in Natural Cytotoxicity Mediated by Human Natural Killer Cells. *Journal of Experimental Medicine* **190,** 1505–1516. ISSN: 0022-1007. https://doi.org/10.1084/jem.190.10.1505 (1999).

18. Muccio, L. *et al.* Late Development of FcεRγneg Adaptive Natural Killer Cells Upon Human Cytomegalovirus Reactivation in Umbilical Cord Blood Transplantation Recipients. *Frontiers in Immunology* **9.** ISSN: 1664-3224. https://www.frontiersin.org/journals/immunology/articles/10.3389/fimmu.2018.01050 (2018).

19. Arnon, T. I., Markel, G. & Mandelboim, O. Tumor and viral recognition by natural killer cells receptors. *Semin Cancer Biol* **16,** 348–58. ISSN: 1044-579x. https://doi.org/10.1016/j.semcancer.2006.07.005 (2006).

20. Schlecker, E. *et al.* Metalloprotease-Mediated Tumor Cell Shedding of B7-H6, the Ligand of the Natural Killer Cell–Activating Receptor NKp30. *Cancer Research* **74,** 3429–3440. ISSN: 0008-5472. https://doi.org/10.1158/0008-5472.CAN-13-3017 (2014).

21. Reiners, K. S. *et al.* Soluble ligands for NK cell receptors promote evasion of chronic lymphocytic leukemia cells from NK cell anti-tumor activity. *Blood* **121,** 3658–3665. ISSN: 0006-4971. https://doi.org/10.1182/blood-2013-01-476606 (2013).

22. Bauer, S. *et al.* Activation of NK Cells and T Cells by NKG2D, a Receptor for Stress-Inducible MICA. *Science* **285,** 727–729. https://www.science.org/doi/abs/10.1126/science.285.5428.727 (1999).

23. Sivori, S. *et al.* 2B4 functions as a co-receptor in human NK cell activation. *Eur J Immunol* **30,** 787–93. ISSN: 0014-2980. https://doi.org/10.1002/1521-4141(200003)30:3%3C787::AID-IMMU787%3E3.0.CO;2-I (2000).

24. Lee, K. M. *et al.* 2B4 acts as a non-major histocompatibility complex binding inhibitory receptor on mouse natural killer cells. *J Exp Med* **199,** 1245–54. ISSN: 0022-1007. https://doi.org/10.1084/jem.20031989 (2004).

25. Carrillo-Bustamante, P., Keşmir, C. & de Boer, R. J. The evolution of natural killer cell receptors. *Immunogenetics* **68,** 3–18. ISSN: 0093-7711. https://doi.org/10.1007/s00251-015-0869-7 (2016).

26. Quatrini, L. *et al.* Human NK cells, their receptors and function. *Eur J Immunol* **51,** 1566–1579. ISSN: 0014-2980. https://doi.org/10.1002/eji.202049028 (2021).

27. Raulet, D. H. & Vance, R. E. Self-tolerance of natural killer cells. *Nature Reviews Immunology* **6,** 520–531. ISSN: 1474-1741. https://doi.org/10.1038/nri1863 (2006).

28. Prager, I. & Watzl, C. Mechanisms of natural killer cell-mediated cellular cytotoxicity. *Journal of Leukocyte Biology* **105,** 1319–1329. ISSN: 0741-5400. https://doi.org/10.1002/JLB.MR0718-269R (2019).

29. Guo, Y., Chen, J., Zhao, T. & Fan, Z. Granzyme K degrades the redox/DNA repair enzyme Ape1 to trigger oxidative stress of target cells leading to cytotoxicity. *Molecular Immunology* **45,** 2225–2235. ISSN: 0161-5890. https://www.sciencedirect.com/science/article/pii/S0161589007008681 (2008).

30. Zhao, T. *et al.* Granzyme K cleaves the nucleosome assembly protein SET to induce single-stranded DNA nicks of target cells. *Cell Death and Differentiation* **14,** 489–499. ISSN: 1476-5403. https://doi.org/10.1038/sj.cdd.4402040 (2007).

31. Cullen, S. P. *et al.* Nucleophosmin Is Cleaved and Inactivated by the Cytotoxic Granule Protease Granzyme M during Natural Killer Cell-mediated Killing*. *Journal of Biological Chemistry* **284,** 5137–5147. ISSN: 0021-9258. https://www.sciencedirect.com/science/article/pii/S0021925820709737 (2009).

32. Prager, I. & Watzl, C. Mechanisms of natural killer cell-mediated cellular cytotoxicity. *J Leukoc Biol* **105,** 1319–1329. ISSN: 0741-5400. https://doi.org/10.1002/JLB.MR0718-269R (2019).

33. Johnstone, R. W., Frew, A. J. & Smyth, M. J. The TRAIL apoptotic pathway in cancer onset, progression and therapy. *Nature Reviews Cancer* **8,** 782–798. ISSN: 1474-1768. https://doi.org/10.1038/nrc2465 (2008).

34. Rosenberg, S. A. *et al.* Use of tumor-infiltrating lymphocytes and interleukin-2 in the immunotherapy of patients with metastatic melanoma. *New England Journal of Medicine* **319,** 1676–1680. ISSN: 0028-4793. https://doi.org/10.1056/NEJM198812223192527 (1988).

35. Zhang, P., Zhang, G. & Wan, X. Challenges and new technologies in adoptive cell therapy. *Journal of Hematology and Oncology* **16,** 97. ISSN: 1756-8722. https://doi.org/10.1186/s13045-023-01492-8 (2023).

36. Rohaan, M. W., Wilgenhof, S. & Haanen, J. B. A. G. Adoptive cellular therapies: the current landscape. *Virchows Archiv* **474,** 449–461. ISSN: 1432-2307. https://doi.org/10.1007/s00428-018-2484-0 (2019).

37. Rezvani, K. Adoptive cell therapy using engineered natural killer cells. *Bone Marrow Transplantation* **54,** 785–788. ISSN: 1476-5365. https://doi.org/10.1038/s41409-019-0601-6 (2019).

38. Liu, E. *et al.* Use of CAR-Transduced Natural Killer Cells in CD19-Positive Lymphoid Tumors. *N Engl J Med* **382,** 545–553. https://doi.org/10.1056/nejmoa1910607 (2020).

39. Dagher, O. K. & Posey, A. D. Forks in the road for CAR T and CAR NK cell cancer therapies. *Nature Immunology* **24,** 1994–2007. ISSN: 1529-2916. https://doi.org/10.1038/s41590-023-01659-y (2023).

40. Maalej, K. M. *et al.* CAR-cell therapy in the era of solid tumor treatment: current challenges and emerging therapeutic advances. *Molecular Cancer* **22,** 20. ISSN: 1476-4598. https://doi.org/10.1186/s12943-023-01723-z (2023).

41. Page, A., Chuvin, N., Valladeau-Guilemond, J. & Depil, S. Development of NK cell-based cancer immunotherapies through receptor engineering. *Cellular and Molecular Immunology.* ISSN: 2042-0226. https://doi.org/10.1038/s41423-024-01145-x (2024).

42. Vivier, E. *et al.* Natural killer cell therapies. *Nature* **626,** 727–736. ISSN: 1476-4687. https://doi.org/10.1038/s41586-023-06945-1 (2024).

43. Hatjiharissi, E. *et al.* Increased natural killer cell expression of CD16, augmented binding and ADCC activity to rituximab among individuals expressing the FcγRIIIa-158 V/V and V/F polymorphism. *Blood* **110,** 2561–2564. ISSN: 0006-4971. https://doi.org/10.1182/blood-2007-01-070656 (2007).

44. Laskowski, T. J., Biederstädt, A. & Rezvani, K. Natural killer cells in antitumour adoptive cell immunotherapy. *Nature Reviews Cancer* **22,** 557–575. ISSN: 1474-1768. https://doi.org/10.1038/s41568-022-00491-0 (2022).

45. Fang, F., Wang, W., Chen, M., Tian, Z. & Xiao, W. Technical advances in NK cell-based cellular immunotherapy. *Cancer Biol Med* **16,** 647–654. ISSN: 2095-3941. https://doi.org/10.20892/j.issn.2095-3941.2019.0187 (2019).

46. Berrien-Elliott, M. M., Jacobs, M. T. & Fehniger, T. A. Allogeneic natural killer cell therapy. *Blood* **141,** 856–868. ISSN: 0006-4971. https://doi.org/10.1182/blood.2022016200 (2023).

47. Suck, G. *et al.* NK-92: an 'off-the-shelf therapeutic' for adoptive natural killer cell-based cancer immunotherapy. *Cancer Immunology, Immunotherapy* **65,** 485–492. ISSN: 1432-0851. https://doi.org/10.1007/s00262-015-1761-x (2016).

48. Klingemann, H. The NK-92 cell line 30 years later: its impact on natural killer cell research and treatment of cancer. *Cytotherapy* **25,** 451–457. ISSN: 1465-3249. https://doi.org/10.1016/j.jcyt.2022.12.003 (2023).

49. Maki, G., Klingemann, H. G., Martinson, J. A. & Tam, Y. K. Factors Regulating the Cytotoxic Activity of the Human Natural Killer Cell Line, NK-92. *Journal of Hematotherapy and Stem Cell Research* **10,** 369–383. https://www.liebertpub.com/doi/abs/10.1089/152581601750288975 (2001).

50. Solocinski, K. *et al.* Overcoming hypoxia-induced functional suppression of NK cells. *Journal for ImmunoTherapy of Cancer* **8,** e000246. https://jitc.bmj.com/content/jitc/8/1/e000246.full.pdf (2020).

51. Schönfeld, K. *et al.* Selective Inhibition of Tumor Growth by Clonal NK Cells Expressing an ErbB2/HER2-Specific Chimeric Antigen Receptor. *Molecular Therapy* **23,** 330–338. ISSN: 1525-0016. https://www.sciencedirect.com/science/article/pii/S1525001616300430 (2015).

52. Tonn, T. *et al.* Treatment of patients with advanced cancer with the natural killer cell line NK-92. *Cytotherapy* **15.** doi: 10.1016/j.jcyt.2013.06.017, 1563–1570. ISSN: 1465-3249. https://doi.org/10.1016/j.jcyt.2013.06.017 (2013).

53. Williams, B. A. *et al.* A phase I trial of NK-92 cells for refractory hematological malignancies relapsing after autologous hematopoietic cell transplantation shows safety and evidence of efficacy. *Oncotarget* **8.** ISSN: 1949-2553. https://www.oncotarget.com/article/19204/text/ (2017).

54. García Aponte, O. F., Kozma, B., Egger, D., Kasper, C. & Herwig, C. Kinetics of NK-92 growth and functionality in pseudo-static cultures. *Biochemical Engineering Journal* **196,** 108929. ISSN: 1369-703X. https://doi.org/10.1016/j.bej.2023.108929 (2023).

55. Dai, Z., Wu, Z., Jia, S. & Wu, G. Analysis of amino acid composition in proteins of animal tissues and foods as pre-column o-phthaldialdehyde derivatives by HPLC with fluorescence detection. *Journal of Chromatography B* **964,** 116–127. ISSN: 1570-0232. https://doi.org/10.1016/j.jchromb.2014.03.025 (2014).

56. Jochems, P., Schad, G. & Kraft, V. Fast and Sensitive Analysis of Amino Acids Using Automated Pre-Column Derivatization. *The Application Notebook* **33,** 395–396 (2018).

57. Brunner, K. T., Mauel, J., Cerottini, J. C. & Chapuis, B. Quantitative assay of the lytic action of immune lymphoid cells on 51-Cr-labelled allogeneic target cells in vitro; inhibition by isoantibody and by drugs. *Immunology* **14,** 181–96. ISSN: 0019-2805 (1968).

58. Neville, M. E. 51Cr-uptake assay a sensitive and reliable method to quantitate cell viability and cell death. *Journal of Immunological Methods* **99,** 77–82. ISSN: 0022-1759. https://doi.org/10.1016/0022-1759(87)90034-2 (1987).

59. Neri, S., Mariani, E., Meneghetti, A., Cattini, L. & Facchini, A. Calcein-Acetyoxymethyl Cytotoxicity Assay: Standardization of a Method Allowing Additional Analyses on Recovered Effector Cells and Supernatants. *Clinical Diagnostic Laboratory Immunology* **8,** 1131–1135. https://doi.org/10.1128/cdli.8.6.1131-1135.2001 (2001).

60. Korzeniewski, C. & Callewaert, D. M. An enzyme-release assay for natural cytotoxicity. *J Immunol Methods* **64,** 313–20. ISSN: 0022-1759. https://doi.org/10.1016/0022-1759(83)90438-6 (1983).

61. Parhamifar, L., Andersen, H. & Moghimi, S. M. Lactate dehydrogenase assay for assessment of polycation cytotoxicity. *Methods Mol Biol* **948,** 13–22. ISSN: 1064-3745. https://doi.org/10.1007/978-1-62703-140-0_2 (2013).

62. Van Engeland, M., Nieland, L. J. W., Ramaekers, F. C. S., Schutte, B. & Reutelingsperger, C. P. M. Annexin V-Affinity assay: A review on an apoptosis detection system based on phosphatidylserine exposure. *Cytometry* **31,** 1–9. ISSN: 0196-4763. https://doi.org/10.1002/(SICI)1097-0320(19980101)31:1%3C1::AID-CYTO1%3E3.0.CO;2-R (1998).

63. Robinson, J. P. Flow cytometry: past and future. *BioTechniques* **72,** 159–169. https://www.future-science.com/doi/abs/10.2144/btn-2022-0005 (2022).

64. Joanna, D. *et al.* Ammonia inhibits antitumor activity of NK cells by decreasing mature perforin. *bioRxiv,* 2023.11.20.567708. http://biorxiv.org/content/early/2023/11/21/2023.11.20.567708.abstract (2023).

65. Lunt, S. Y. & Vander Heiden, M. G. Aerobic Glycolysis: Meeting the Metabolic Requirements of Cell Proliferation. *Annual Review of Cell and Developmental Biology* **27,** 441–464. ISSN: 1530-8995. https://www.annualreviews.org/content/journals/10.1146/annurev-cellbio-092910-154237 (2011).

66. Kornberg, M. D. The immunologic Warburg effect: Evidence and therapeutic opportunities in autoimmunity. *Wiley Interdiscip Rev Syst Biol Med* **12,** e1486. ISSN: 1939-5094. https://doi.org/10.1002/wsbm.1486 (2020).

67. Son, S. *et al.* Direct observation of mammalian cell growth and size regulation. *Nature Methods* **9,** 910–912. ISSN: 1548-7105. https://doi.org/10.1038/nmeth.2133 (2012).

68. Miettinen, T. P. & Björklund, M. Mitochondrial Function and Cell Size: An Allometric Relationship. *Trends in Cell Biology* **27,** 393–402. ISSN: 0962-8924. https://doi.org/10.1016/j.tcb.2017.02.006 (2017).

69. Liu, S. in *Bioprocess Engineering (Second Edition)* (ed Liu, S.) 629–697 (Elsevier, 2017). ISBN: 978-0-444-63783-3. https://www.sciencedirect.com/science/article/pii/B9780444637833000113.

70. Cong, J. Metabolism of Natural Killer Cells and Other Innate Lymphoid Cells. *Front Immunol* **11,** 1989. ISSN: 1664-3224. https://doi.org/10.3389/fimmu.2020.01989 (2020).

71. Assmann, N. *et al.* Srebp-controlled glucose metabolism is essential for NK cell functional responses. *Nature Immunology* **18,** 1197–1206. ISSN: 1529-2916. https://doi.org/10.1038/ni.3838 (2017).

72. Lamas, B. *et al.* Leptin modulates dose-dependently the metabolic and cytolytic activities of NK-92 cells. *J Cell Physiol* **228,** 1202–9. ISSN: 0021-9541. https://doi.org/10.1002/jcp.24273 (2013).

73. Choi, C. & Finlay, D. K. Optimising NK cell metabolism to increase the efficacy of cancer immunotherapy. *Stem Cell Research and Therapy* **12,** 320. ISSN: 1757-6512. https://doi.org/10.1186/s13287-021-02377-8 (2021).

74. Surace, L. *et al.* Polarized mitochondria as guardians of NK cell fitness. *Blood Adv* **5.** 2473-9537, 26–38. https://doi.org/10.1182/bloodadvances.2020003458 (2021).

75. Ma, E. H. *et al.* Serine Is an Essential Metabolite for Effector T Cell Expansion. *Cell Metabolism* **25,** 345–357. ISSN: 1550-4131. https://doi.org/10.1016/j.cmet.2016.12.011 (2017).

76. Rosenberg, J. & Huang, J. CD8(+) T Cells and NK Cells: Parallel and Complementary Soldiers of Immunotherapy. *Curr Opin Chem Eng* **19,** 9–20. ISSN: 2211-3398. https://doi.org/10.1016/j.coche.2017.11.006 (2018).

77. Terrén, I., Orrantia, A., Vitallé, J., Zenarruzabeitia, O. & Borrego, F. NK Cell Metabolism and Tumor Microenvironment. *Frontiers in Immunology* **10.** ISSN: 1664-3224. https://www.frontiersin.org/articles/10.3389/fimmu.2019.02278 (2019).

78. Geeraerts, S. L., Heylen, E., De Keersmaecker, K. & Kampen, K. R. The ins and outs of serine and glycine metabolism in cancer. *Nature Metabolism* **3,** 131–141. ISSN: 2522-5812. https://doi.org/10.1038/s42255-020-00329-9 (2021).

79. Terrén, I. *et al.* Modulating NK cell metabolism for cancer immunotherapy. *Seminars in Hematology* **57,** 213–224. ISSN: 0037-1963. https://www.sciencedirect.com/science/article/pii/S003719632030041X (2020).

80. Yoo, H. C., Yu, Y. C., Sung, Y. & Han, J. M. Glutamine reliance in cell metabolism. *Experimental and Molecular Medicine* **52,** 1496–1516. ISSN: 2092-6413. https://doi.org/10.1038/s12276-020-00504-8 (2020).

81. Loftus, R. M. *et al.* Amino acid-dependent cMyc expression is essential for NK cell metabolic and functional responses in mice. *Nature Communications* **9,** 2341. ISSN: 2041-1723. https://doi.org/10.1038/s41467-018-04719-2 (2018).

82. Martí i Líndez, A.-A. & Reith, W. Arginine-dependent immune responses. *Cellular and Molecular Life Sciences* **78,** 5303–5324. ISSN: 1420-9071. https://doi.org/10.1007/s00018-021-03828-4 (2021).

83. Kuo, M. T., Chen, H. H. W., Feun, L. G. & Savaraj, N. Targeting the Proline Glutamine Asparagine Arginine Metabolic Axis in Amino Acid Starvation Cancer Therapy. *Pharmaceuticals* **14,** 72. ISSN: 1424-8247. https://www.mdpi.com/1424-8247/14/1/72 (2021).

84. Lamas, B. *et al.* Altered functions of natural killer cells in response to L-Arginine availability. *Cellular Immunology* **280,** 182–190. ISSN: 0008-8749. https://www.sciencedirect.com/science/article/pii/S0008874912002213 (2012).

85. Wu, J. *et al.* Asparagine enhances LCK signalling to potentiate CD8+ T-cell activation and anti-tumour responses. *Nature Cell Biology* **23,** 75–86. ISSN: 1476-4679. https://doi.org/10.1038/s41556-020-00615-4 (2021).

86. Krall, A. S., Xu, S., Graeber, T. G., Braas, D. & Christofk, H. R. Asparagine promotes cancer cell proliferation through use as an amino acid exchange factor. *Nature Communications* **7,** 11457. ISSN: 2041-1723. https://doi.org/10.1038/ncomms11457 (2016).

87. Martin, S. J. *et al.* Early redistribution of plasma membrane phosphatidylserine is a general feature of apoptosis regardless of the initiating stimulus: inhibition by overexpression of Bcl-2 and Abl. *Journal of Experimental Medicine* **182,** 1545–1556. ISSN: 0022-1007. https://doi.org/10.1084/jem.182.5.1545 (1995).

88. Denecker, G. *et al.* Phosphatidyl serine exposure during apoptosis precedes release of cytochrome c and decrease in mitochondrial transmembrane potential. *FEBS Letters* **465,** 47–52. ISSN: 0014-5793. https://febs.onlinelibrary.wiley.com/doi/abs/10.1016/S0014-5793%2899%2901702-0 (2000).

89. Taheri, F. *et al.* L-Arginine regulates the expression of the T-cell receptor zeta chain (CD3zeta) in Jurkat cells. *Clin Cancer Res* **7,** 958s–965s. ISSN: 1078-0432 (2001).

90. Orange, J. S. Formation and function of the lytic NK-cell immunological synapse. *Nature Reviews Immunology* **8,** 713–725. ISSN: 1474-1741. https://doi.org/10.1038/nri2381 (2008).

91. Bryceson, Y. T., March, M. E., Barber, D. F., Ljunggren, H.-G. & Long, E. O. Cytolytic granule polarization and degranulation controlled by different receptors in resting NK cells. *Journal of Experimental Medicine* **202,** 1001–1012. ISSN: 0022-1007. https://doi.org/10.1084/jem.20051143 (2005).

92. Hoffmann, S. C., Cohnen, A., Ludwig, T. & Watzl, C. 2B4 Engagement Mediates Rapid LFA-1 and Actin-Dependent NK Cell Adhesion to Tumor Cells as Measured by Single Cell Force Spectroscopy. *The Journal of Immunology* **186,** 2757–2764. ISSN: 0022-1767. https://doi.org/10.4049/jimmunol.1002867 (2011).

93. Fauriat, C., Long, E. O., Ljunggren, H.-G. & Bryceson, Y. T. Regulation of human NK-cell cytokine and chemokine production by target cell recognition. *Blood* **115,** 2167–2176. ISSN: 0006-4971. https://doi.org/10.1182/blood-2009-08-238469 (2010).

94. Judge, S. J., Murphy, W. J. & Canter, R. J. Characterizing the Dysfunctional NK Cell: Assessing the Clinical Relevance of Exhaustion, Anergy, and Senescence. *Frontiers in Cellular and Infection Microbiology* **10.** ISSN: 2235-2988. https://www.frontiersin.org/articles/10.3389/fcimb.2020.00049 (2020).

95. Myers, J. A. *et al.* Balanced engagement of activating and inhibitory receptors mitigates human NK cell exhaustion. *JCI Insight* **7.** ISSN: 2379-3708. https://doi.org/10.1172/jci.insight.150079 (2022).

96. Bi, J. & Tian, Z. NK Cell Exhaustion. *Front Immunol* **8,** 760. ISSN: 1664-3224. https://doi.org/10.3389/fimmu.2017.00760 (2017).

97. Klausner, R. D., Donaldson, J. G. & Lippincott-Schwartz, J. Brefeldin A: insights into the control of membrane traffic and organelle structure. *J Cell Biol* **116.** 1540-8140, 1071–80. ISSN: 0021-9525. https://doi.org/10.1083/jcb.116.5.1071 (1992).

98. Mollenhauer, H. H., James Morré, D. & Rowe, L. D. Alteration of intracellular traffic by monensin; mechanism, specificity and relationship to toxicity. *Biochimica et Biophysica Acta (BBA) - Reviews on Biomembranes* **1031,** 225–246. ISSN: 0304-4157. https://doi.org/10.1016/0304-4157(90)90008-Z (1990).

99. Borrego, F., Robertson, M. J., Ritz, J., Peña, J. & Solana, R. CD69 is a stimulatory receptor for natural killer cell and its cytotoxic effect is blocked by CD94 inhibitory receptor. *Immunology* **97.** 1365-2567, 159–65. ISSN: 0019-2805. https://doi.org/10.1046%2Fj.1365-2567.1999.00738.x (1999).

100. Kedia-Mehta, N. *et al.* Natural Killer Cells Integrate Signals Received from Tumour Interactions and IL2 to Induce Robust and Prolonged Anti-Tumour and Metabolic Responses. *Immunometabolism* **1,** e190014. ISSN: 2633-0407. https://doi.org/10.20900/immunometab20190014 (2019).

101. Borrego, F., Robertson, M. J., Ritz, J., Peña, J. & Solana, R. CD69 is a stimulatory receptor for natural killer cell and its cytotoxic effect is blocked by CD94 inhibitory receptor. *Immunology* **97.** 1365-2567, 159–65. ISSN: 0019-2805. https://doi.org/10.1046%2Fj.1365-2567.1999.00738.x (1999).

102. Xie, J.-H., Li, Y.-Y. & Jin, J. The essential functions of mitochondrial dynamics in immune cells. *Cellular and Molecular Immunology* **17,** 712–721. ISSN: 2042-0226. https://doi.org/10.1038/s41423-020-0480-1 (2020).

103. Zheng, X. *et al.* Mitochondrial fragmentation limits NK cell-based tumor immunosurveillance. *Nature Immunology* **20,** 1656–1667. ISSN: 1529-2916. https://doi.org/10.1038/s41590-019-0511-1 (2019).

Appendix

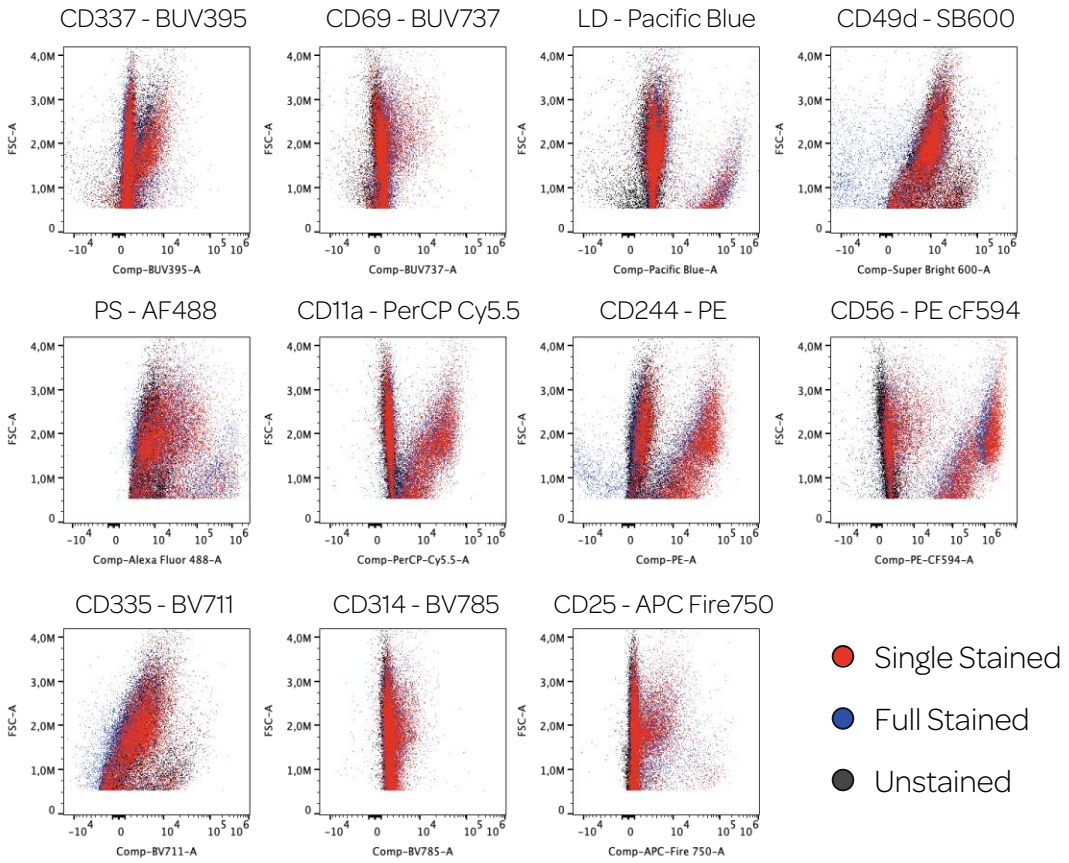

Figure A1: Overlay of unmixed spectral flow cytometry data: surface panel. NK-92 cells were co-cultured with K-562 cells at a 1:1 ratio, followed by harvesting. Subsequently, cells were either stained with one fluorophore-conjugated antibody (single stained) or the complete antibody panel (full-stained). An unstained sample was used as a background control. For the corresponding antibody concentrations, see chapter 3. Depicted are the overlays of single-stained, full-stained, and unstained sample dot plots. Notably, the markers CD244 and CD49d are overcompensated for K-562 cells, yet this does not impact the characterization of NK-92 cells. Robust unmixing is evident, as the dot plots of full-stained (blue) and single-stained (red) align well.

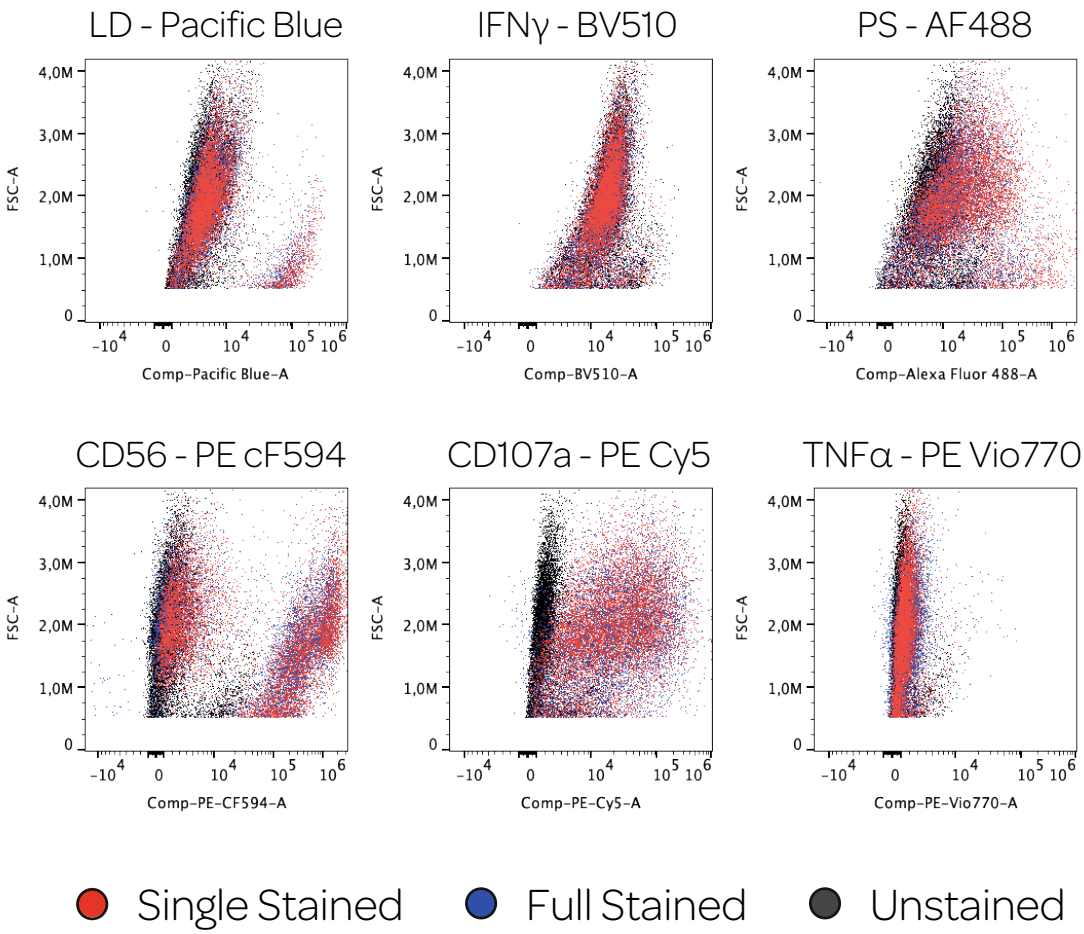

Figure A2: Overlay of unmixed spectral flow cytometry data: cytokine panel. NK-92 cells were co-cultured with K-562 cells at a 1:1 ratio, followed by harvesting. Subsequently, cells were either stained with one fluorophore-conjugated antibody (single stained) or the complete antibody panel (full-stained). An unstained sample was used as a background control. For the corresponding antibody concentrations, see chapter 3. Depicted are the overlays of single-stained, full-stained, and unstained sample dot plots. Robust unmixing is evident, as the dot plots of full-stained (blue) and single-stained (red) align well.